Defense Special Weapons Agency
Alexandria, VA 22310-3398

DSWA-TR-97-13

Worldwide Cloud Forecasts with Neural Networks

Kenneth A. Poehls, et al.
Pacific-Sierra Research Corp.
2901 28th Street
Santa Monica, CA 90405-2938

May 1998

Technical Report

CONTRACT No. DNA 001-94-C-0149

DESTRUCTION NOTICE:

Destroy this report when it is no longer needed.
Do not return to sender.

PLEASE NOTIFY THE DEFENSE SPECIAL WEAPONS AGENCY, ATTN: CSTI, 6801TELEGRAPH ROAD, ALEXANDRIA, VA 22310-3398, IF YOUR ADDRESS IS INCORRECT, IF YOU WISH IT DELETED FROM THE DISTRIBUTION LIST, OR IF THE ADDRESSEE IS NO LONGER EMPLOYED BY YOUR ORGANIZATION.

DISTRIBUTION LIST UPDATE

This mailer is provided to enable DSWA to maintain current distribution lists for reports. (We would appreciate your providing the requested information.)

NOTE:
Please return the mailing label from the document so that any additions, changes, corrections or deletions can be made easily. For distribution cancellation or more information call DSWA/IMAS (703) 325-1036.

☐ Add the individual listed to your distribution list.

☐ Delete the cited organization/individual.

☐ Change of address.

NAME: _____

ORGANIZATION: _____

OLD ADDRESS	CURRENT ADDRESS
_____	_____
_____	_____
_____	_____

TELEPHONE NUMBER: ( ) _____

DSWA PUBLICATION NUMBER/TITLE	CHANGES/DELETIONS/ADDITIONS, etc.) *(Attach Sheet if more Space is Required)*
_____	_____
_____	_____
_____	_____

DSWA OR OTHER GOVERNMENT CONTRACT NUMBER: _____

CERTIFICATION OF NEED-TO-KNOW BY GOVERNMENT SPONSOR (if other than DSWA):

SPONSORING ORGANIZATION: _____

CONTRACTING OFFICER OR REPRESENTATIVE: _____

SIGNATURE: _____

CUT HERE AND RETURN

DEFENSE SPECIAL WEAPONS AGENCY
ATTN: IMAS
6801 TELEGRAPH ROAD
ALEXANDRIA, VA 22310-3398

DEFENSE SPECIAL WEAPONS AGENCY
ATTN: IMAS
6801 TELEGRAPH ROAD
ALEXANDRIA, VA 22310-3398

REPORT DOCUMENTATION PAGE

Form Approved
OMB No. 0704-0188

1. AGENCY USE ONLY (Leave blank)	2. REPORT DATE	3. REPORT TYPE AND DATES COVERED
	980501	Technical 940826 - 970430

4. TITLE AND SUBTITLE
Worldwide Cloud Forecasts with Neural Networks

5. FUNDING NUMBERS
C - DNA 001-94-C-0149
PE - 62715H
PR - AC
TA - BA
WU - DH00114

6. AUTHOR(S)
Kenneth A. Poehls, David M. Crandall, Kevin O'Rouke, and Kenneth E. Heikes

7. PERFORMING ORGANIZATION NAME(S) AND ADDRESS(ES)
Pacific-Sierra Research Corp.
2901 28th Street
Santa Monica, CA 90405-2938

8. PERFORMING ORGANIZATION REPORT NUMBER
PSR Report 2692

9. SPONSORING/MONITORING AGENCY NAME(S) AND ADDRESS(ES)
Defense Special Weapons Agency
6801 Telegraph Road
Alexandria, VA 22310-3398
WEL/Smith

10. SPONSORING/MONITORING AGENCY REPORT NUMBER
DSWA-TR-97-13

11. SUPPLEMENTARY NOTES
This work was sponsored by the Defense Special Weapons Agency under RDT&E RMC Code B4662D BA 00114 4400A AC 25904D.

12a. DISTRIBUTION/AVAILABILITY STATEMENT
Approved for public release; distribution is unlimited.

12b. DISTRIBUTION CODE

13. ABSTRACT (*Maximum 200 words*)

Most approaches to weather and cloud forecasting entail the use of a large numerical weather prediction code. This project investigated an alternative approach to cloud forecasting based upon using a neural network (NN) to analyze and combine the basic meteorological elements of persistence, advection and evolution.

The Worldwide Cloud Prediction Model (WCPM) is based upon a pixel-by-pixel implementation of a NN. The temporal evolution and advection are estimated from past satellite and numerical weather prediction data. Persistence of cloud properties at a pixel is estimated from past data. The forecast is based upon this pixel level analysis and is almost independent of changes in neighboring pixels. Over the limited data available, the NN performed somewhat better in tropical regions than the current HRCP model. The approach demonstrated the ability to predict both the advection and evolution of clouds. Performance was best in regions of significant cloud cover, regions of scattered clouds were smeared. RMS prediction errors of ~20% were typical for the WCPM as compared to rms errors of ~30% for tropical HRCP predictions. An alternative, fully object-oriented approach to the NN is outlined to improve the performance and forecast sharpness in regions of scattered clouds.

14. SUBJECT TERMS
Weather Neural Networks Cloud Forecasting

15. NUMBER OF PAGES
112

16. PRICE CODE

17. SECURITY CLASSIFICATION OF REPORT	18. SECURITY CLASSIFICATION OF THIS PAGE	19. SECURITY CLASSIFICATION OF ABSTRACT	20. LIMITATION OF ABSTRACT
UNCLASSIFIED	UNCLASSIFIED	UNCLASSIFIED	SAR

NSN 7540-280-5500

Standar d Form 298 ((rev. 2-89)
Precribed by ANSI Sta. 239-18
298-102

CLASSIFIED BY:

N/A since Unclassified.

DECLASSIFY ON:

N/A since Unclassified.

SUMMARY

Most approaches to weather and cloud forecasting entail the use of a large numerical weather prediction code. These codes assimilate many forms of current weather data and then propagate that weather into the future using the governing dynamic equations. PSR has developed a cloud forecast model based on a neural network (NN) intended for eventual (by FY2002) integration into the Cloud Depiction and Forecast System II (CDFS II) at Air Force Global Weather Central. Work to date indicates a capability to analyze and forecast clouds can be accomplished on a single workstation and satellite data feed within a theater of operations, potentially with no connection to a weather center.

The cloud forecast model is founded on established forecast principles combined with promising new analysis techniques. The model is based on three fundamental processes: persistence, advection and evolution. These processes encompass the full range of atmospheric time and length scales that influence short- and extended-range cloud forecasts. Current meteorological methods are used to define the basic elements of each process but a NN is employed to analyze and combine the elements.

The current PSR worldwide cloud prediction model (WCPM) is based upon a pixel-by-pixel implementation of a NN. The advection of clouds within a pixel is traced through time. The temporal evolution of a pixel is estimated from past data. The persistence of cloud properties at a pixel is estimated from past data. The forecast is based upon this pixel level analysis and is almost independent of changes in neighboring pixels.

The NN was trained on SERCAA cloud images from both the Mediterranean Sea and the Central/South America region. Forecasts up to 12 hours were calculated and compared to truth. The approach demonstrated the ability predict both the advection and evolution of clouds.

The approach has considerable difficulty forecasting scattered clouds. This is not surprising given that the scattered clouds are completely random in both location and evolution. The best results were therefore obtained by training on and predicting median filtered clouds. RMS prediction errors of ~20% were typical for the WCPM as compared to rms errors of ~30% for tropical HRCP predictions. The dominant errors arise from over-predicting scattered clouds. The scattered clouds also were found to adversely affect the forecast sharpness by smearing the forecast.

The limited amount of data available for training severely impacted the ability of the NN to forecast. A NN should be trained on a variety of situations. Our data is dominated by evolved

cloud fields with scattered clouds. Advection is therefore not well represented in the data, neither are days with more than 25% cloud fraction. It is obvious what the NN best predicts. This can be remedied only by further training. Further training will not improve the forecast of random clouds, however.

It is felt that both of these problems can be repaired by modifying the pixel-by-pixel forecast approach. An object-oriented approach was described that better represents the regional weather situation. Pixels are no longer independent of their surroundings but depend upon the nature of approach (and receding) weather conditions. The object-oriented approach addresses the scattered cloud problem by including randomness as part of object descriptions.

CONVERSION TABLE

Conversion factors for U.S. Customary to metric (SI) units of measurement

MULTIPLY → / TO GET ←	BY → / BY ←	TO GET / DIVIDE
angstrom	1.000 000 x E -10	meters (m)
atmosphere (normal)	1.013 25 x E +2	kilo pascal (kPa)
bar	1.000 000 x E +2	kilo pascal (kPa)
barn	1.000 000 x E -28	meter^2 (m^2)
British thermal unit (thermochemical)	1.054 350 x E +3	joule (J)
calorie (thermochemical)	4.184 000	joule (J)
cal (thermochemical)/cm^2	4.184 000 x E -2	mega joule/m^2 (MJ/m^2)
curie	3.700 000 x E +1	*giga becquerel (GBq)
degree (angle)	1.745 329 x E -2	radian(rad)
degree Fahrenheit	$t_K = (t°f + 459.67)/1.8$	degree kelvin (K)
electron volt	1.602 19 x E -19	joule (J)
erg	1.000 000 x E -7	joule (J)
erg/second	1.000 000 x E -7	watt (W)
foot	3.048 000 x E -1	meter (m)
foot-pound-force	1.355 818	joule (J)
gallon (U.S. liquid)	3.785 412 x E -3	meter^3 (m^3)
inch	2.540 000 x E -2	meter (m)
jerk	1.000 000 x E +9	joule (J)
joule/kilogram (J/kg) (radiation dose absorbed)	1.000 000	Gray (Gy)
kilotons	4.183	terajoules
kip (1000 lbf)	4.448 222 x E +3	newton (N)
kip/inch^2 (ksi)	6.894 757 x E +3	kilo pascal (kPa)
ktap	1.000 000 x E +2	newton-second/m^2 (N-s/m^2)
micron	1.000 000 x E -6	meter (m)
mil	2.540 000 x E -5	meter (m)
mile (international)	1.609 344 x E +3	meter (m)
ounce	2.834 952 x E -2	kilogram (kg)
pound-force (lbs avoirdupois)	4.448 222	newton (N)
pound-force inch	1.129 848 x E -1	newton-meter (N m)
pound-force/inch	1.751 268 x E +2	newton/meter (N/m)
pound-force/foot^2	4.788 026 x E -2	kilo pascal (kPa)
pound-force/inch^2 (psi)	6.894 757	kilo pascal (kPa)
pound-mass (lbm avoirdupois)	4.535 924 x E -1	kilogram (kg)
pound-mass-foot^2 (moment of inertia)	4.214 011 x E -2	kilogram-meter^2 (kg m^2)
pound-mass/foot^3	1.601 846 x E +1	kilogram/meter^3 (kg/m^3)
rad (radiation dose absorbed)	1.000 000 x E -2	**Gray (Gy)
roentgen	2.579 760 x E -4	coulomb/kilogram (C/kg)
shake	1.000 000 x E -8	second (s)
slug	1.459 390 x E +1	kilogram (k)
torr (mm Hg, 0°C)	1.333 22 x E -1	kilo pascal (kPa)

*The becquerel (Bq) is the SI unit of radioactivity; 1 Bq = 1 event/s.

**The Gray (Gy) is the SI unit of absorbed radiation.

TABLE OF CONTENTS

FIGURES

FIGURES (Continued)

TABLES

SECTION 1
INTRODUCTION

Most approaches to weather and cloud forecasting entail the use a large numerical weather prediction code. These codes assimilate many forms of current weather data and then propagate that weather into the future using the governing dynamic equations. An alternative approach to cloud forecasting is developed here. The new cloud forecast model is based on a neural network (NN) intended for eventual (in FY2002) integration into the Cloud Depiction and Forecast System II (CDFS II) at Air Force Global Weather Central.

The cloud forecast model is founded on established forecast principles combined with promising new analysis techniques. The model is based on three fundamental processes: persistence, advection and evolution. These processes encompass the full range of atmospheric time and length scales that influence short- and extended-range cloud forecasts. Current meteorological methods are used to define the basic elements of each process but a NN is employed to analyze and combine the elements. While NNs have only recently been applied to meteorological problems (McCann, 1992; Blankert, 1993; Welch, et al., 1992), they are widely used for problems such as pattern recognition where formal analysis is often ineffective. NNs are attractive for cloud forecasting because they (1) are robust in the face of incomplete data, (2) readily accept data from widely divergent sources, (3) are fast once trained, and (4) can model nonlinear relationships.

The worldwide cloud prediction model (WCPM) is based upon a pixel-by-pixel implementation of a NN. The advection of clouds within a pixel is traced through time. The temporal evolution of a pixel is estimated from past satellite and numerical weather prediction data. The persistence of cloud properties at a pixel is estimated from past data. The forecast is based upon this pixel level analysis and is almost independent of changes in neighboring pixels.

This report documents the three stages of project development. First, individual modules were developed to forecast clouds using only advection, persistence, or evolution. A separate NN was developed for each module. Second, a rigorous analysis was performed on the selected predictors in an effort to reduce redundancy and eliminate noisy or useless predictors. A unified NN was developed that simultaneously utilized the advection, persistence and evolution predictors. Lastly, the quality of the resulting forecasts was evaluated using skill scores on data not used for NN training.

The cloud forecast model developed can easily run in a standard work station environment. Over the limited data available for verification, the NN developed was found to perform some-

what better in tropical regions than the current High-Resolution Cloud Prognosis (HRCP) model. Lack of data prevented testing on a global basis.

Performance was best in regions of significant cloud cover. Poor forecast sharpness was associated with regions of scattered clouds. The NN smeared the scattered clouds uniformly across the region. This was due both to the limited training set and to the pixel-by-pixel approach. Based upon the forecast capabilities of WCPM, an alternative, fully object-oriented approach to the NN is outlined to improve the performance and forecast sharpness in regions of scattered clouds.

SECTION 2
THE NATURE OF CLOUD FORECASTING

All forecasting problems start with a conceptual model of the required phenomenon to be forecast, in our case clouds, which must in some way conform to the way the clouds are sampled. Our basic requirement is to forecast cloud fraction and altitude, including at least four cloud layers (if present), on a global (or regional) basis. Several *conceptual models* are possible to describe the same cloud distribution, yet which result in different *forecast model* parameterizations. Models differ in terms of the parameterization of the clouds themselves, and in the parameterization of the cloud distributions.

The primary source of cloud data for the following development and analysis is SERCAA Level 3 or 4 cloud data (Gustafson, et al., 1994). The SERCAA cloud data is parameterized in terms of cloud fraction (in four layers) and (eventually) cloud type. A complete nephanalysis is performed on high resolution imagery (2 to 5 km pixel resolution) to estimate cloud fraction at a $1/16^{th}$ mesh scale (approximately 25×25 km). A *minimum* requirement for computer forecasting is pixel-by-pixel cloud fraction; cloud type designators are useless. Neither descriptor provides cloud *image* information (information that relates clouds at one pixel to clouds at neighboring pixels). Neither descriptor provides information about the randomness in the cloud scene.

A typical cloud scene (Figure 2-1) can best be described as several spatially and/or temporally correlated features with both mean and random cloud properties. The mean properties (shape, area, average cloud cover) of features A, B, C and D are potentially predictable; the random properties (the pixel-by-pixel cloud fractions) are not predictable, although their statistics might well be. Here feature A has a mean cloud fraction (23%) and cloud top temperature (300 °K). The random cloud distribution within the feature might be described by higher moments or a fractal dimension, but is only predictable in a statistical sense.

Feature D is an example of a relatively stable cloud distribution with very low cloud fraction. Only isolated clouds (a few pixels each) are present that appear to jump around from temporal image to temporal image. Here, either the clouds are evolving and/or advecting much more rapidly than the sampling time so a consistent picture of the detailed clouds is not available. The clouds appear to be randomly distributed throughout the feature although the total cloud fraction is relatively constant.

Figure 2-1. Cloud scene from the Mediterranean Sea and North Africa showing several cloud features (A, B, C, D). North is approximately to the left on the image.

The remaining clouds not included in the four features are random with temporal sampling. It might be possible to predict a mean "background" cloud fraction but not its spatial distribution.

The above discussion of predictable and random clouds is highly contingent upon the data resolution and sampling time. A much higher sampling rate (than one image per hour) would allow smaller clouds to be better tracked. Higher resolution (than the $1/16^{th}$ mesh SERCAA data) would allow smaller significant features to be defined. At some resolution, however, clouds are randomly created and destroyed. The conditions under which clouds form, grow or diminish are predictable, however, clouds are known to form randomly in space within those conditions.

Therefore, the detailed cloud distribution within regions of light clouds will always be a random process and not predictable.

Two parameterizations of cloud distributions can be considered. The most straightforward conceptual model is the **generalized model**. The clouds are located in space by a pixel designator (i,j) and the cloud top height (or IR brightness temperature). Each pixel can conceivably have clouds at several heights. Each pixel is in many ways independent of adjacent pixels. Minimal nephanalysis or pre-processing of the cloud images is required.

An alternative conceptual model is a **layered model**. Here, the clouds are pre-processed into L finite thickness layers. The layers can be of either fixed or floating height and thickness. Each layer is independent of the other layers. The layering imposes an implicit physical relationship between clouds in the same layer. Complete nephanalysis and considerable pre-processing of the cloud images are required.

The former parameterization is the most general and provides the more exact representation of the available cloud data. The data is fully represented in terms of cloud fractions, pixel location, and cloud top heights. In doing so, however, it stresses the forecast algorithms because more parameters must be predicted. Generality is lost if layering is imposed, but the forecast algorithms need not forecast cloud top height at independent pixels. This is a great advantage in that clouds at many adjacent pixels are usually related in origin through (spatially) smoothly varying atmospheric conditions (weather systems or fronts).

The generalized model is preferred because it de-emphasizes the nephanalysis and will be investigated first. The layered model may be pursued at a later time. The final choice will be based upon the model robustness to various cloud scenarios and upon prediction performance

SECTION 3
MODEL DEVELOPMENT AND REFINEMENT

A pixel-by-pixel NN algorithm is adopted as the generalized approach to cloud forecasting. The approach is based upon the assumption that a forecast is possible based solely upon the past, current and approaching clouds to a single pixel. The pixel-by-pixel implementation was chosen to minimize and simplify the data input into the neural network. Each pixel is treated separately and is only loosely connected to surrounding pixels through the latitude and longitude inputs. No formal synoptic weather inputs are employed in this approach.

The forecast code is designed around a unified NN (described in Section 3.4) with major weather inputs representing *advection* of clouds, *persistence* of clouds, and *evolution* of clouds along with several influence parameters. The general structure of the code is illustrated in Figure 3-1. This final form is somewhat different from the original configuration that employed a separate NN for each module input and a NN to combine the individual forecasts. The latter was abandoned in favor of the unified approach to reduce the redundancy of the input parameters.

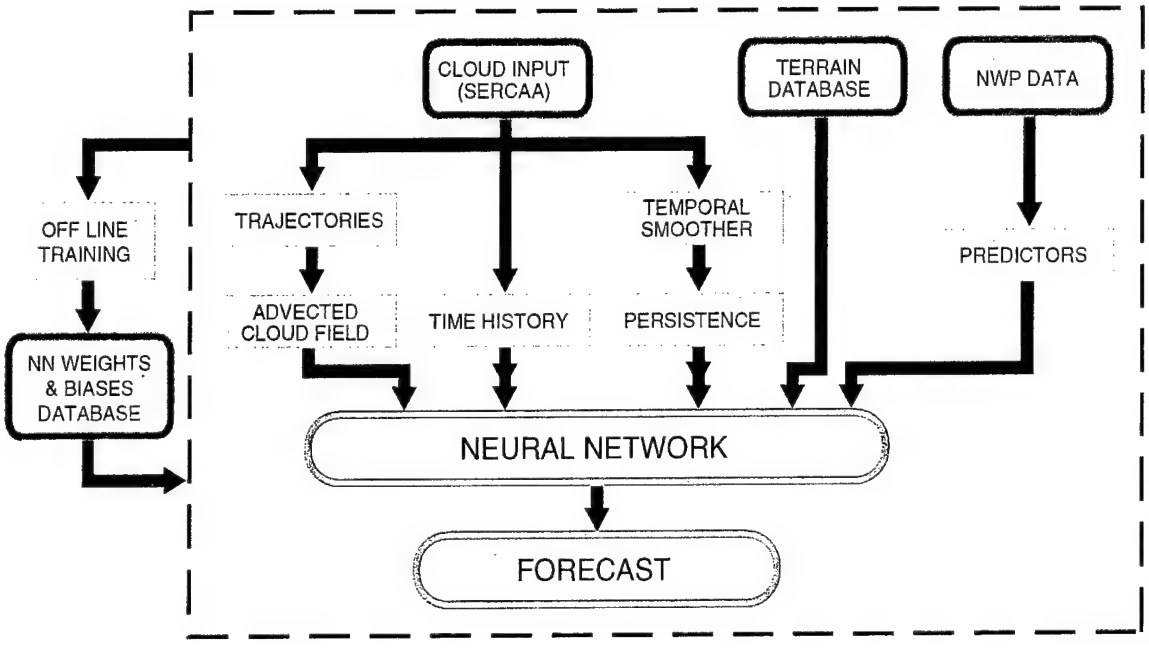

Figure 3-1. General structure of the code.

The weather inputs are divided into two categories: cloud observation data and meteorological parameter input. The *advection* and *persistence* modules represent the former while the *evolution* module represents the latter. For this study's purposes, the cloud observation data is taken from SERCAA level 3 nephanalysis. Navy Operational and Global Atmospheric Prediction System (NOGAPS) numerical analysis and forecasts are used for the meteorological parameter inputs. See Appendix A for a description of SERCAA and NOGAPS data.

The model will be described below essentially in the same way it was developed, as individual algorithms that were eventually merged into a single neural network. It should be remembered, however, that although the algorithms are separately described, there was never any intention that they would perform well as stand alone modules.

3.1 ADVECTION DEPENDENCE.

The advection module has significantly evolved from its original incarnation. The stand-alone model was based upon somewhat more than simple advection and assumed that clouds do not depend on location, season, or local time – kinematic assumption – and that the clouds will follow the same trajectory and undergo the same changes during the next 12 hours as during the previous 12 hours. The original NN module therefore included the following components (totaling 200 input values):

1. Advection of the current time clouds to the forecast time;
2. Current clouds at hourly increments upwind;
3. Previous clouds at hourly increments upwind.

Only the first input was retained in the final advection inputs. The purpose of the latter two inputs was to describe how the clouds were changing as they were advected. These inputs were dropped because of noise. Both cloud time series were found to be white noise sequences. The noise originated from two sources: errors in the advection trajectory and in cloud sampling. Both were aggravated by the fact that the data is dominated by broken clouds in both EASA and CNSA.

A detailed analysis of the performance of the advection estimation algorithm resulted in a major change in the approach. The previous approach was purposely simple:

- Wind vectors were estimated for the previous hour.
- Forecast time wind vectors were obtained by simply multiplying the 1 hour vectors by the forecast time.
- Clouds were moved based upon the vectors.

It was hoped that the neural network would correct for poor wind estimates. Instead, it was found that poor wind estimates (when advection actually was the primary process) degraded the performance of the persistence and evolution inputs. Based upon this, two improvements to the advection module were instituted. A progressive wind vector advection algorithm replaced the simple single wind vector prediction, and a smoothing algorithm was developed for the wind field.

The previously employed advection algorithm was simple and efficient for short-term forecasts or wind fields with little curvature. When significant curvature exists, as occurs in flow about a major high or low pressure system, the simple linear approach produces extremely poor results. To rectify this a *progressive vector* advection module was created.

The clouds at a mesh point are advected using the following algorithm illustrated in Figure 3-2:

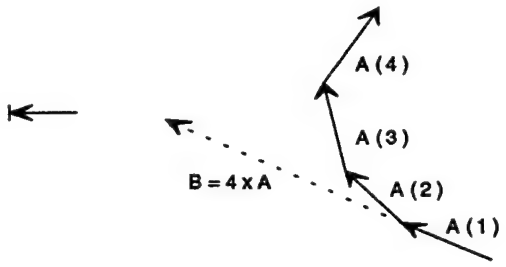

Figure 3-2. In cases of significant curvature to the wind field, the progressive vector method (A) retains more accuracy than the linear extrapolation method (B).

- The wind field for the most recent hour is assumed to be the best estimate of the wind field in the future.
- The clouds at a mesh point are advected forward 1 hour in time to a new mesh point using the wind vector at the current point.
- The wind vector at the new point is used to advect the clouds forward an additional 1 hour in time.
- The previous step is repeated until the desired forecast time is attained.

This procedure better retains the overall shape of the cloud formations as long as the current wind field accurately reflects the future wind field and the clouds are predominately advected (as opposed to evolved).

The correlation analysis results in an inconsistent wind field, e.g. the field is not smooth and vectors often cross. To help alleviate (but not completely eliminate this problem) a smoothing process has been added to the wind field estimate. We have advection data defined on a 2D grid with lots of gaps – cloudless grid points with no good advection estimate. A weighted least squares smoother interpolator was developed.

The input data is on a grid of dimensions $n_x \times n_y$, with grid points at positions $x = 1,2,\ldots,n_x$ and $y = 1,2,\ldots,n_y$. The input data consists of three pieces of data for each grid point: $u(x,y)$ is the x component of the advection, $v(x,y)$ is the y component, and $w(x,y)$ is the weight. w is constructed from the correlation data: for good pixels, w is the correlation value (between 0 and 1 – no negative values); for bad pixels, w is set to zero. For bad pixels we should also set u and v to zero.

The data is fit by a set of smooth 2D basis functions. We'll specify the basis functions later, but for now let n_b be the number of basis functions used, and the basis functions are $B_b(x,y)$ for $b = 1,2,\ldots n_b$, defined for all x and y. The smoothed advection functions are linear superpositions of the basis functions, with some coefficients:

$$\begin{aligned} u_{smooth}(x,y) &= \sum_{b=1}^{n_b} a_b B_b(x,y) \\ v_{smooth}(x,y) &= \sum_{b=1}^{n_b} b_b B_b(x,y) \end{aligned} \qquad (3.1)$$

The coefficients are determined by doing a weighted fit to the advection data. This is the standard linear least squares fitting result, with weights. For the u data, define the variance

$$\sigma_x^2 \equiv \frac{1}{n_x n_y} \sum_{x=1}^{n_x} \sum_{y=1}^{n_y} w(x,y)\left[u(x,y) - u_{smooth}(x,y)\right]^2 \quad . \qquad (3.2)$$

Make the following definitions for the scalar UU, the vector BU, and the $n_b \times n_b$ matrix BB:

$$UU \equiv \frac{1}{n_x n_y} \sum_{x,y} w(x,y) u(x,y)^2$$

$$BU_b \equiv \frac{1}{n_x n_y} \sum_{x,y} w(x,y) B_b(x,y) u(x,y) \quad . \tag{3.3}$$

$$BB_{bb'} \equiv \frac{1}{n_x n_y} \sum_{x,y} w(x,y) B_b(x,y) B_{b'}(x,y)$$

With these and some math, the variance is

$$\sigma_x^2 = UU - 2\sum_b a_b BU_b + \sum_{b,b'} a_b a_{b'} BB_{b,b'} \quad . \tag{3.4}$$

Minimizing this with respect to a_b gives a solution in terms of the inverse of the matrix BB:

$$a_b = \sum_{b'} BB^{-1}{}_{b,b'} \cdot BU_{b'} \quad , \tag{3.5}$$

and with this the variance is

$$\sigma_x^2 = UU - \sum_{b,b'} BU_b \cdot BB^{-1}{}_{b,b'} \cdot BU_{b'} \quad . \tag{3.6}$$

The variance is useful to calculate, because it gives us a feeling for how well we're fitting the data.

If the basis functions were orthogonal, so that

$$BB_{bb'} = \frac{1}{n_x n_y} \sum_{x,y} w(x,y) B_b(x,y) B_{b'}(x,y) \tag{3.7}$$

was zero for $b \neq b'$, then the matrix would be diagonal and the inversion trivial. However, because of the arbitrary weights w in the equation, it is impossible to choose orthogonal basis functions. We will just choose simple basis functions, and have to live with the matrix inversion.

Figures 3-3 and 3-4 show an example calculation for the Mediterranean wind field. First, the north and east components of the wind field are estimated for individual cloudy pixels (Figures 3-3a and c). These are then smoothed and interpolated to produce the wind field used for advection (Figures 3-3b and d). The results of the advection are shown in Figure 3-4. Here, the

original (T_0) clouds are advected 12 hours based upon the old and the new smoothed T_0 wind field. The results are compared to truth 12 hours later. Both approaches suffer from the fact that the cloud motion is not dominated by advection throughout the region; the clouds over southern Europe (to the left) are not moving but are evolving. Over northern Africa where advection is more dominant, the new model provides a better advection only forecast.

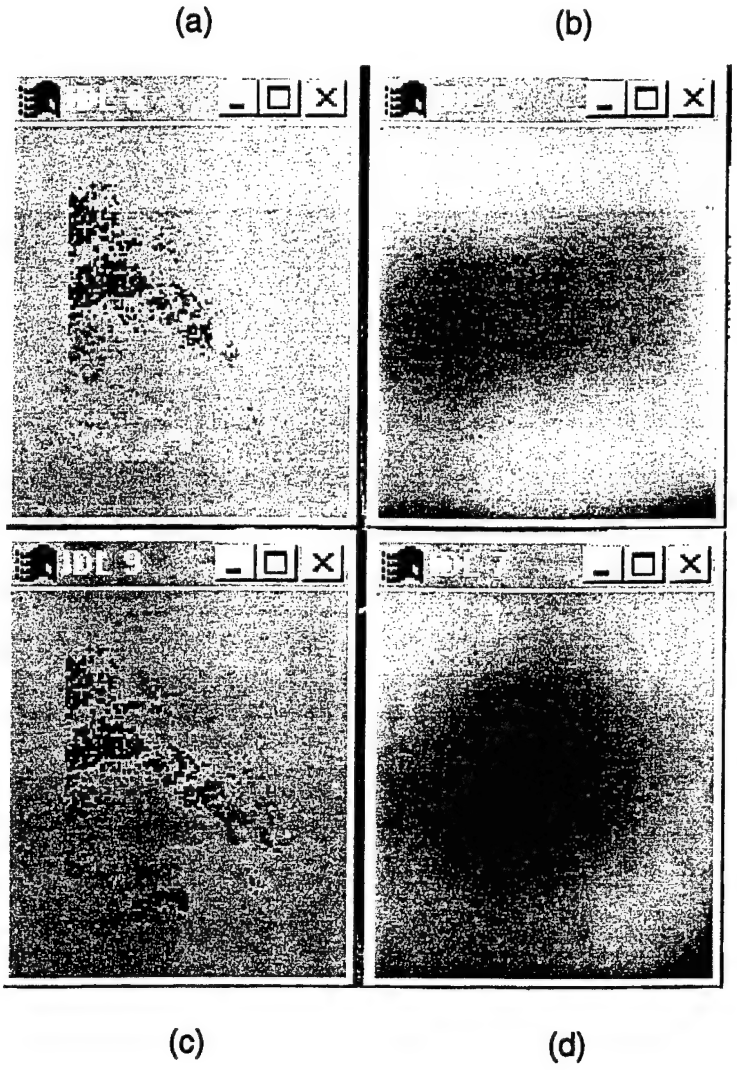

Figure 3-3. Cloud advection calculation using a 4th order fit for the EMDA.

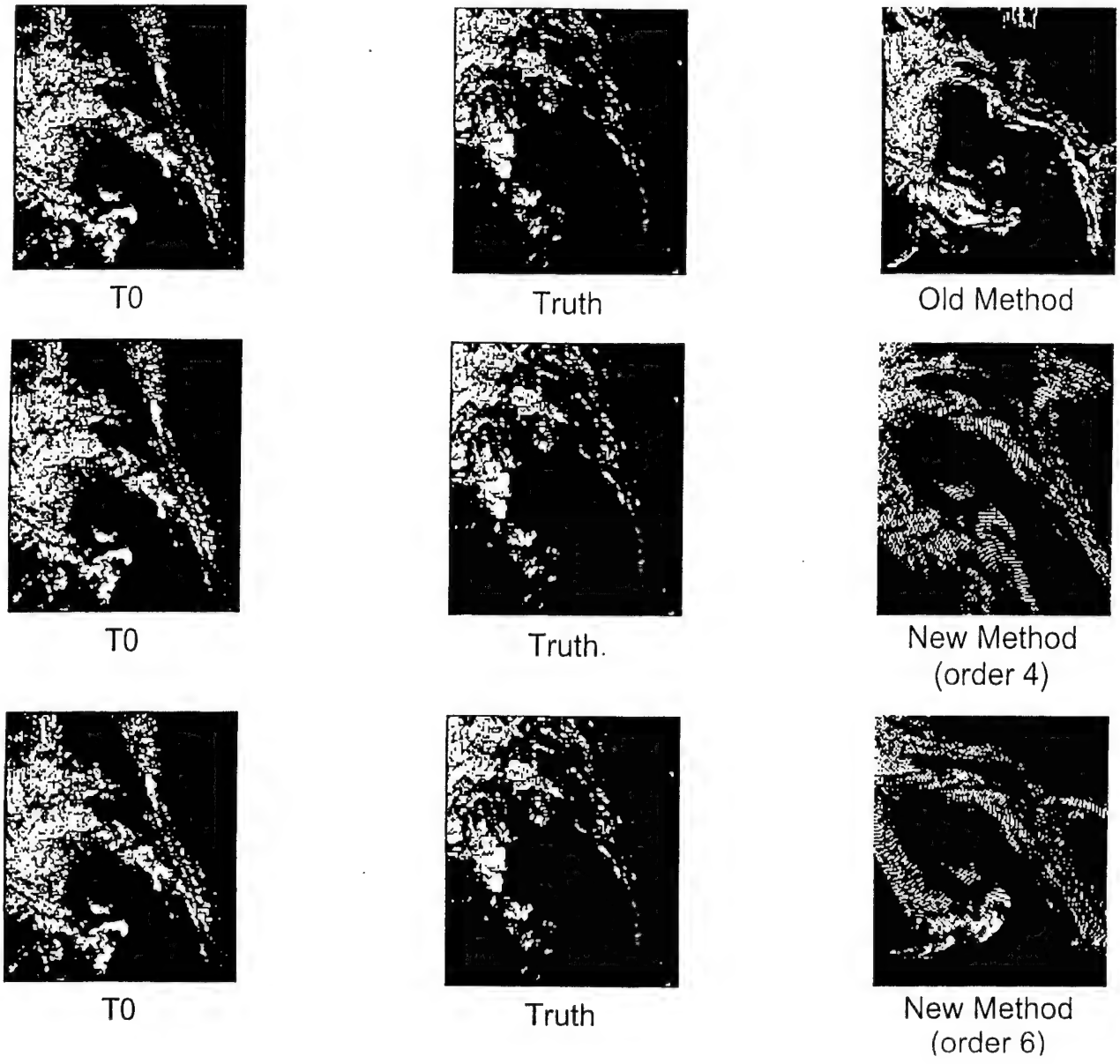

Figure 3-4. Cloud advection results.

3.2 PERSISTENCE DEPENDENCE.

Persistence is the tendency of weather to change slowly or to predictably repeat itself after some time interval. A forecast that merely persists current weather is usually the best short-term (0 to 3 hours) predictor. Some current tropical forecast models rely solely on simple persistence and a variation of it, diurnal persistence. Analyses by Salby, et al. (1991) indicate that a better persistence forecast might be obtained by including a more complete time history of cloud behavior. In particular, Salby, et al. noted strong regionally-dependent semi-diurnal and 4-day cycles associated with easterly waves in the tropics. A cloud history function that spans at least four days might improve forecasts.

The dominance of persistence in the SERCAA data areas is best represented by power spectral analysis. The power spectra were obtained by analyzing 2000 9-day hourly time series from random locations.

The results of the spectral analysis for EASA March 1993 tropical and mid-latitude ocean and land are shown in Figures 3-5 through 3-8. For cloud fraction, the top line corresponds to total cloud fraction and the lines below are fore SERCAA layers 1 through 4, respectively. For cloud height, starting at the top, the lines correspond to SERCAA layers 1 through 4, respectively.

As expected, the data show a definite diurnal cycle over tropical land areas. No trends of any sort are apparent over ocean areas or at temperate latitudes. In fact, with the exception of the diurnal peaks, the spectra are representative of a white noise process with a very long term trend superimposed. The results for layers 3 and 4 represent pure white noise processes. These results do not preclude the presence of long period cycles but more likely reflect poor resolution of the lower cloud layers by the SERCAA nephanalysis.

The above results do require a significant modification to the anticipated persistence modeling approach. The proposed approach called for an auto-regressive model using a 6-day time series to capture the easterly wave 4-day cycle. The data clearly does not support such a model. Limited data also precludes model dependence upon geographic region and time of year. Given these constraints a simpler approach to a persistence model was adopted that only includes a 12 hour cloud history and an average diurnal input.

The 12 hour cloud history is simply input by including the current time cloud characterization along with cloud characterization for 1, 3, 6, and 12 hours past. This data is meant to establish the near-time trend in cloud parameters.

The diurnal cycle in cloud parameters is input by averaging the cloud parameters from 24, 48, and 72 hours before the *forecast time*. This approach appears, and is, simple but was chosen for its robustness. The diurnal input can be averaged in several different ways and still be input. A recursive filter with a three day weight is an obvious choice for an operational system. The choice of weighting should be based upon information available upon longer term weather trends. A semi-diurnal or 4 day cycle can be input instead of the diurnal input.

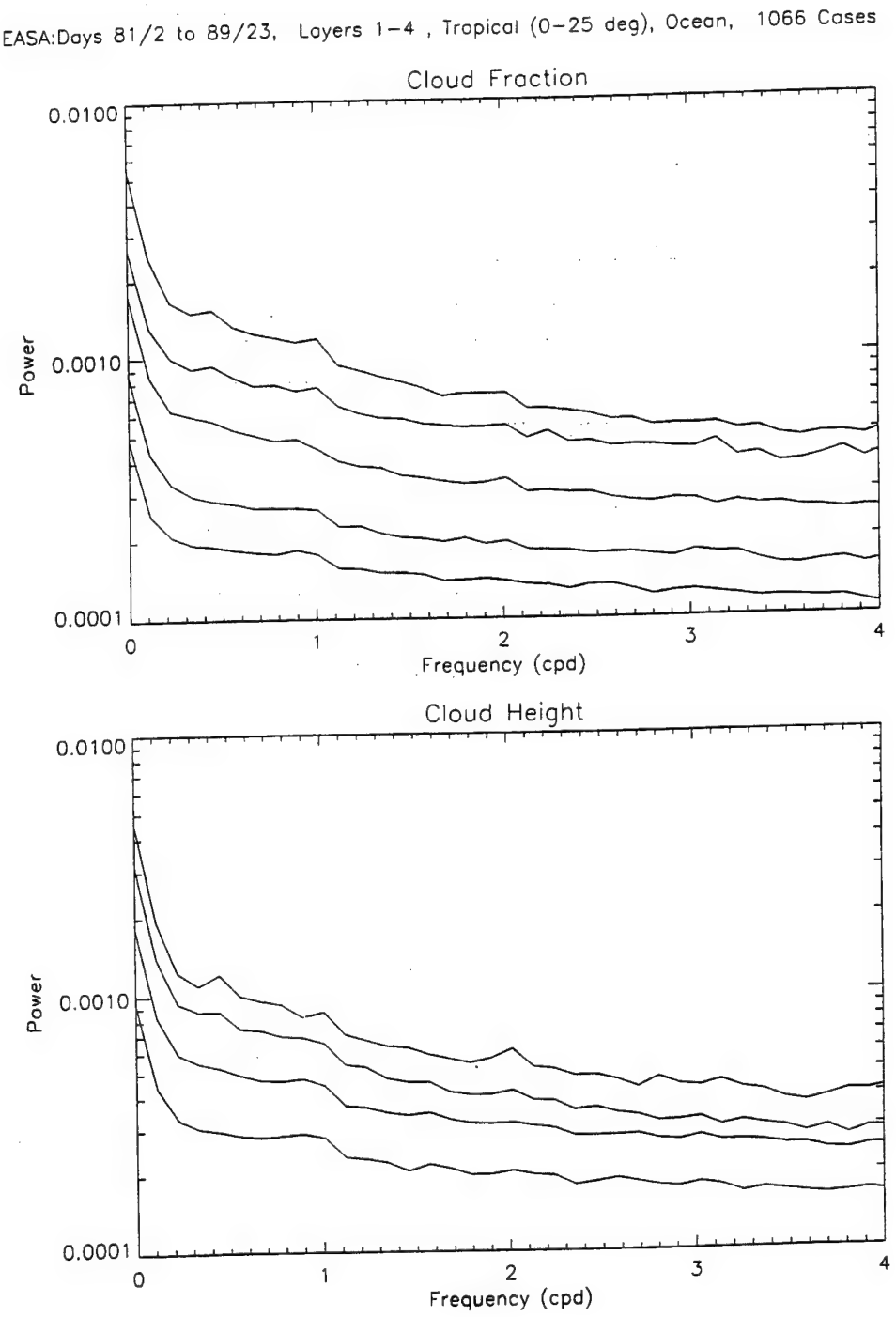

Figure 3-5. Spectral analysis of cloud history in EASA March 1993 over tropical ocean regions.

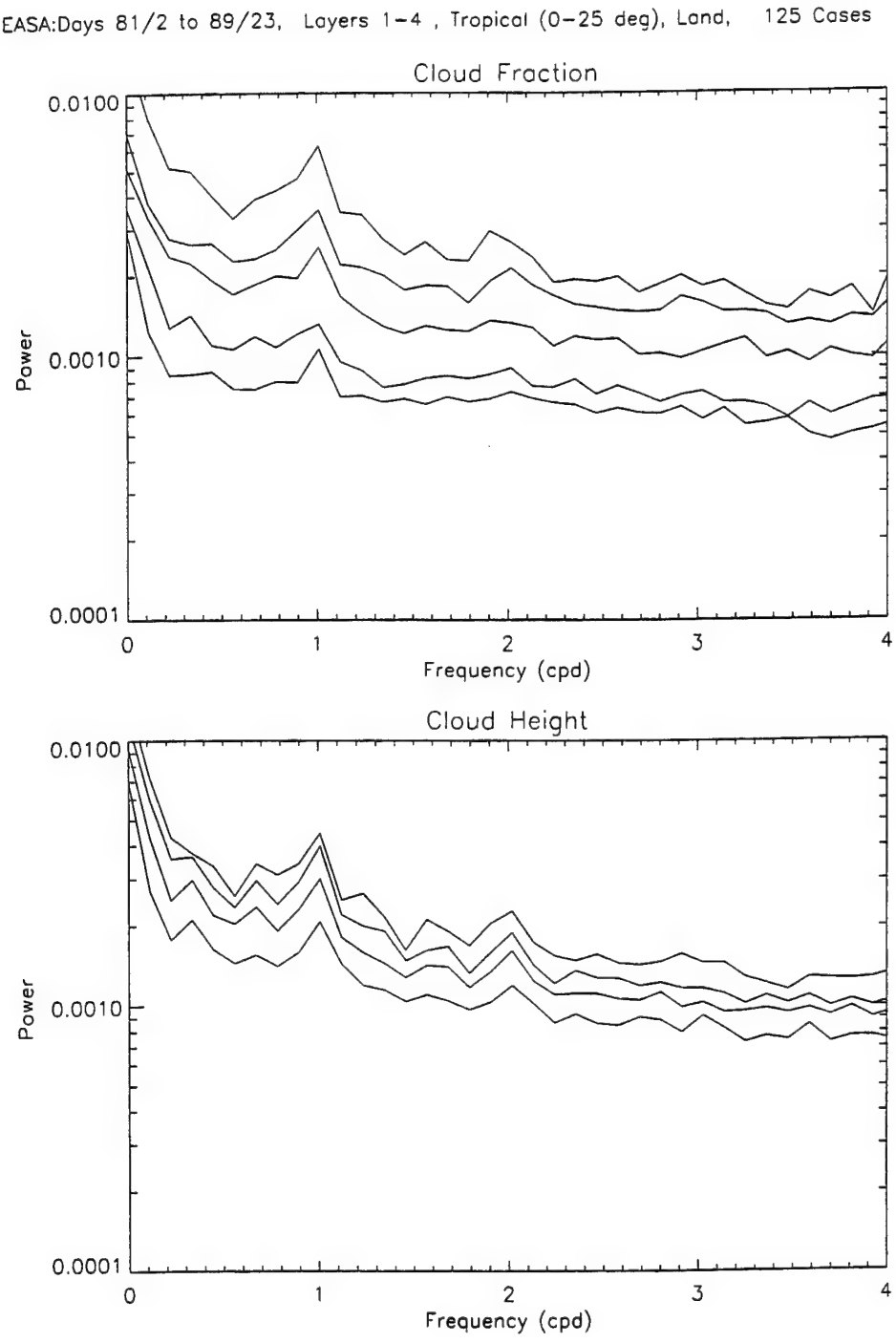

Figure 3-6. Spectral analysis of cloud history in EASA March 1993 over tropical land regions.

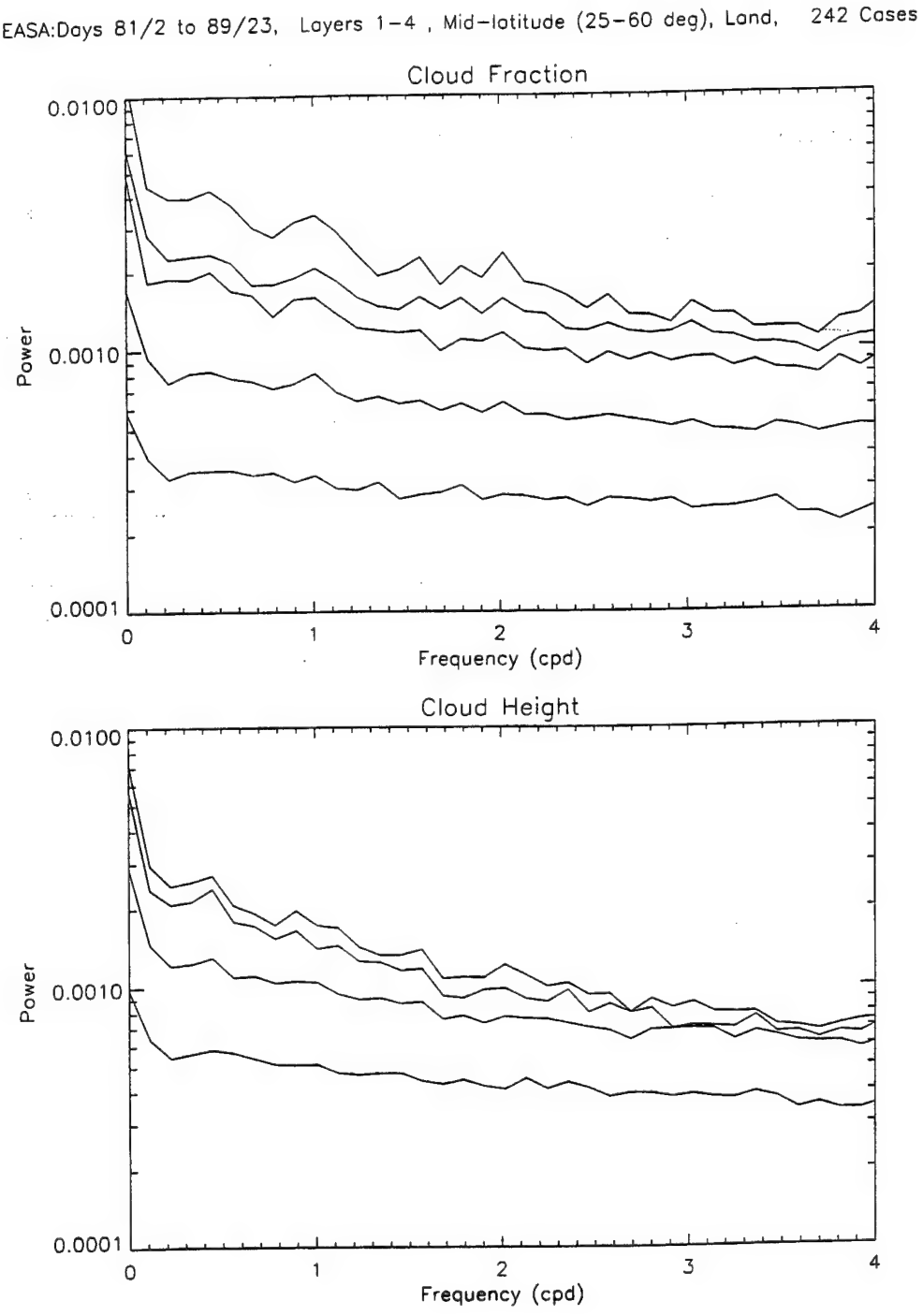

Figure 3-7. Spectral analysis of cloud history in EASA March 1993 over mid-latitude ocean regions.

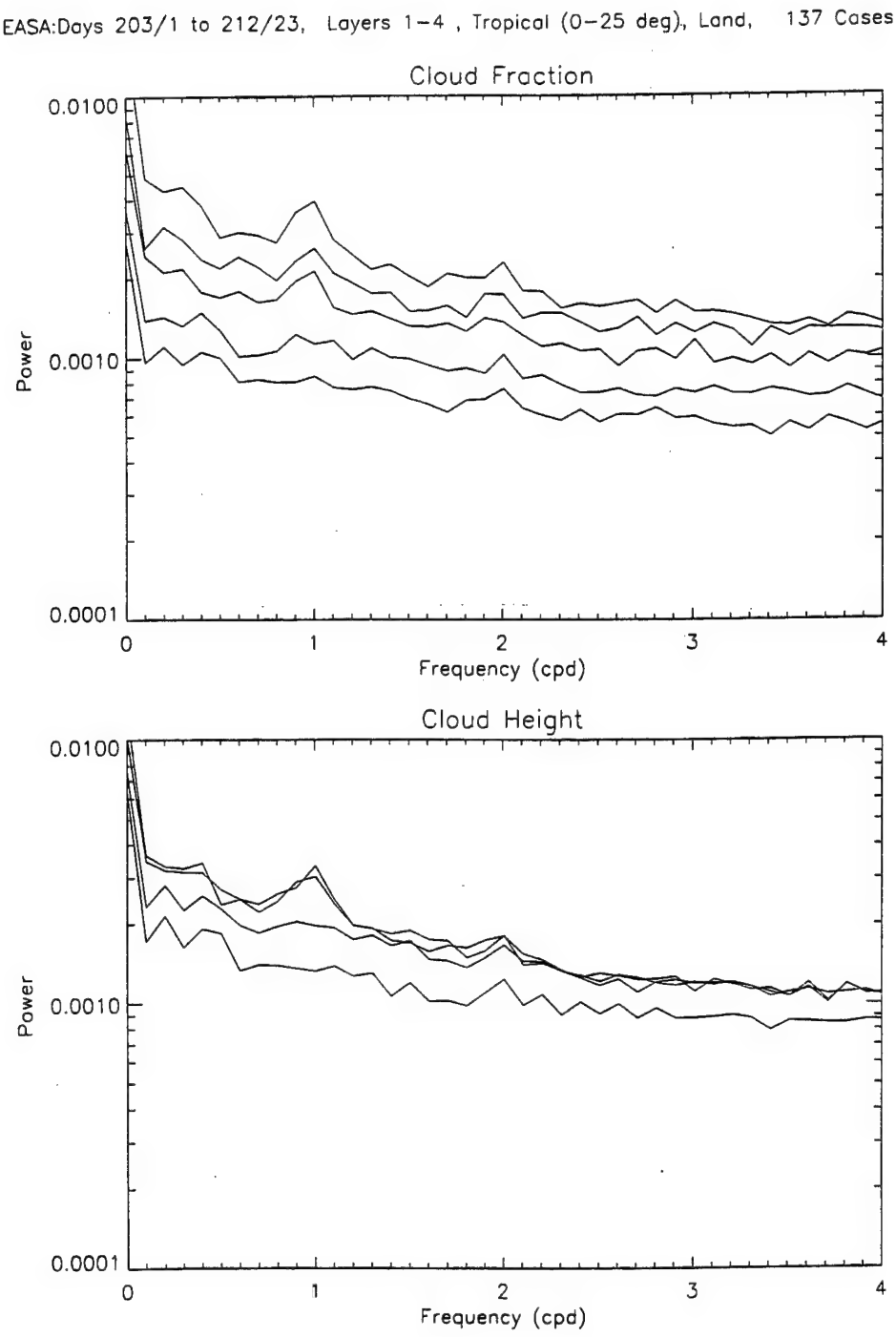

Figure 3-8. Spectral analysis of cloud history in EASA March 1993 over mid-latitude land regions.

Table 3-1 summarizes both the minimal and normal data requirements for the persistence algorithm. The minimum requirements refer to data requirements necessary for a cold start. Therefore the model can be started with only the previous day's data. Normal operation requires three previous days of data.

Table 3-1. Persistence model data requirements.

Minimum Requirements	Normal Requirements
t_0	t_0
t_0 - 1 (hours)	t_0 - 1 (hours)
t_0 - 3	t_0 - 3
t_0 - 6	t_0 - 6
t_0 - 12	t_0 - 12
$t_{forecast}$ - 24	$t_{forecast}$ - av(24, 48, 72)

Three quantities are input for each of the times (except diurnal) in Table 3-1. For each identified layer of clouds these include: (1) time delay from t_0; (2) cloud fraction at the time delay; (3) cloud top temperature at the time delay.

3.3 EVOLUTION DEPENDENCE.

Like persistence, the evolution algorithm depends on local characteristics such as topography, geography, latitude and time-of-day, but whereas the persistence and advection algorithms merely extrapolate cloud behavior in time and space, the evolution algorithm exploits atmospheric dynamics to predict clouds by engaging the output of a numerical weather prediction (NWP) model. Since the military intends to consolidate all NWP functions under FNMOC, and since NOGAPS is the Navy's global forecast model, it is likely that NOGAPS data will be the source of NWP data in future AF cloud forecast systems. Therefore, the decision was made to rely exclusively on NOGAPS as the source for NWP data.

Since NWP models generally do not predict clouds directly, it is necessary to relate the model output data to the cloud fields. The standard procedure for doing this is termed Model Output Statistics (MOS). The first step in the MOS approach is to define a set of *predictors* based on NWP forecast data. Predictors are not limited to NWP data and may include, for example, the current observed cloud fields. The predictors are then related to the forecast clouds (*predictands*) by means of a regression analysis on historical data. Our approach is similar ex-

cept that we use a neural network to relate predictors to predictands. The advantage of the neural network approach is that possible nonlinear and cross-product relationships between predictors are automatically ferreted out by the neural network to produce a better estimate of the predictand. The predictors are drawn from a pool of potential predictors that include elemental and derived variables based on NOGAPS data.

There is a large disparity in the resolutions of predictors based on NOGAPS data and predictands based on SERCAA data. NOGAPS provides a global analysis and a 12-hour forecast twice daily at 00 and 12 Z on a 2.5 × 2.5 degree latitude/longitude grid. The resolution at 60° N is 139 km, decreasing to 278 km at the equator. In contrast, SERCAA data is available hourly (nominally) and the resolution of 16th-mesh SERCAA data at 60° N is 23.8 km, increasing toward the equator. The current NOGAPS operational model is higher resolution (0.75 × 0.75 degree) but unfortunately no archived data is available for the 1993 and 1994 times corresponding to the SERCAA data sets. Figure 3-9 is an example of a NOGAPS analysis of mean sea level (MSL) pressure. The EASA region is outlined at NOGAPS resolution. (Note, there is an error in NOGAPS depiction of the century. It should show 1993 rather than 1893.)

Table 3-2 shows the variables considered in the search for cloud field predictors. The first 6 variables are elemental NOGAPS model output data. The remaining variables, beginning with divergence, are derived from the elemental variables. The height variable refers to the height of the pressure (hPa) surface. All variables, other than MSL pressure and surface (SFC) temperature, are defined on pressure surfaces listed across the top to the table. Vapor pressure (and thus relative humidity) is available only to 300 hPa. Divergence and vorticity are associated with vertical motion in the atmosphere at mid- to upper-latitudes and therefore likely to be correlated with clouds. Relative humidity is obviously linked with cloudiness. Temperature advection, vorticity advection, wind speed, and wind shear are often associated with developing storm systems. Temperature difference and thickness between pressure surfaces are measures of atmospheric stability.

Each predictor listed in Table 3-2 is used in three different ways. First, we simply take the predictor defined by the 12-hour forecast as it stands. Second, we subtract the zonal average from the 12-hour forecast value. Last, we define a trend based on the predictor at forecast time and its 12-hour forecast value. All calculations are performed on the NOGAPS 2.5 × 2.5 degree grid and interpolated to the SERCAA 16th-mesh grid. Predictors are only compared to total cloud fraction and no attempt is made to discriminate predictors as a function of cloud layer,

Figure 3-9. NOGAPS analysis of mean sea level pressure.

Table 3-2. Evolution module predictors.*

PREDICTOR	HEIGHT																
	MSL	SFC	1000	850	700	500	400	300	200	150	100	50	70	20	30	10	925
PRESSURE	■																
HEIGHT	■	■	■	■	■	■	■	■	■	■	■	■	■	■	■	■	■
TEMPERATURE		■	■	■	■	■	■	■	■	■	■	■	■	■	■	■	■
VAPOR PRES			■	■	■	■	■	■									
ZONAL VEL			■	■	■	■	■	■	■	■	■	■	■	■	■	■	■
MERIDNL VEL			■	■	■	■	■	■	■	■	■	■	■	■	■	■	■
DIVERGENCE			■	■	■	■	■	■	■	■	■	■	■	■	■	■	■
VORTICITY			■	■	■	■	■	■	■	■	■	■	■	■	■	■	■
REL HUMID			■	■	■	■	■	■									
TEMP ADV			■	■	■	■	■	■	■	■	■	■	■	■	■	■	■
VORTICITY ADV			■	■	■	■	■	■	■	■	■	■	■	■	■	■	■
THICKNESS			■	■	■	■	■	■	■	■	■	■	■	■	■	■	■
WIND SPEED			■	■	■	■	■	■	■	■	■	■	■	■	■	■	■
WIND SHEAR			■	■	■	■	■	■	■	■	■	■	■	■	■	■	■
TEMP DIFF			■	■	■	■	■	■	■	■	■	■	■	■	■	■	■

* Blocked area indicate the heights for which predictor data is available.

height, geography, or latitude zone. The 3 forms of 15 predictors at 17 heights result in pool of 618 potential predictors (not all variables are available at all heights).

The next step is to identify the predictors that show the highest degree of association with the predictands. Several measures of association were considered. One approach is to compare the chi-square, entropy, and Spearman rank correlation values calculated from a contingency table of predictor versus predictand. The analyses based on contingency tables all produced similar results. For example, if the chi-square value was high, then so were the other measures of association. We also performed a matrix correlation between predictor and predictand. The best correlated predictors produced by this analysis significantly differed from those ranked high based on the contingency table. Visual comparisons of predictor and predictand in both cases led us to choose correlation as the best measure of association.

The correlation between predictor and predictand was then calculated for all times in each data set. The absolute values of correlation were averaged and ranked. Predictors that were related were eliminated to reduce redundancy. For example, if vapor pressure and relative humidity at a given height were both found to be highly correlated with total cloud fraction, then only the

higher ranked predictor was kept. Similarly, only the higher ranked zonal wind or total wind speed was kept, since the zonal wind vector usually accounts for most of the wind speed magnitude. Also, only the higher ranked fundamental variable or its zonal perturbation was kept, not both. Table 3-3 shows the 25 top-ranked predictors for the March and July EASA data sets. Figures 3-10 and 3-11 illustrate the close correlation between total cloud fraction observed at 00 Z on 29 July 1993 and the relative humidity based on a 12-hour forecast made at 12 Z on 28 July 1993 for EASA.

Table 3-3. 25 top-ranked predictors for EASA data sets.

MARCH			JULY		
400 hPa	VAPP	TREND	400 hPa	VAPP	
700 hPa	VOR		500 hPa	RH	
850 hPa	VOR		300 hPa	VAPP	
500 hPa	SPEED		850 hPa	U_GRD	
300 hPa	SPEED		925 hPa	U_GRD	
700 hPa	SPEED		700 hPa	RH	
200 hPa	SPEED		1000 hPa	U_GRD	
400 hPa	SPEED		700 hPa	U_GRD	
700 hPa	SHEAR		500 hPa	U_GRD	
100 hPa	T_DIF		300 hPa	VAPP	
925 hPa	VOR		850 hPa	SHEAR	
150 hPa	SPEED		400 hPa	VAPP	TREND
100 hPa	SHEAR		200 hPa	DIV	
500 hPa	VAPP	TREND	400 hPa	T_DIF	TREND
50 hPa	T_DIF –		925 hPa	HGT –	
10 hPa	U_GRD –	TREND	850 hPa	HGT –	
700 hPa	RH	TREND	850 hPa	RH	
200 hPa	T_DIF –	TREND	400 hPa	U_GRD	
500 hPa	VOR		1000 hPa	HGT –	
300 hPa	THICK	TREND	0 MSL	PRES –	
300 hPa	TMP	TREND	10 hPa	U_GRD	TREND
1000 hPa	VOR		925 hPa	DIV –	
400 hPa	TMP	TREND	1000 hPa	DIV –	
850 hPa	VOR	TREND	700 hPa	HGT –	
850 hPa	HGT –		50 hPa	U_GRD –	

Once the best predictors were identified, a set of vectors was generated for neural network training. Each training vector contains 37 input and 16 output elements. The input elements consists of predictors (25), current cloud fraction fields (4), elevation (1), time-of-day (2), latitude (1), longitude (2) and terrain slope (2). The output elements are 4 cloud fraction fields at 3, 6, 9, and 12 hours (16). The 25 top-ranked predictors were first calculated on the 2.5 x 2.5 degree NOGAPS grid and then interpolated to the 16th-mesh SERCAA grid. Predictors were

Figure 3-10. SERCAA total cloud fraction observed at 00 Z on 29 July 1993.

Figure 3-11. NOGAPS relative humidity 12-hour forecast for Figure 3-9.

selected from 500 random locations within the region for each time in the data set. The times used for training are determined by the NWP forecast cycle. Only times where NWP data is available at the forecast time (Figure 3-12a) are used. The model has not been tested for times where NWP data is not synchronized with the forecast (Figure 3-12b). The last 12-hour period in the data set encompassing a NWP forecast cycle is reserved for validation. There are typically 15 times in each data set, excluding the last 12-hour period, where NWP data is synchronized with the forecast time. As a result, the training set for each data set consists of about 7500 (500×15) training vectors.

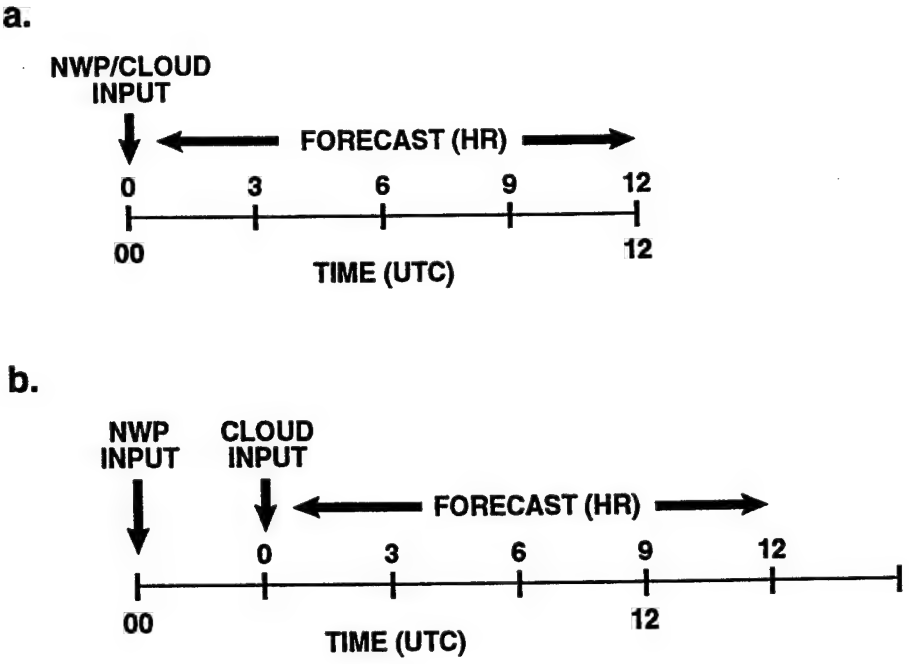

Figure 3-12. Evolution data feed: (a) forecast cycle tested in the current model configuration, (b) example of another forecast cycle the model must eventually handle.

Figures 3-13 and 3-14 show 3, 6, 9, and 12-hour forecasts produced by the evolution algorithm alone for EASA. The forecasts are produced for the last 12-hour period in each data set. The neural network weight/bias sets were not trained on this data, so these forecasts are an indication of how well the neural network performs on new data. Forecast times are 00 Z on 30 March 1993 (Julian day 89) and 31 July 1993 (Julian day 212) for EASA. Images are displayed in the 16th-mesh coordinate system so each panel is oriented with the equator near the top and 60° N near the lower right corner. SERCAA data was not provided for southern latitudes and this

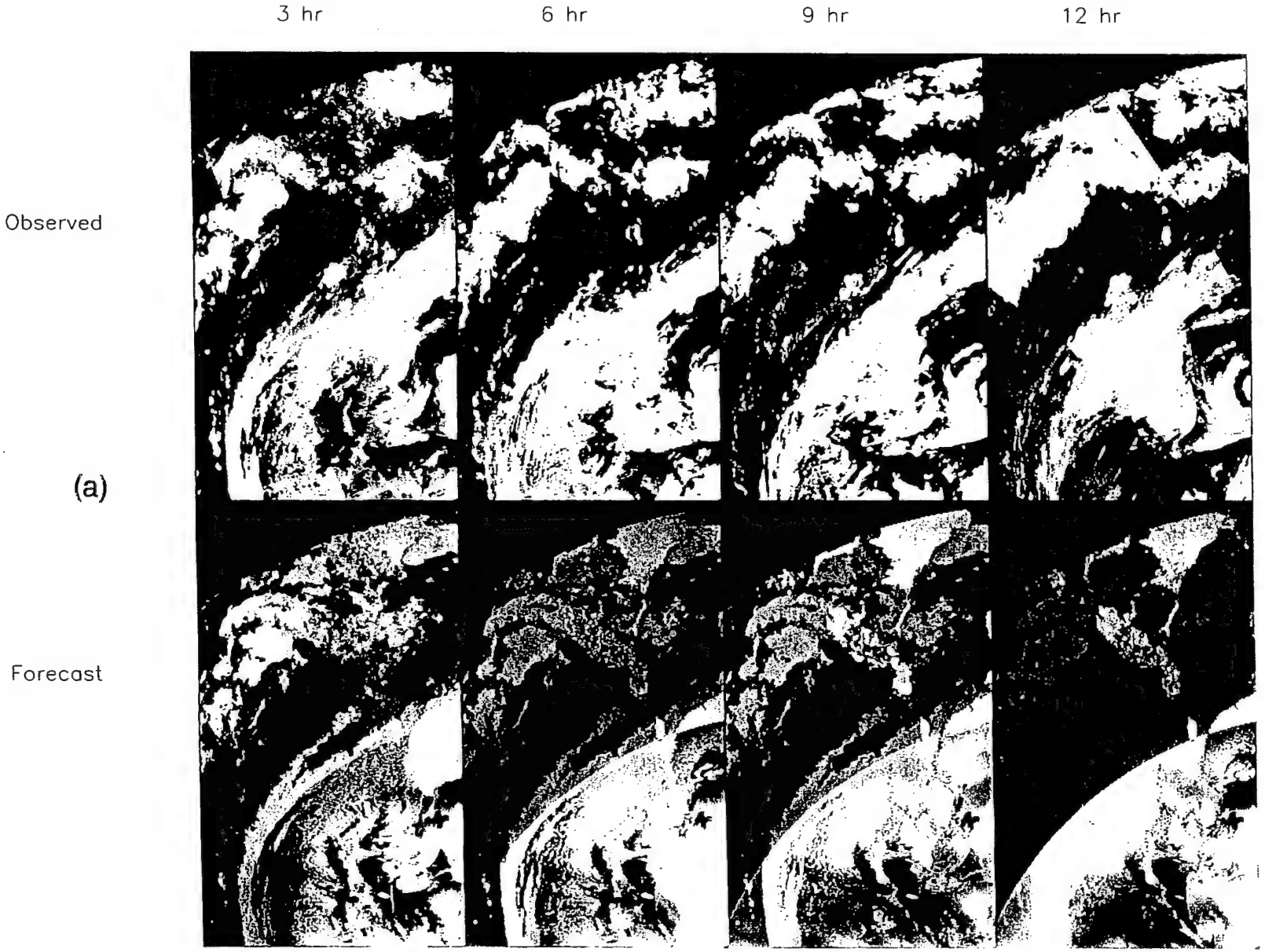

Figure 3-13. Evolution module forecast for EASA for day 89: (a) total cloud fraction, and (b) layer 1 cloud fraction.

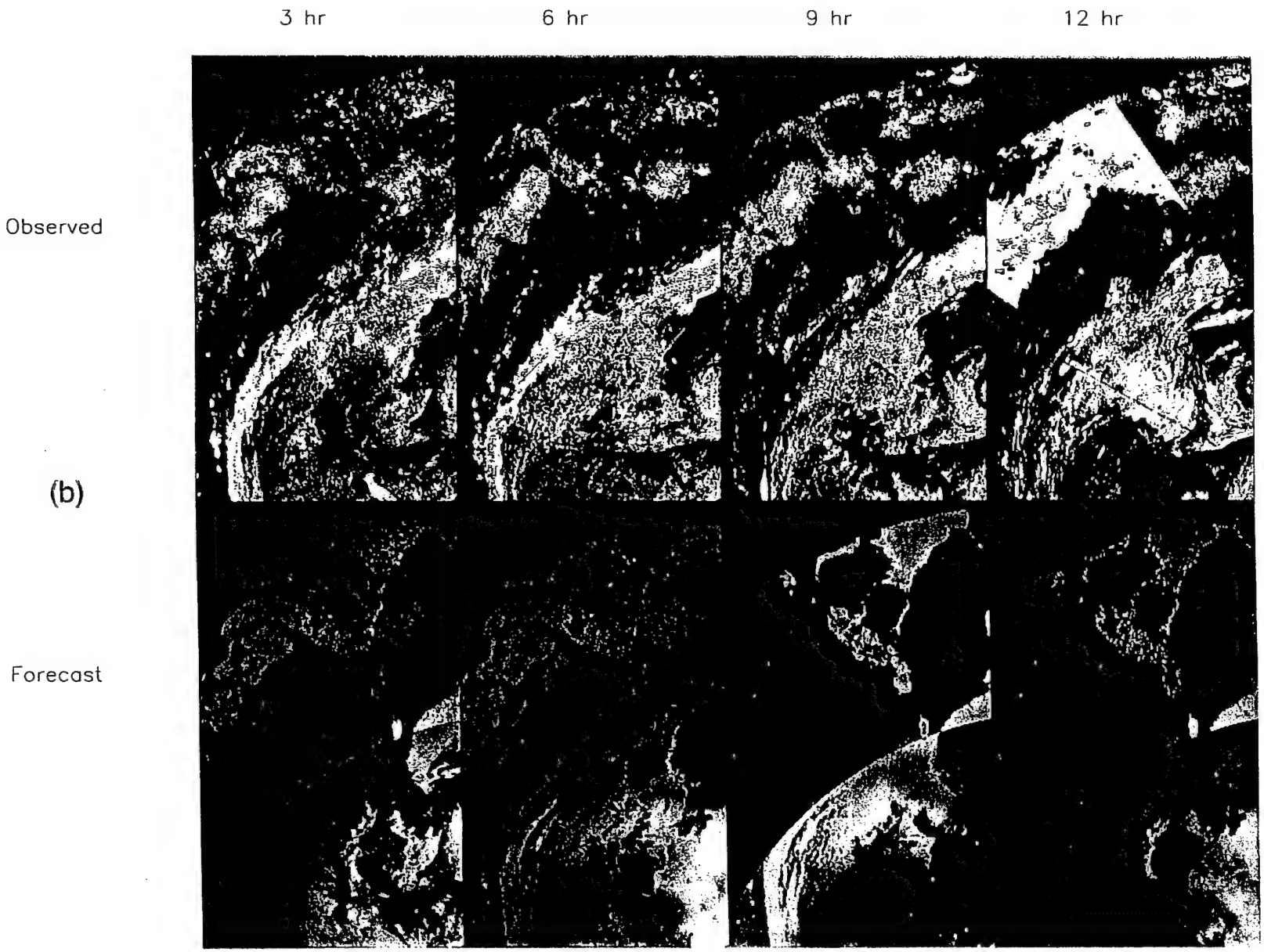

Figure 3-13. Evolution module forecast for EASA for day 89: (a) total cloud fraction, and (b) layer 1 cloud fraction (Continued).

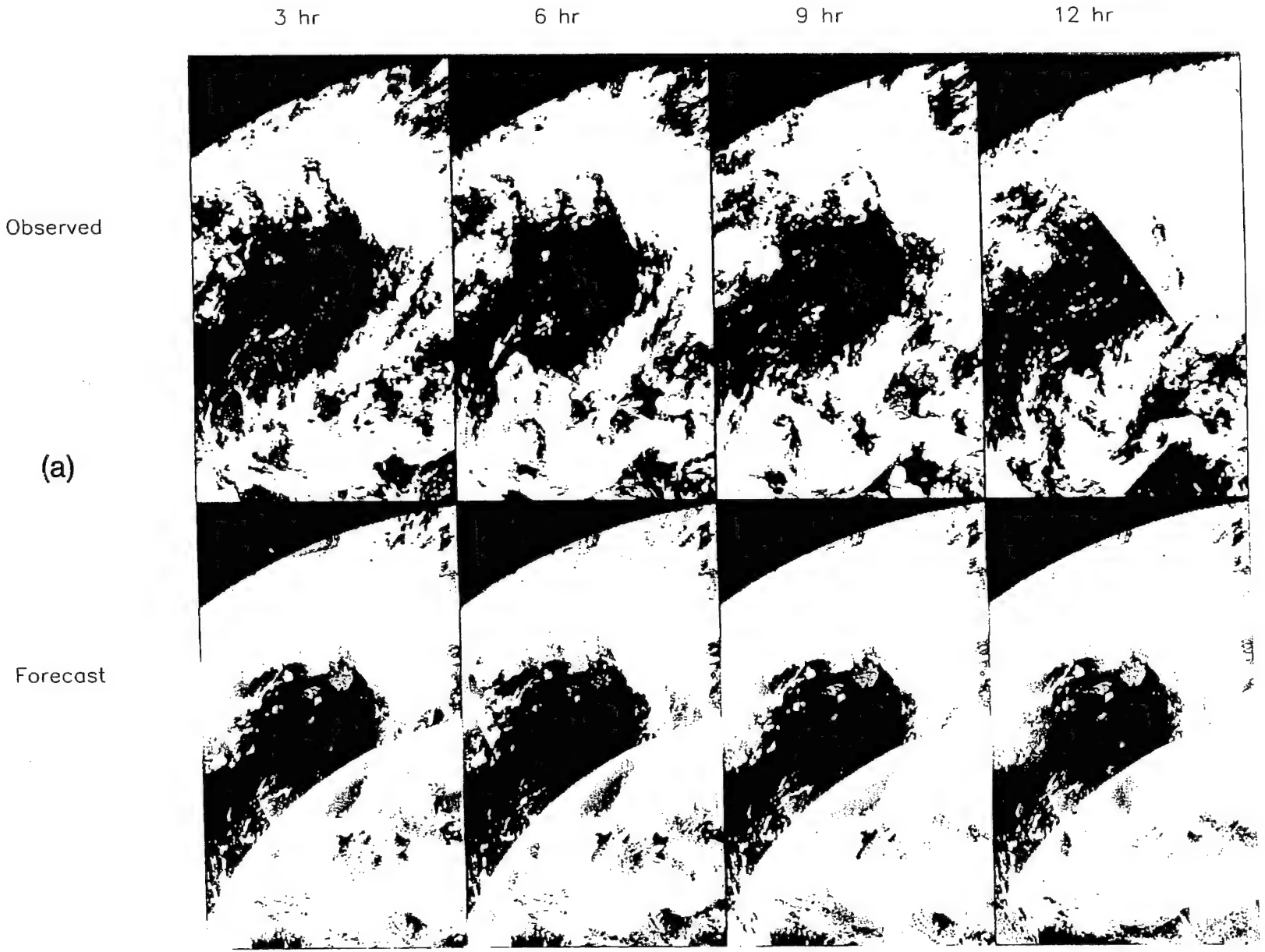

Figure 3-14. Evolution module forecast for EASA for day 212: (a) total cloud fraction, and (b) layer 1 cloud fraction.

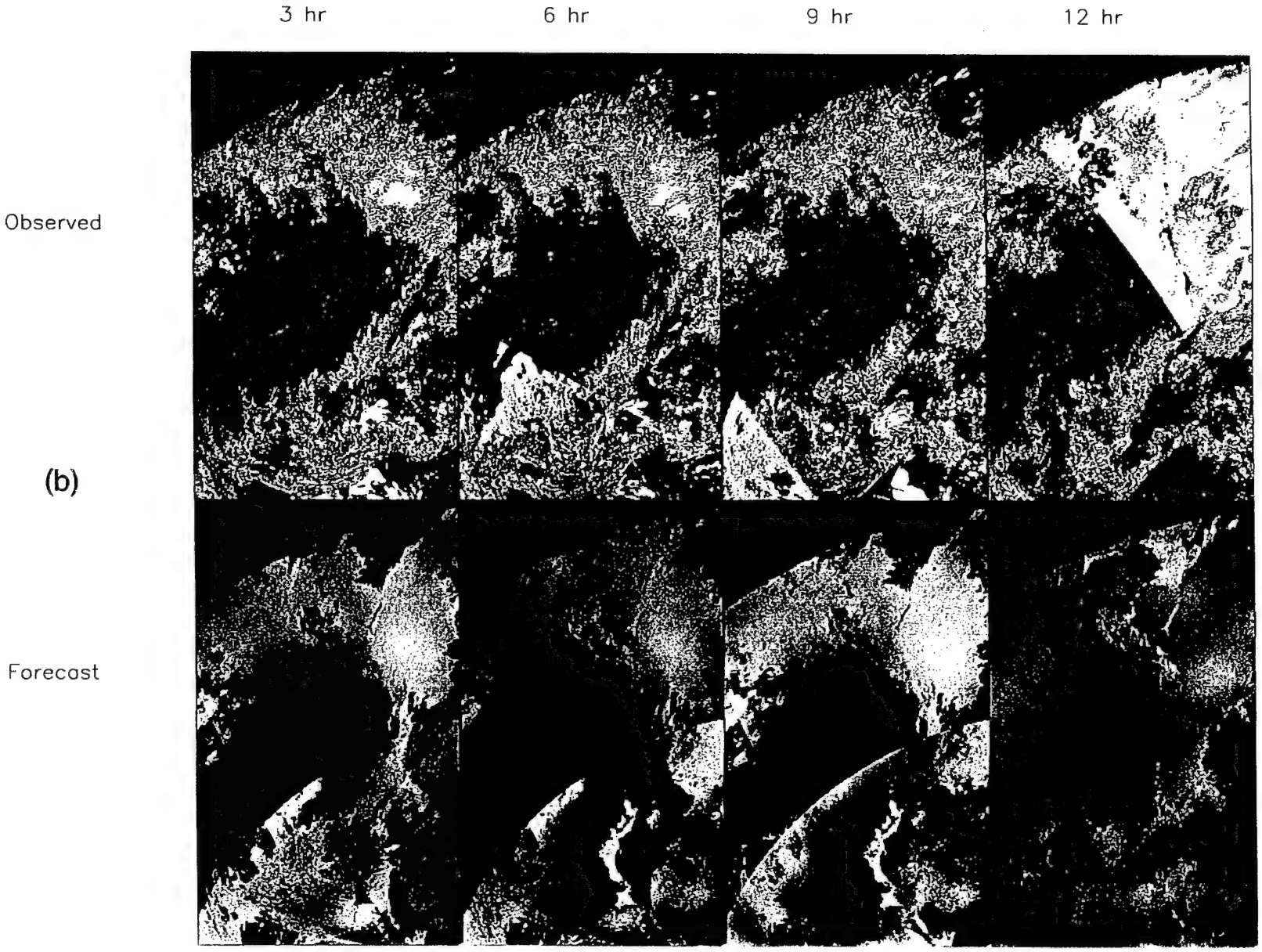

Figure 3-14. Evolution module forecast for EASA for day 212: (a) total cloud fraction, and (b) layer 1 cloud fraction (Continued).

accounts for the arc near the top of each panel defined by the absence of clouds. Wedges of discontinuous cloud fraction in the observed clouds are an artifact of the SERCAA merge process. The wedges are the result of improper geometric corrects or calibration of multiple satellites before merge. Discontinuities in the forecast images are visible where there is a transition between weight/bias set predictions for a specific latitude zone and geography. An example is the transition between latitude zones at 25° N across the center of most forecasts images.

These results are preliminary and are only indicative of the performance of the evolution algorithm. Evolution inputs will be further refined when the three algorithms are combined. There are some encouraging features from the evolution only algorithm. Figure 3-13 indicates reasonable cloud development over land in the tropics. The light area visible near the top and center-right of the forecast panels in Figure 3-13 shows cloud development coincident with Borneo. The outline of Borneo is apparent in the observed clouds (top panels), but not as sharply defined. Similarly, cloud development is predicted over the Philippines but not the surrounding ocean. At mid-latitudes (lower half of Figures 3-13 and 3-14), the general pattern of the observed cloud field is predicted but features are not as well defined as in the tropics.

3.4 COMBINED NEURAL NETWORK.

Combining the individual algorithms consisted of two interactive parts. First, the general form of the NN was established. Second, the final selection of the input vectors was made based upon NN prediction performance. Both are discussed in the following sections.

The fully-connected, feed-forward-back-propagation NN shown in Figure 3-15 was adopted for use on this project. The NN has 28 (the final number of inputs) input nodes, two hidden-layers (12 and 10 nodes each) and three output nodes for a total of 430 degrees of freedom. Several other variations on the number of hidden layers and the number of nodes in the hidden-layers were attempted. This was by no means an exhaustive study but several trends pointed toward the current selection. Greatly increasing the number of nodes in the hidden-layers significantly improved the training error but not the prediction error. A single hidden-layer performed more poorly. Reducing the hidden-layer nodes degraded the prediction capability.

3.4.1 Neural Network Training.

Training takes place on a batch of input vectors selected at random from the population of training vectors. The objective of training is to reduce the sum squared difference between the

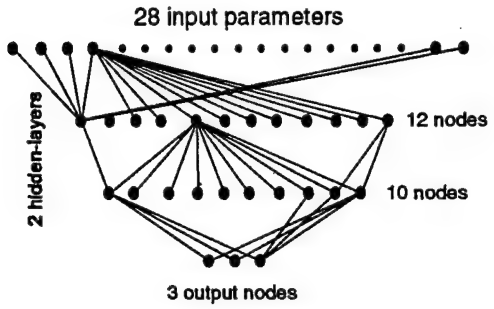

Figure 3-15. Neural network configuration.

neural network output and target cloud fields. The weight/bias set giving the least error is sought using a line minimization approach. Line minimization attempts to quickly hunt down the minimum of a two-dimensional curve by successively fitting parabolas to a region that brackets the minimum. This is usually more efficient than iterative methods where the minimum is found by taking a series of steps in the direction of greatest decreasing error (gradient descent), particularly if the minimum lies within a broad, shallow region of the curve. The error surface is actually multidimensional, the dimension depending on the number of weights and biases in the network. The search for a global minimum on the multidimensional error surface is reduced to a series two-dimensional searches by iteratively finding the minimum in first one direction, then another. Gradient descent moves in the direction of maximal error reduction. We employ a more efficient search that proceeds in the so-called conjugate gradient direction, which is a compromise between the previous search direction and that of gradient descent. The path defined by conjugate gradient directions tends to approach the minimum smoothly, eliminating inefficient zigzags inherent in the gradient descent approach.

The NN was extensively trained on the best and longest data set, the first six days of EMDA data (days 73 through 78). The following procedure was followed:

1. An input file was created for all descriptors of each available (some were missing) hourly image.
2. One-third of all pixels were randomly selected from the first three days of data.
3. The NN was trained for 100 iterations on this training set.
4. The process was repeated for the second three days of data but the training was started with the previously obtained nodal weights.

The above procedure guaranteed that training included a distribution of available latitudes, longitudes, times of day and land types. (Dividing the data into two three-day pieces was based upon a computer limitation.) The NN was trained on a total of approximately 500,000 independent input vectors.

Training was stopped after 100 iterations in all cases. It was found that 95% of the training was accomplished in the first 25 to 35 iterations. Little improvement in training was realized after that point. In general, the training error varied from 15 to 20% when raw data was used as input; a 5% improvement was realized when median filtered data was used for training (see Section 4.2).

The greatest shortcoming of the training was a lack of variety in the cloud cover. A quick perusal of the cloud images in Appendix A results in the conclusion that the data set is best characterized by scant cloud cover. For the most part, clouds are confined to coastal areas around Italy, Greece and Turkey with variable clouds in North Africa. No instances of heavy clouds are recorded. More robust training is required in the future if better prediction performance is to be achieved.

The same procedure was followed for training the NN on the CNSA data. As indicated in Table A-1, Appendix A, far fewer image hours of data were available. To overcome the lack of data, the training commenced using the weights obtained from the EASA training.

3.4.2 Training Vector Definition.

The final input vector definition was selected based upon an input parameter sensitivity study. The most straightforward method of determining which input parameters are important is to selectively omit parameters from the training process (Butler and Meredith, 1996). The removal of a parameter can affect NN performance in three ways: 1) if the parameter is important the NN performance is degraded, 2) if the parameter is unimportant, the NN performance is unchanged, and 3) if the parameter acts like a noise source, the NN performance is improved. Parameters that fall into the last category should be eliminated. Parameters that fall into the second category should be strongly considered for removal because their inclusion increases the training requirements and adds undesired degrees-of-freedom to the network.

A detailed study of all possible parameter combinations was obviously not performed. Instead, the study focused on the persistence input, the evolution parameters and the influence parameters (latitude, longitude, land type, elevation, etc.). Table 3-4 presents the qualitative results of the study. Two important results emerge. First, the *elevation* input degrades the NN performance.

Second, individually removing any of the many evolution parameters does not affect the NN performance, however, removing all of the evolution parameters degrades NN performance.

Based upon these results, the evolution parameters were re-evaluated in terms of the applicable atmospheric physics to select a much reduced input parameter set. The primary atmospheric condition that favors cloud formation is the uplift of warm moist air. This can be characterized by the NOGAPS *relative humidity, velocity divergence,* and *temperature* parameters at various altitudes. A new evolution predictor set of relative humidity, velocity divergence and temperature at five altitudes (Sea level, 100, 300, 500 and 850 hPa) was tested. Five altitudes provided redundant information. Two altitudes (850 and 500 mBars) provided the best compromise. Temperature was found to provide no meaningful NN performance and was eliminated from the predictors. The final predictors are listed in Table 3.5. The basic results reflect the most important predictors found by others. In reviewing the predictors (used and not used) it is important to remember that these were chosen based upon NN performance with a particular, limited set of tropical cloud data. Other scenarios might require some additions or adjustments to these predictors. More extensive NN training might reduce the training error and result in additional predictors becoming important.

Table 3-4. Skill scores for NN forecasts (cloud fraction).

Training Data	Sharp Obs.	Sharp For.	Brier	ESS	G20/20
2 hour forecast					
all*	0.97	0.67	0.12	0.26	0.62
elevation removed	0.97	0.77	0.13	0.33	0.67
lat/lon removed	0.97	0.77	0.14	0.21	0.67
longitude removed	0.97	0.70	0.13	0.32	0.62
land type removed	0.97	0.54	0.15	0.27	0.50
evol removed	0.97	0.71	0.11	0.32	0.65
evol removed except div850	0.97	0.74	0.12	0.32	0.67
elev. evolution <500 removed	0.97	0.74	0.12	0.29	0.66
div @ 850,500 only†	0.97	0.70	0.12	0.22	0.64
rh @ 850,500 only†	0.97	0.71	0.12	0.36	0.65
tmp @ 850,500 only†	0.97	0.74	0.11	0.39	0.67
temp & div @ 850,500 only†	0.97	0.75	0.12	0.33	0.67
rh & div @ 850,500 only†	0.97	0.73	0.12	0.39	0.66
tmp & rh @ 850,500 only†	0.97	0.76	0.12	0.32	0.68
evol @ 850,500 only†	0.97	0.68	0.12	0.29	0.63
3 hour forecast					
all*	0.97	0.67	0.13	0.28	0.60
elevation removed	0.97	0.75	0.13	0.31	0.66
lat/lon removed	0.97	0.78	0.14	0.19	0.67
longitude removed	0.97	0.68	0.13	0.32	0.61
land type removed	0.97	0.51	0.16	0.25	0.47
evol removed	0.97	0.69	0.12	0.32	0.63
evol removed except div850	0.97	0.71	0.12	0.30	0.64
elev. evolution <500 removed	0.97	0.71	0.12	0.31	0.64
div @ 850,500 only†	0.97	0.68	0.12	0.22	0.63
rh @ 850,500 only†	0.97	0.69	0.13	0.33	0.63
tmp @ 850,500 only†	0.97	0.73	0.12	0.31	0.66
temp & div @ 850,500 only†	0.97	0.74	0.12	0.33	0.66
rh & div @ 850,500 only†	0.97	0.71	0.13	0.33	0.64
tmp & rh @ 850,500 only†	0.97	0.75	0.12	0.34	0.67
evol @ 850,500 only†	0.97	0.66	0.12	0.30	0.61
6 hour forecast					
all*	0.97	0.64	0.13	0.30	0.58
elevation removed	0.97	0.75	0.14	0.31	0.66
lat/lon removed	0.97	0.74	0.14	0.17	0.64
longitude removed	0.97	0.68	0.14	0.29	0.60
land type removed	0.97	0.48	0.18	0.21	0.44
evol removed	0.97	0.61	0.13	0.32	0.57
evol removed except div850	0.97	0.68	0.13	0.28	0.63
elev. evolution <500 removed	0.97	0.67	0.12	0.30	0.61
div @ 850,500 only†	0.97	0.65	0.13	0.27	0.59
rh @ 850,500 only†	0.97	0.67	0.14	0.30	0.60
tmp @ 850,500 only†	0.97	0.73	0.13	0.30	0.66

Table 3-4. Skill scores for NN forecasts (cloud fraction) (Continued).

6 hour forecast (continued)					
temp & div @ 850,500 only†	0.97	0.73	0.13	0.26	0.65
rh & div @ 850,500 only†	0.97	0.70	0.14	0.30	0.63
tmp & rh @ 850,500 only†	0.97	0.74	0.13	0.26	0.66
9 hour forecast					
all*	0.97	0.59	0.13	0.37	0.55
elevation removed	0.97	0.74	0.13	0.31	0.66
lat/lon removed	0.97	0.77	0.14	0.26	0.66
longitude removed	0.97	0.72	0.14	0.29	0.62
land type removed	0.97	0.49	0.17	0.18	0.45
evol removed	0.97	0.59	0.14	0.27	0.54
evol removed except div850	0.97	0.73	0.13	0.32	0.66
elev. evolution <500 removed	0.97	0.65	0.12	0.38	0.59
div @ 850,500 only†	0.97	0.72	0.12	0.24	0.65
rh @ 850,500 only†	0.97	0.69	0.14	0.27	0.61
tmp @ 850,500 only†	0.97	0.78	0.13	0.33	0.68
temp & div @ 850,500 only†	0.97	0.71	0.13	0.22	0.63
rh & div @ 850,500 only†	0.97	0.71	0.13	0.32	0.64
tmp & rh @ 850,500 only†	0.97	0.73	0.13	0.33	0.65
evol @ 850,500 only†	0.97	0.70	0.12	0.32	0.64
12 hour forecast					
all*	0.97	0.62	0.13	0.28	0.56
elevation removed	0.97	0.72	0.13	0.33	0.65
lat/lon removed	0.97	0.81	0.15	0.17	0.67
longitude removed	0.97	0.75	0.14	0.27	0.64
land type removed	0.97	0.57	0.17	0.18	0.51
evol removed	0.97	0.62	0.13	0.25	0.56
evol removed except div850	0.97	0.81	0.13	0.23	0.71
elev. evolution <500 removed	0.97	0.67	0.12	0.22	0.60
div @ 850,500 only†	0.97	0.74	0.13	0.18	0.65
rh @ 850,500 only†	0.97	0.68	0.13	0.24	0.61
tmp @ 850,500 only†	0.97	0.81	0.13	0.28	0.71
temp & div @ 850,500 only†	0.97	0.72	0.13	0.32	0.64
rh & div @ 850,500 only†	0.97	0.73	0.13	0.30	0.65
tmp & rh @ 850,500 only†	0.97	0.76	0.13	0.30	0.67
evol @ 850,500 only†	0.97	0.76	0.13	0.26	0.68

*This set has a duplicate t0 parameter included.
†These sets have elevation removed

Table 3.5. Final Predictors

NN Predictors
UT of forecast time
Δt before forecast
Latitude
Longitude
Advected cloud fraction
Advected cloud top temperature
TCF at t_0
CTT at t_0
TCF at t_0-1 hour
CTT at t_0-1 hour
Δt from forecast
TCF at t_0-3 hour
CTT at t_0-3 hour
Δt from forecast
TCF at t_0-6 hour
CTT at t_0-6 hour
Δt from forecast
TCF at t_0-12 hour
CTT at t_0-12 hour
Δt from forecast
Clouds/no clouds flag
Relative humidity @ 850 hPa
Relative humidity @ 500 hPa
Velocity Divergence @ 850 hPa
Velocity Divergence @ 500 hPa
TCF at t_0-24 hours (Averaged over past 3 days)
CTT at t_0-24 hours (Averaged over past 3 days)
Land type

SECTION 4
MODEL PERFORMANCE

Model performance is not easily quantifiable due to the variability of the realizable cloud scenes. At this point in development and training, model performance is not robust. Nevertheless, the model performance must be quantified. Toward this, the next two sections discuss the performance of the *pixel-by-pixel* model trained on raw images or *median filtered* images.

Six forecast times not originally included in the NN training were selected for evaluation. The times were selected to provide the largest cloud scene variability that this data set allows. The model forecasts were then characterized by standard skill score figures-of-merit: equitable skill score (ESS), 20/20 score, Brier's score, and scene correlation. For a discussion of each see Appendix B.

Before reviewing the results, however, it will be beneficial to reconsider the discussion in Section 2 dealing with the conceptual model of the clouds. It was stated that only some fraction of the clouds were predictable while the remainder were considered to be random. To get an idea of how this affects the skill scores, Figure 4-1 shows two cloud scenes separated by one hour that were analyzed. The skill scores obtained are shown in Table 4-1. The 20/20 score indicates that 93% of the pixels are within ±20% of each other and the Brier score indicates a small rms error; this is what the eye sees. Even though the cloud scenes appear to be remarkably similar the ESS is quite low because the score reflects the detail not easily seen by eye. The correlation score is higher than the ESS because it does not penalize for incorrect forecasts.

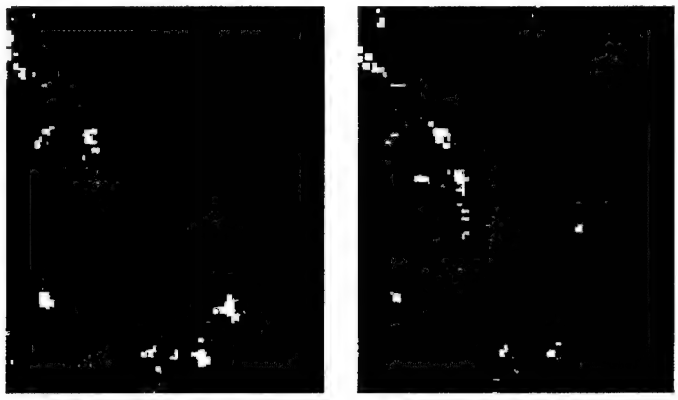

(a) 7909 (b) 7910

Figure 4-1. Consecutive hours of total cloud cover in EMDA.

Table 4-1. Skill scores comparing consecutive hours of total cloud cover from EMDA shown in Figure 4-1.

Skill Score	Value
Brier	.04
ESS	.27
20/20	.93
Correlation	.41

The same pattern of scores is expected when comparing forecasts to truth in Sections 4.1 and 4.2. The overall picture will be statistically correct but it will be smeared due to a tendency of the NN to forecast an average value for the random component. The smearing results in a very small or negative ESS, especially when the full resolution of the data is analyzed. A better ESS will be achieved using the median filtered data. Large ESS cannot be expected when forecasting with temporally or spatially aliased images.

4.1 PIXEL-BY-PIXEL NN.

The training vector sets and the training process are described in Section 3.4. Raw (unfiltered, unsmoothed) pixel data from days 71 through 78 were input for training. Figure 4-2 is an example of a prediction for day 79. Table 4-2 shows the resulting skill scores.

The rms error (the square root of the Brier score) range from 17% to 27%, generally increasing with forecast duration. The basic problem with the forecasts is the smearing of the clouds. Not shown in the color scale is the fact that there is a low (<10%) cloud fraction forecast over virtually the entire area. As the length of the forecast increases, the pervasive low cloud fraction grows.

The low cloud fraction does not affect the 20/20 scores for short forecasts but is the primary reason it drops at longer forecasts. The background level comes up. Also, the NN fails to forecast high cloud fractions, a further result of the smearing.

The smearing is a direct result of randomness in the cloud field and the small size of the training set. Clear improvements are evident when the size of the training set is doubled from three to six days. There is no reason to expect that this trend will not continue for several doublings in training set size.

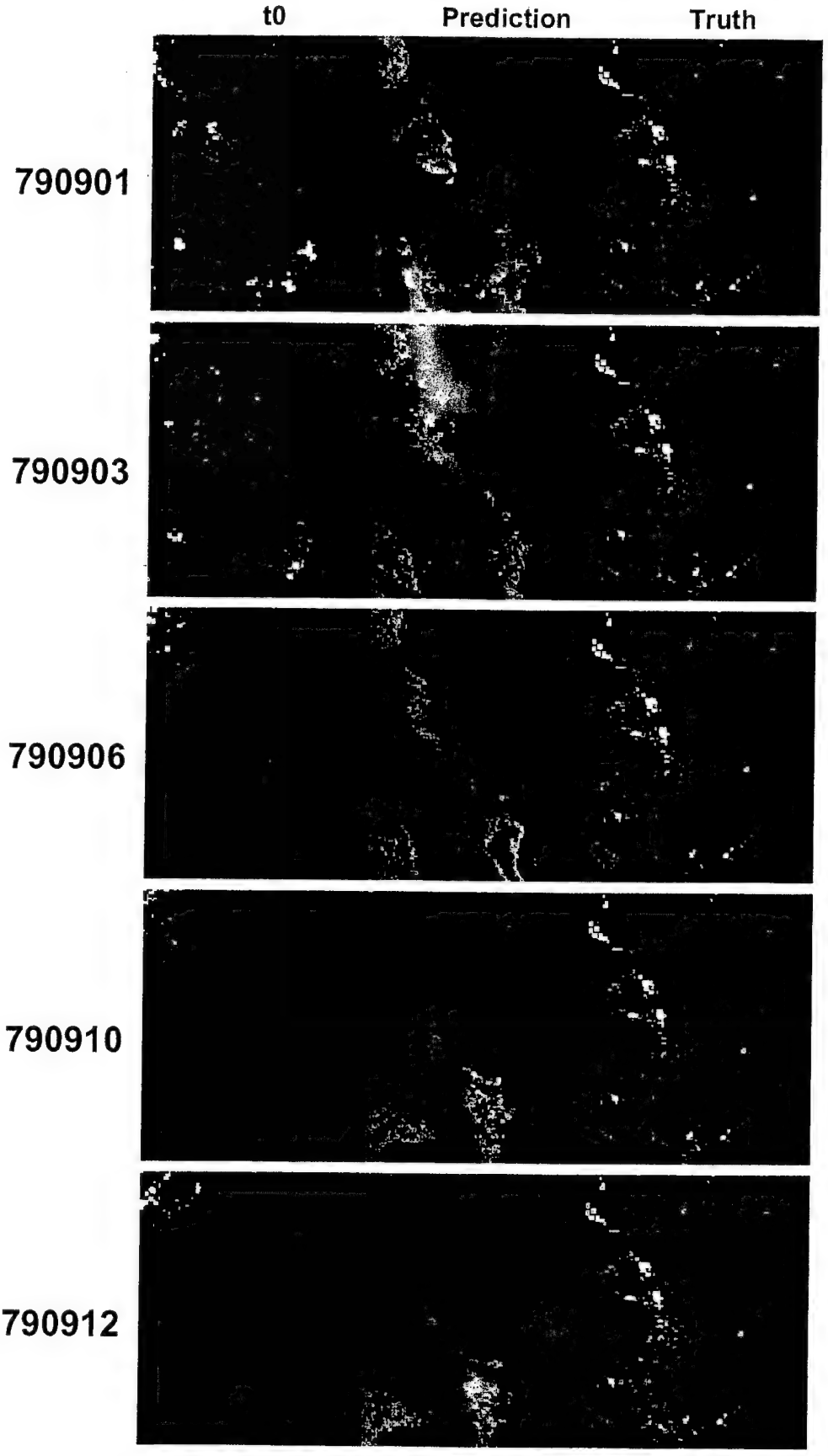

Figure 4-2. Total cloud cover forecasts for unfiltered pixel-by-pixel EMDA data on day 79.

Table 4-2 Skill scores for day 79 forecast.

Skill Score	Forecast Duration (hours)				
	1	3	6	10	12
Brier	.03	.04	.04	.07	.05
ESS	.29	.11	.06	.02	.02
20/20	.91	.85	.83	.71	.77

4.2 MEDIAN FILTERED NN.

As discussed in Section 2, much of the cloud field is random, not predictable. Yet, the NN discussed in Section 4.1 was trained using data including this random cloud content. In the best of all worlds where training data is not at a premium, the random cloud data would cause no problem; the NN would learn to treat the random fluctuations as a source of noise. This cannot be expected from a limited (6 days) training set, however.

The above problem is addressed by filtering the training data. A median filter was selected because it is a nonlinear filter that maintains the sharpness of cloud boundaries better than a simple smoothing filter. Yet, isolated (random) clouds will not pass through the filter. Figure 4-3 illustrates the effect of a median filter on a cloud image. In the figure, the original cloud image is compared to three levels of filtering. The 7×7 filter removes many of the larger cloud masses. The 3×3 or 5×5 filter removes most of the isolated clouds but maintains the larger cloud groups. The 5×5 filter was selected for training purposes.

Forecasting with the median filtered images (Figures 4-4, 4-5, and Table 4-3) as input has the expected effect. The forecasts are sharper yet. There are far fewer large regions of sparse clouds covering cloudless areas in the truth image.

Several attributes of the NN are evident in the forecasts. First, there appears to be more evolution and persistence in the clouds than advection. When advection clearly dominates the cloud history as on day 81 (Figure 4-6), the NN still tries to evolve the cloud field. The advected feature is apparent in the forecast as the region of highest cloud fraction, but is obscured by forecast regional persistence. The median filtering appears to have little impact on the forecast. Day 79 (Figure 4-4) is dominated by scattered clouds. As the forecast time gets longer, the ability of the NN to forecast the details greatly diminishes until at 12 hours, only the largest cloud groups are forecast. These predictable cloud groups are the result of evolution along the coast of southern Europe.

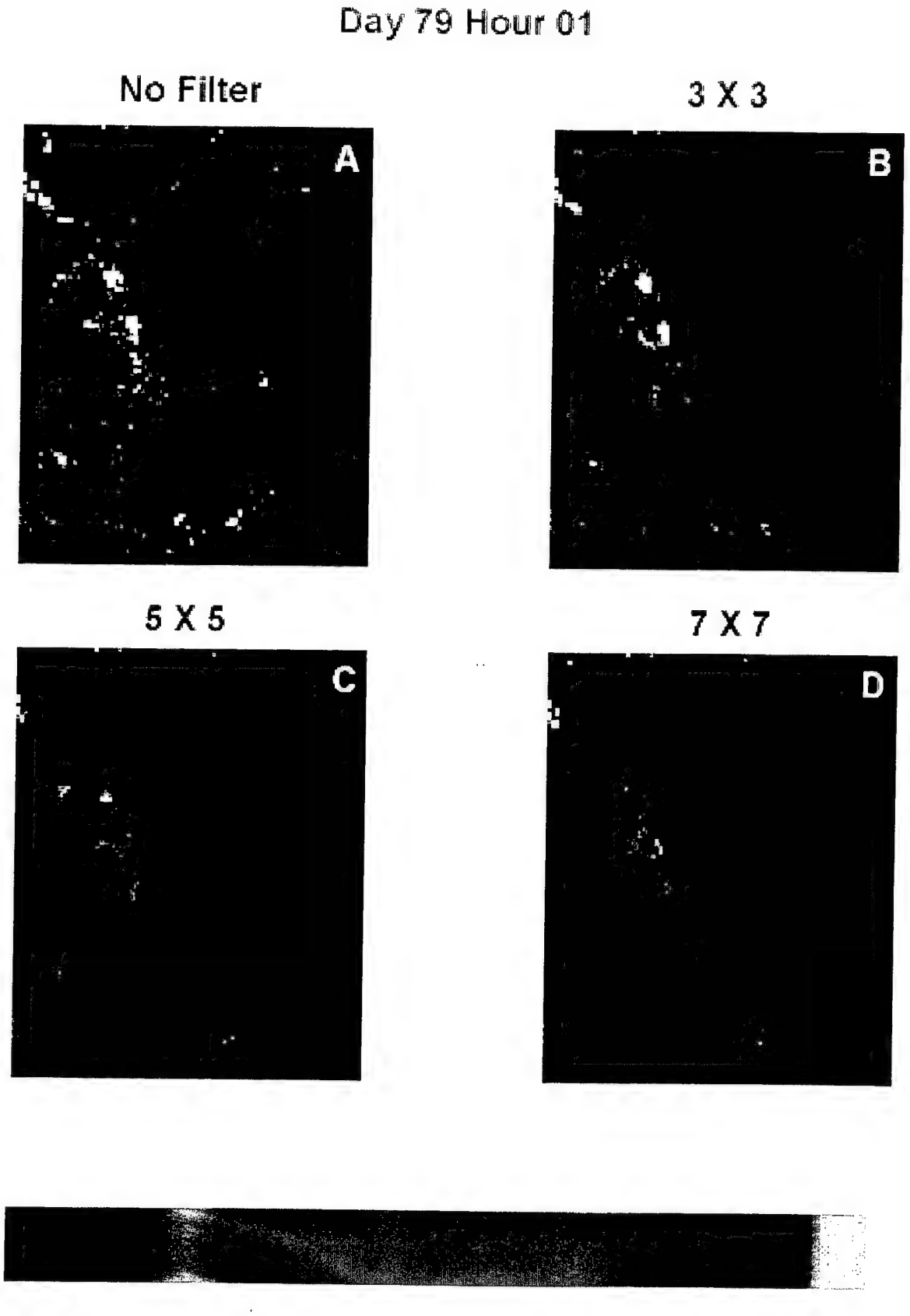

Figure 4-3. Effects of median filtering on the cloud image.

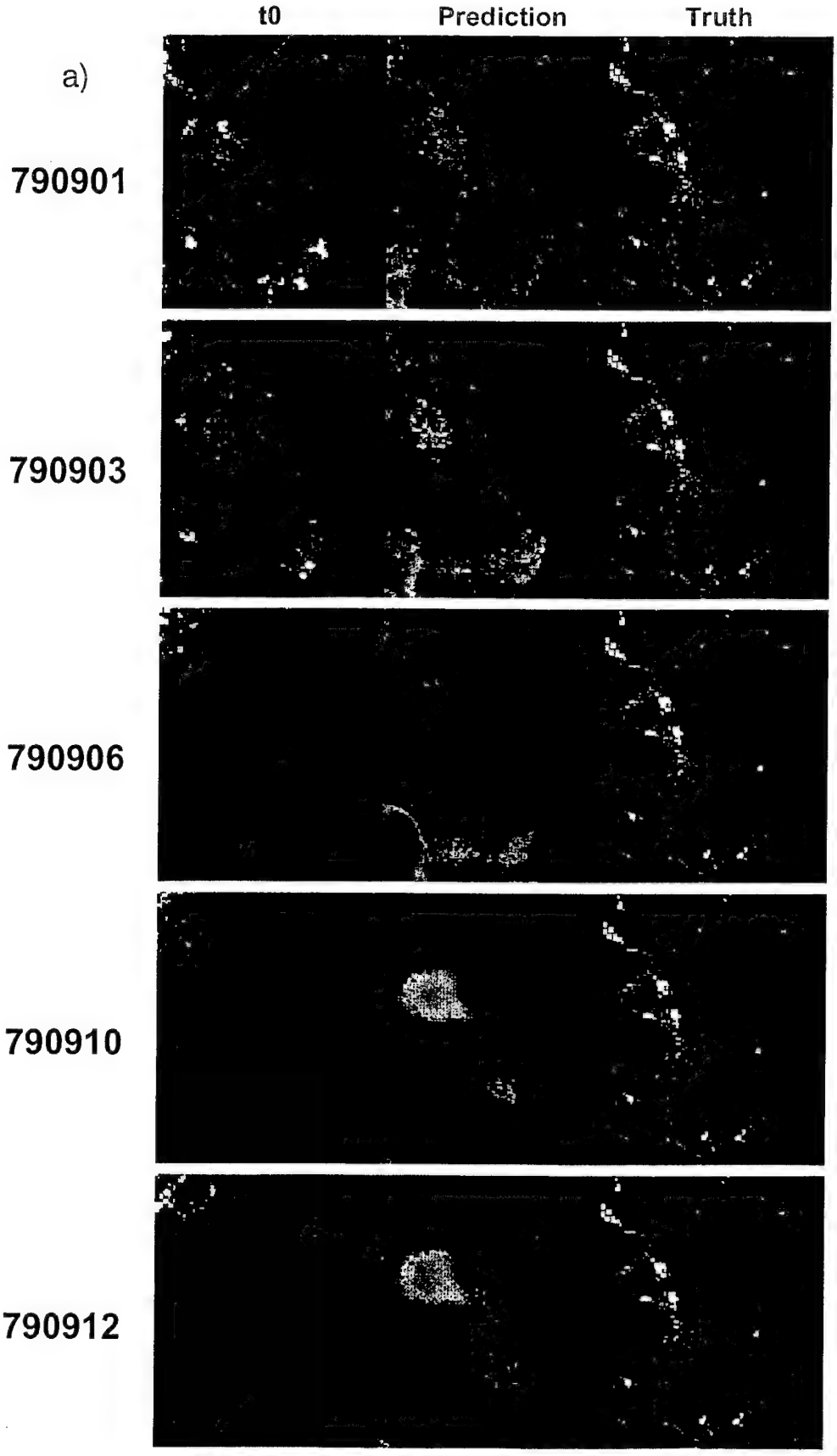

(The number code above denotes the day/time/forecast duration.)

Figure 4-4. Day 79 EMDA forecasts for a neural network trained on median filtered data (a) using unfiltered input, and (b) using median filtered input.

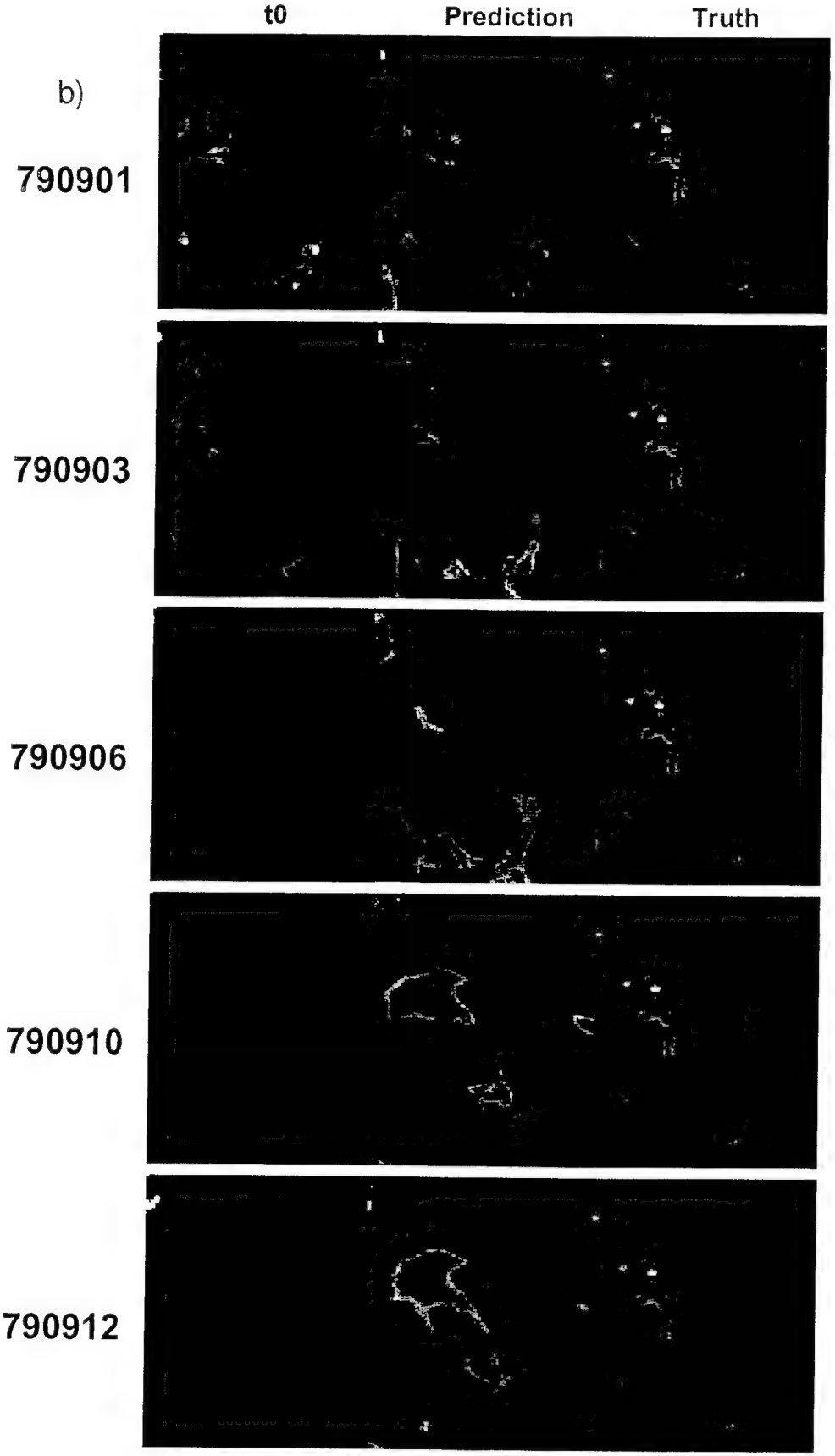

(The number code above denotes the day/time/forecast duration.)

Figure 4-4. Day 79 EMDA forecasts for a neural network trained on median filtered data (a) using unfiltered input, and (b) using median filtered input (Continued).

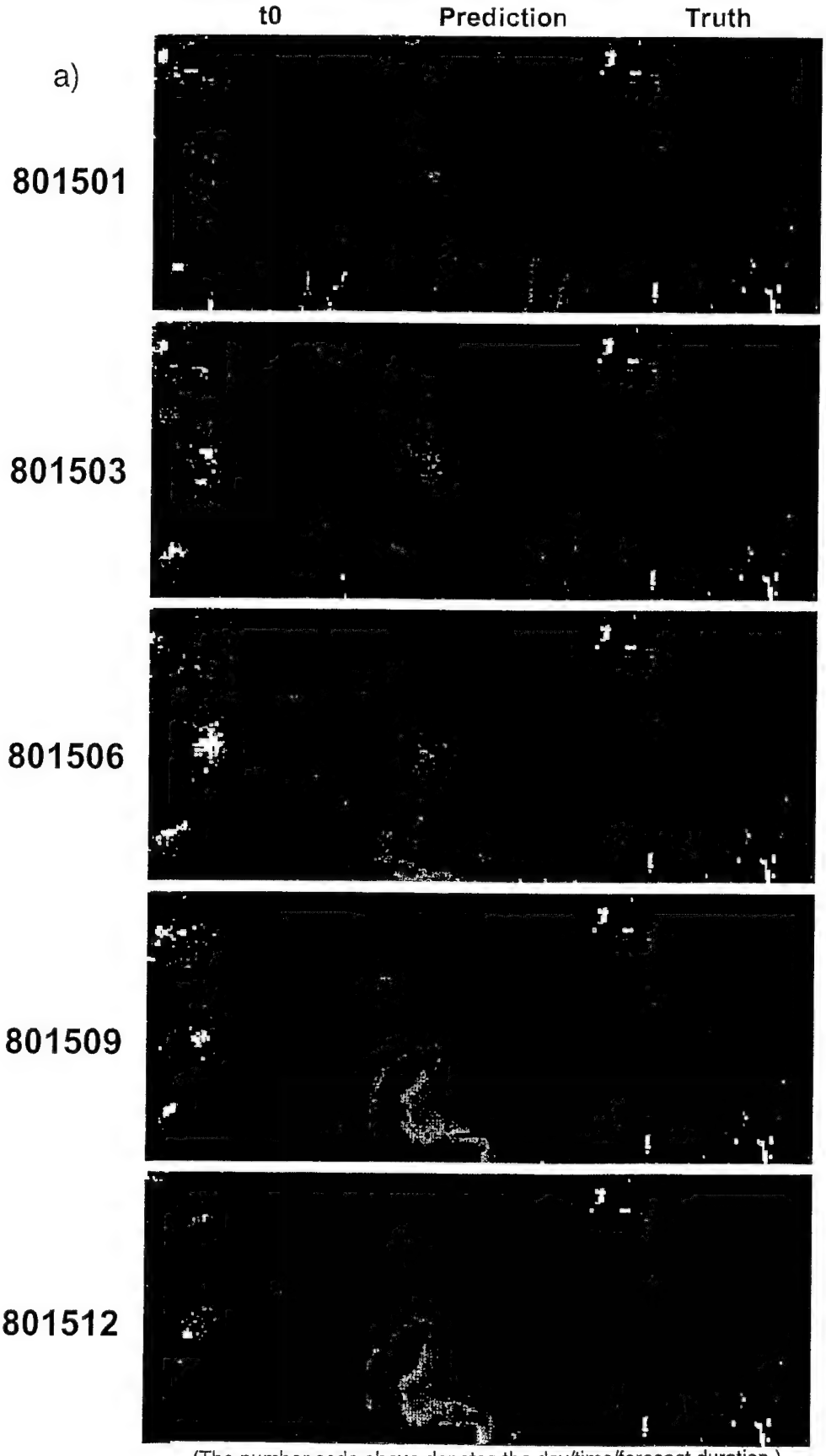

(The number code above denotes the day/time/forecast duration.)

Figure 4-5. Day 80 EMDA forecasts for a neural network trained on median filtered data (a) using unfiltered input, and (b) using median filtered input.

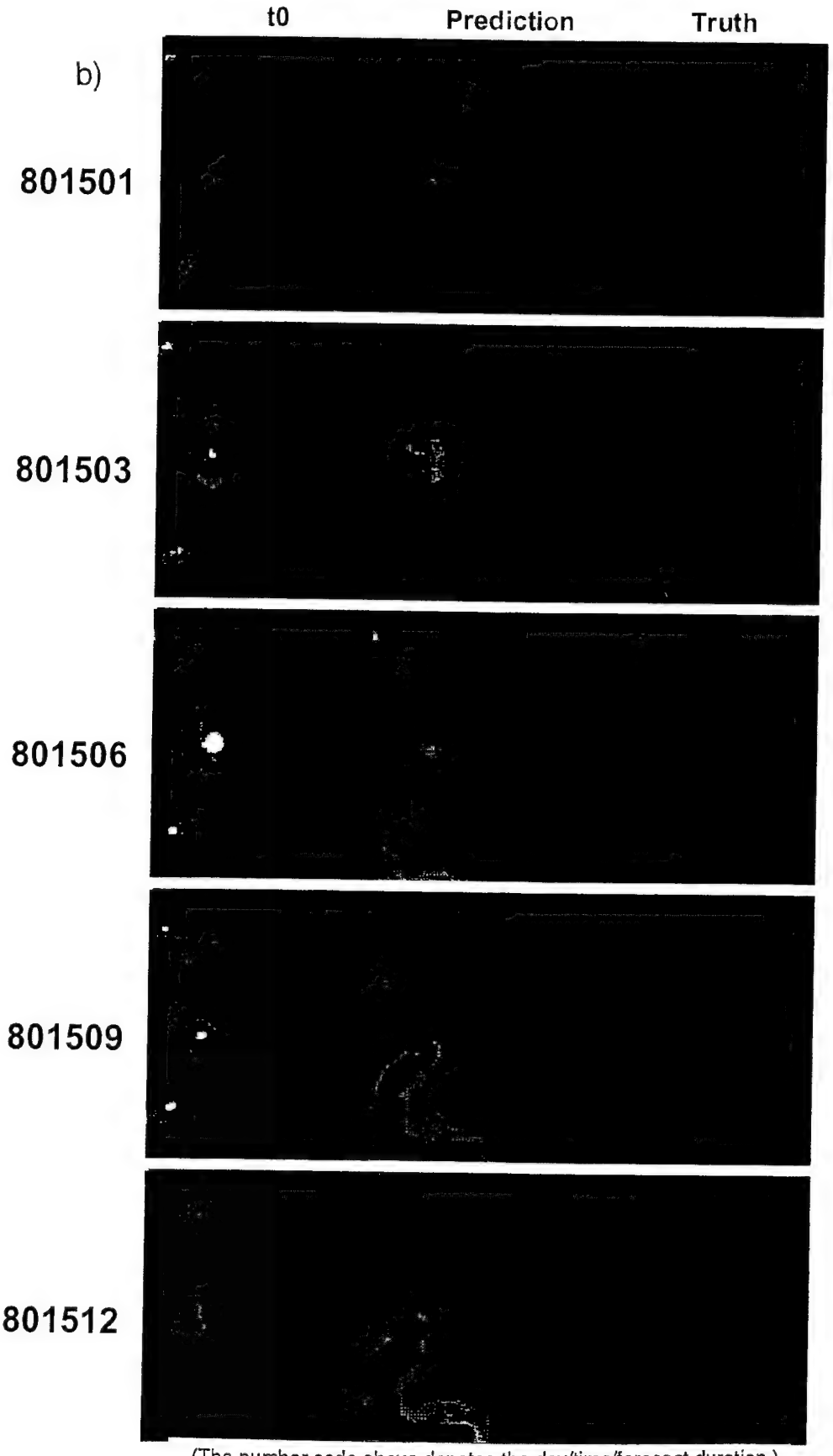

(The number code above denotes the day/time/forecast duration.)

Figure 4-5. Day 80 EMDA forecasts for a neural network trained on median filtered data (a) using unfiltered input, and (b) using median filtered input (Continued).

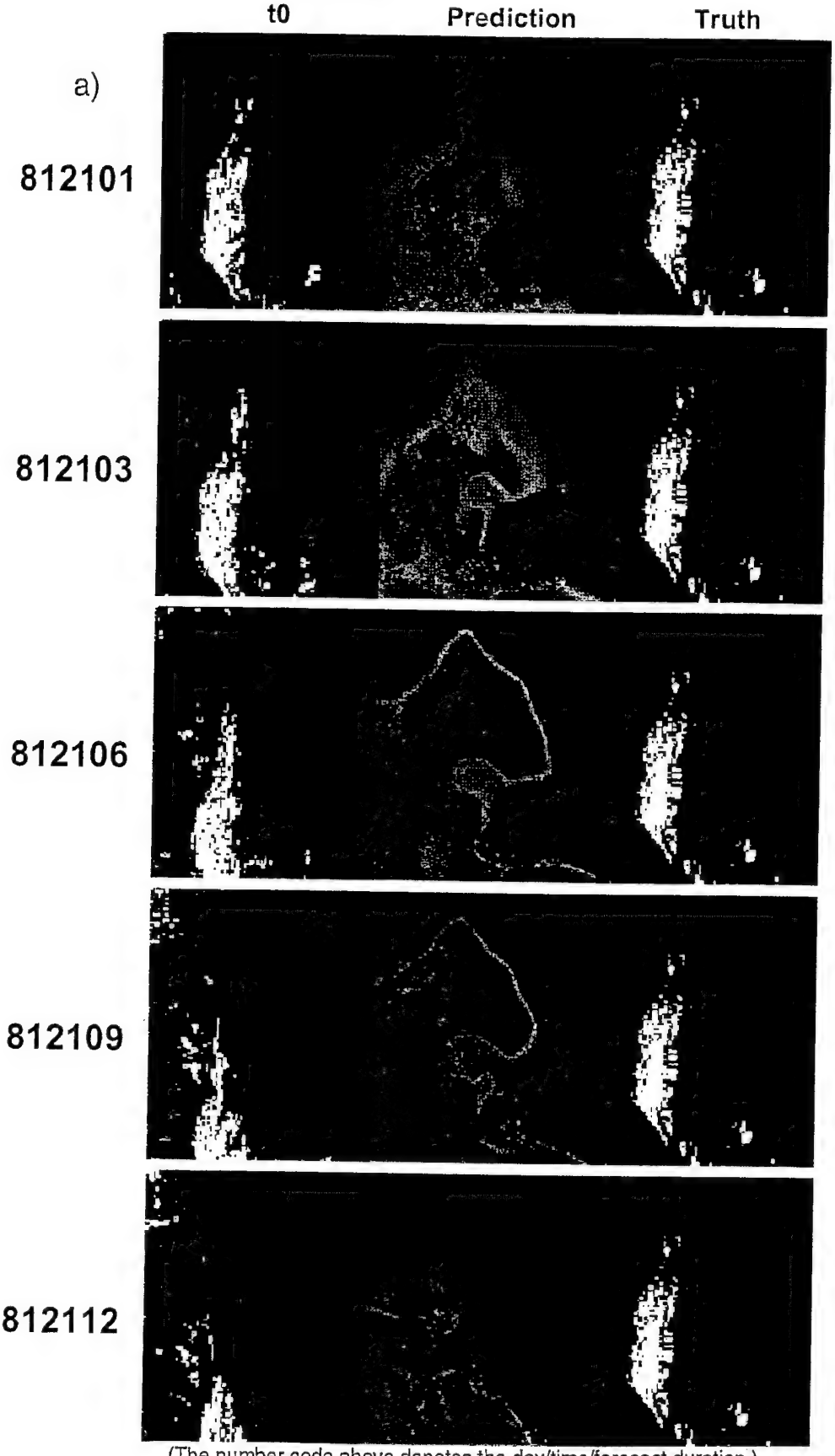

(The number code above denotes the day/time/forecast duration.)

Figure 4-6. Day 81 EMDA forecasts for a neural network trained on median filtered data (a) using unfiltered input, and (b) using median filtered input.

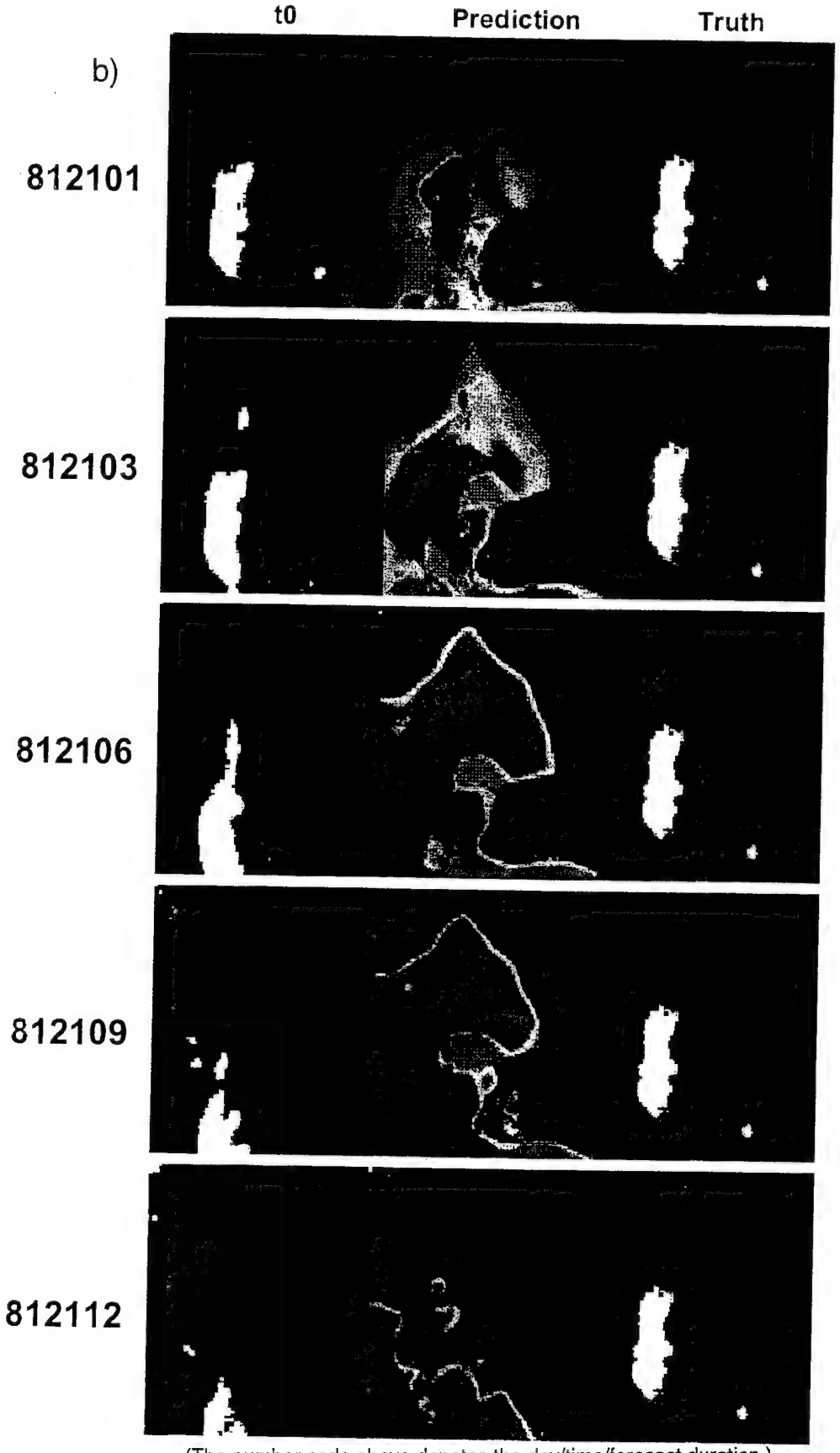

(The number code above denotes the day/time/forecast duration.)

Figure 4-6. Day 81 EMDA forecasts for a neural network trained on median filtered data (a) using unfiltered input, and (b) using median filtered input (Continued).

Table 4-3. Skill scores for median filter training.

	Forecast Duration (Hours)									
	1		3		6		10		12	
Forecast Time	U[1]	MF[2]	U[1]	MF[2]	U[1]	MF[2]	U[1]	MF[2]	U[1]	MF[2]
Day 7909										
Brier	.02	.01	.03	.02	.04	.02	.04	.02	.05	.02
ESS	.30	.18	.03	.02	.50	.02	.04	.05	.03	.05
20/20	.93	.97	.89	.95	.88	.90	.88	.91	.87	.90
Day 8015										
Brier	.02	.00	.03	.01	.02	.01	.05	.04	.05	.05
ESS	.13	.00	.00	-.02	-.02	.00	-.04	-.02	-.04	-.02
20/20	.95	.99	.94	.98	.94	.96	.84	.85	.84	.84
Day 8121										
Brier	.04	.03	.06	.02	.04	.11	.10	.12	.08	.09
ESS	.54	.58	.37	.02	.50	.26	.22	.23	.07	.00
20/20	.88	.92	.69	.95	.88	.52	.54	.55	.75	.76

[1]Unfiltered input; [2]Median filtered input

A limited number of days (and hours during the day) of central American (CNSA) SERCAA cloud images were available for verification. The data set was too small for complete training of a separate NN so the EASA NN was further trained using the available CNSA data. The first four days of CNSA was used for training. No attempt was made to optimize the input predictors as was previously done with EASA; the same predictors were input. The fact that the NN is capable of forecasting in a completely different region than the training region demonstrates the versatility of the approach.

The only reason for any additional training is due to the inclusion of latitude and longitude as predictors. Training on the EASA locations alone resulted in a NN that forecasts *no clouds* outside of the EASA region. In the future this problem should be rectified by eliminating longitude as a predictor and better optimizing the use of land type predictors.

The CNSA images have far more clouds than EASA. Figure A-5 (Appendix A) also shows that the Central American clouds are almost completely dominated by evolution or persistence with little advection evident. Figure 4-7 shows the forecasts for 2300 Z on day 84. Again note that the truth time is constant but the time from which the forecast is made (t_0) changes with the forecast length (1, 2, 6, and 9 hours). The 12 hour forecast is omitted due to data gaps.

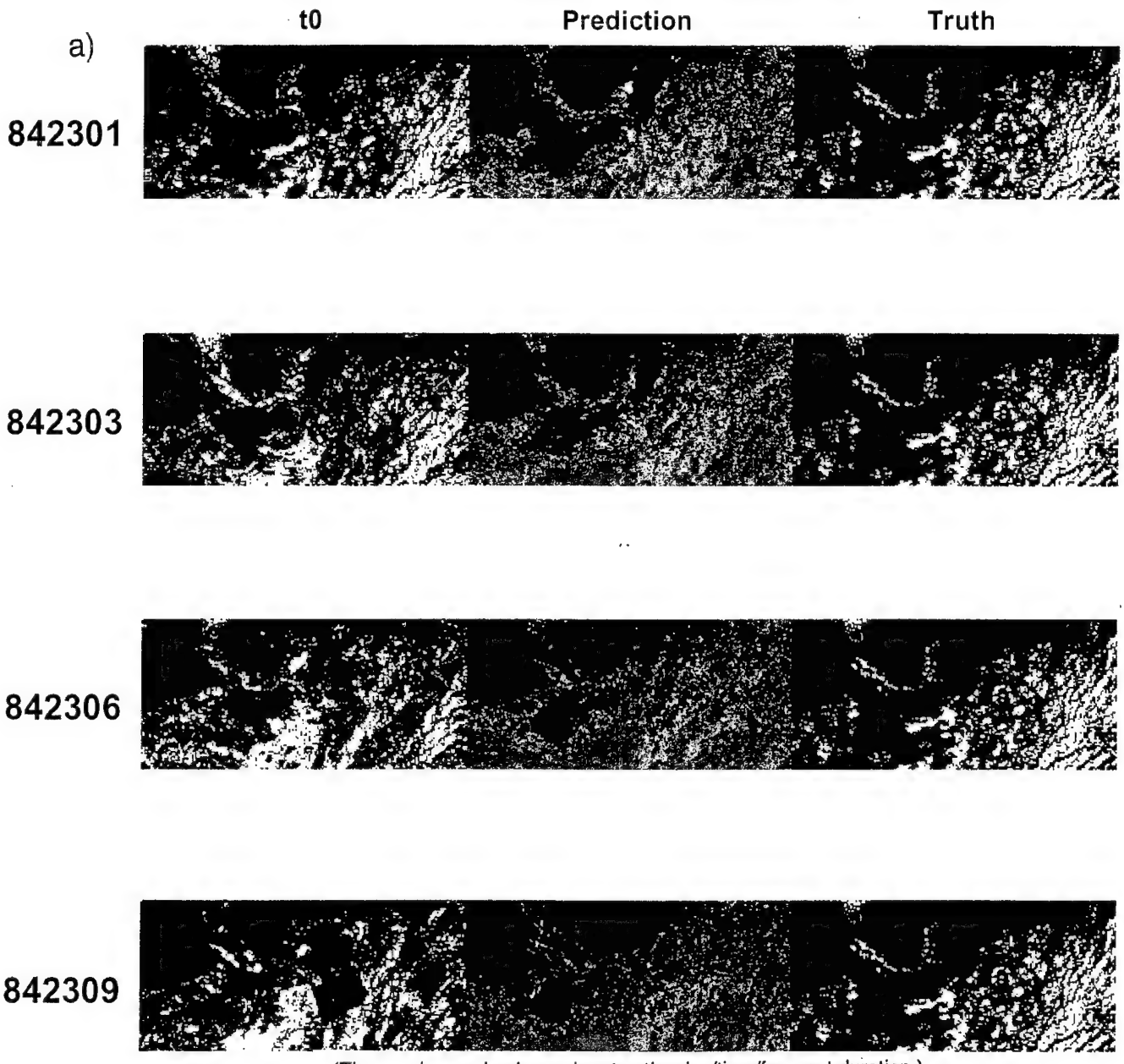

(The number code above denotes the day/time/forecast duration.)

Figure 4-7. Day 84 CNSA forecasts for a neural network trained on median filtered data (a) using unfiltered input, and (b) using median filtered input.

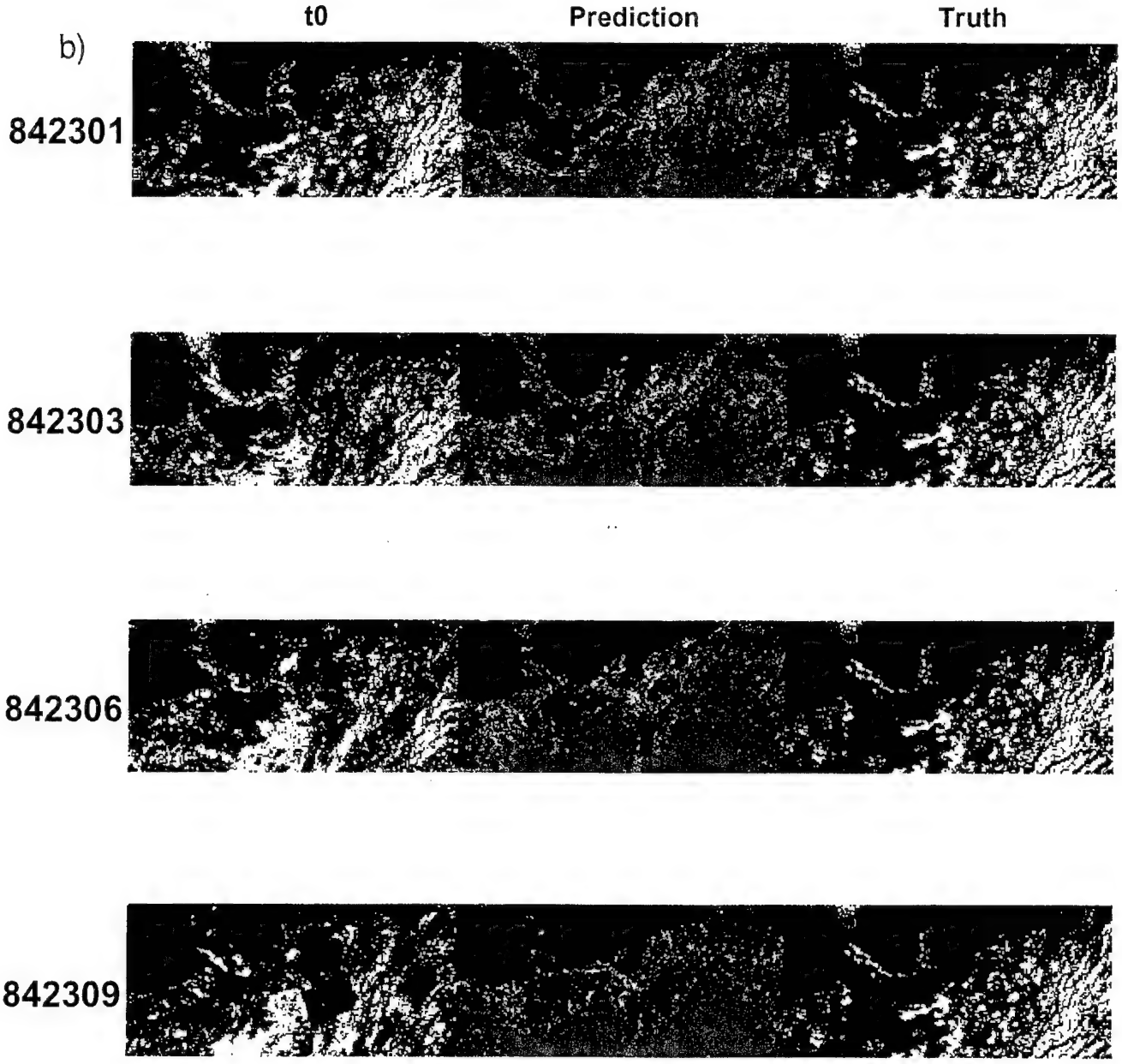

(The number code above denotes the day/time/forecast duration.)

Figure 4-7. Day 84 CNSA forecasts for a neural network trained on median filtered data (a) using unfiltered input, and (b) using median filtered input (Continued).

It is difficult to draw too many conclusions from the CNSA forecasts because the clouds do not change much over the nine hours of the forecast. As a result the forecasts look much like the input advection field which looks much like the truth. The bulk of the clouds are forecast correctly. Again, too many clouds are forecast in some places.

4.3 COMPARISON TO HRCP PERFORMANCE.

Skill score information for overlapping analysis times is not available for HRCP. However, the monthly HRCP verification statistics report provides some insight into the relative performance of the two models (HRCP and WCPM).

HRCP performance is documented in terms of the rms error for 3, 6 and 9 hour forecasts on a monthly basis. No differentiation is made in terms of the local time of the forecast. Performance is also categorized in terms of environmental zones with the tropical zone best for our comparison purposes.

Combining the last fourteen months of performance reports results in an average rms error for 3, 6 and 9 hour forecasts of 29%, 38% and 39% respectively. These should be compared to the square root of the Brier scores previously discussed. Typical Brier scores from WCPM indicate rms errors for 3, 6 and 9 hour forecasts of 17%, 20% and 25%.

Although a significant improvement in forecasting ability is indicated, the comparison might be somewhat deceptive. The WCPM results were obtained for a few realizations in one area; the HRCP results include many realizations in all tropical areas. The WCPM results are for a 16^{th} mesh resolution while the HRCP results are for an 8^{th} (or larger) mesh resolution. Rigorous comparisons should not be made based upon these preliminary results.

SECTION 5

FORECAST IMPROVEMENTS — OBJECT ORIENTED APPROACH

The greater success of the median filtered forecasts and the discussion in Section 2 of cloud randomness strongly suggests a potentially superior approach to cloud forecasting, an object oriented approach. The object oriented approach takes the concept of cloud layers one step farther and isolates cloud "masses, clusters or systems" for analysis. The analysis and forecasting then takes into account spatial correlation and relationships in the clouds and thus becomes more similar to that performed by a meteorologist.

The meteorological "object" information will be obtained from a cloud segmentation and classification analysis of remote sensing multi-spectral and microwave radiometer images combined with available NWP data (e.g. National Meteorological Center data, NOGAPS data, European Center for Medium Range Weather Forecasting data). The segmentation and classification analysis will either replace the nephanalysis or defer the need for a nephanalysis until after the forecast is made. The new process is illustrated in Figure 5-1 by the structure of the NN. The following will discuss the critical aspects of this approach.

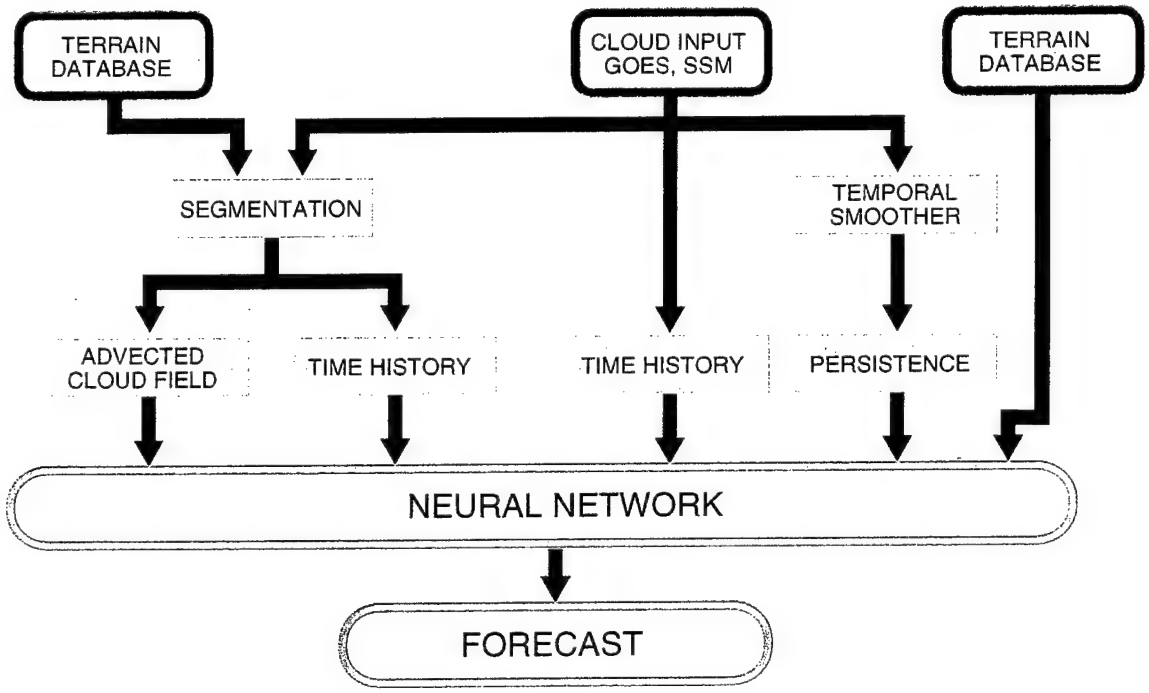

Figure 5-1. Proposed structure of the NN for theater area cloud forecast.

The greatest change proposed in the forecast model is the inclusion of image object advection/persistence/evolution descriptive input. The role of the meteorological objects or weather systems in the analysis will be twofold. First, it will enable a coarser forecast capability at a regional level (about twice the size of the theater area of interest) to be related to cloud properties. Second, it will partially or totally take the place of a nephanalysis in that the cloud fractions and heights will be properties of the objects.

5.1 CLOUD SEGMENTATION.

A variation of the NN cloud segmentation algorithm of Peak and Tag (1988) will be developed to perform the object or weather system identification. Whereas Peak and Tag was mainly interested in isolating contiguous cloud masses from visible satellite data and identifying cloud types, the current need is to identify and characterize a weather system, its motion, and its evolution.

Each weather system will be characterized by its location, physical size, intensity, motion and rate of growth. Associated cloud masses will be characterized in terms of cloud type, height, motion, moisture content, and texture, along with the evolution of these parameters. It is the cloud mass characterization that will form the basis of the forecast.

At this point, it is anticipated that the ***cloud segmentation and description will be performed using multi-spectral and microwave remote sensing as well as NWP input.*** Existing algorithms use one or the other but not both to identify cloud types. Peak and Tag use a hierarchical approach and a NN for segmentation. He can include many size, shape and texture parameters as input to the NN. Formally, the approach can accommodate multi-sensor information or other meteorological information. Peak's segmentation methodology was investigated and rejected for use in the pixel-by-pixel worldwide cloud forecast model but is quite appropriate to an object oriented approach.

Liu, Curry, and Sheu (1995) have classified clouds into non-traditional categories based upon combined infrared and microwave radiometer data to predict precipitation. This approach appears to be more appropriate to cloud and precipitation forecasting than standard cloud classification because the classification (Table 5-1) is based upon those characteristics of the clouds most diagnostic of precipitation. In particular, clouds are classified based upon present and past moisture content and cloud top height. No actual segmentation was attempted. The addition of microwave radiometer data opens the possibility to forecast precipitation of various types as well as cloud thickness.

Table 5-1. Schematic diagram of microwave index (f) versus cloud top temperature for cloud classification.

Thin High-Top Nonprecipitating Cloud	Deep High-Top Nonprecipitating Cloud	Anvil With Stratiform Precipitating Cloud	Deep Convective Precipitating Cloud
Midtop Nonprecipitating Cloud		Midtop Precipitating Cloud	
Warm Nonprecipitating Cloud		Warm Precipitating Cloud	

0.25 0.0 0.75

f(Microwave Index)

(Liu, Curry, and Sheu, 1995)

5.2 CLOUD MOISTURE.

Moisture is obviously a key input into the cloud forecasting model. Numerical weather prediction (NWP) models rely on radiosonde data for moisture field initialization. Numerous techniques were developed in the past 10 years to utilize satellite multi-spectral and microwave radiometer data to infer vertical profiles of water vapor and precipitation in the atmosphere (e.g., Weng and Grody, 1994; Jones and Vonder Haar, 1990; Liu, Curry, and Sheu, 1995). Multi-spectral data (e.g. AVHRR) is effective at estimating water vapor content in clear sky regions, but depends on an accurate temperature profile. If free water is also present, better results are achieved using microwave radiometer systems such as SSM/I and SSM/T-1 or /T-2 (e.g., Falcone et al., 1992; Butler, Meredith, and Stogryn, 1996; Butler, Meredith, and Rosenberg, 1992). Comparisons with radiosonde data are good within the operating zone of the radiosonde. Simulations have also demonstrated the expected sensitivity to upper atmosphere relative humidity (e.g., Butler, Meredith, and Rosenberg, 1992).

5.3 PIXEL-BY-PIXEL DATA.

The pixel data still remains an important part of the forecast input for two reasons. First, ***persistence information*** (e.g., diurnal or multiple day trends) can best be characterized on a pixel-by-pixel basis. Secondly, the pixel-by-pixel data retains the ***highest resolution information***. Neither should be discarded. Advective and evolutionary information will now be relegated to the object level. The number of pixel level model predictors will therefore be greatly reduced.

5.4 UNIVERSAL PARAMETERS.

A NN is relatively unlimited in terms of the quantity of data that can be input. However, once trained, it is severely limited in terms of the types of data it can accept without a complete new training. ***The choice of universal input parameter definition is therefore critical and will be one of the first tasks performed.***

Raw multi-spectral and microwave radiometer data represents brightness temperatures at different frequencies and must be interpreted in terms of frequency. The frequency dependence must be removed before it can be algebraically combined. The frequency dependence is removed if physical parameters such as vapor pressure, free water content, true temperature, etc. are estimated. Similar parameters are estimated from radiosonde data and thus can be easily included in the analysis. Other data such as wind vectors can be directly included into the advection analysis.

SECTION 6
REFERENCES

Blankert, R. L., "Probabilistic Neural Network Approach to Cloud Classification," in *13th Conf. on Weather Analysis and Forecasting Including Symposium on Flash Floods,* Vienna, VA, 2-6 August, 1993, Am. Meteor. Soc., Boston, MA. (UNCLASSIFIED)

Butler, C. T., R. v. Z. Meredith, and A. P. Stogryn, "Retrieving Atmospheric Temperature Parameters from DMSP SSM/T-1 Data with a Neural Network," *J. Geophys. Res.,* Vol. 101, 1996, pp. 7075-7083. (UNCLASSIFIED)

Butler, C. T., R. v. Z. Meredith, and A. Rosenberg, "Retrieving Atmospheric Temperature Profiles from Simulated DMSP Sounder Data with a Neural Network," in *Proceedings of the 1991 Conference on Cloud Impacts on DoD Operations and Systems*, CIDOS, 1992, pp. 325-330. (UNCLASSIFIED)

Falcone, V. J. et al., *SSM/T-2 Calibration and Validation Data Analysis,* Phillips Laboratory, Hanscom AFB, MA, PL-TR-92-2293, 1992. (UNCLASSIFIED)

Gandin, L. S., and A. H. Murphy, "Equitable Skill Scores for Categorical Forecasts," *Mon. Wea. Rev.,* Vol. 120, February 1992, pp. 361-370. (UNCLASSIFIED)

Gustafson, G. B. et al., *Support of Environmental Requirements for Cloud Analysis and Archive (SERCAA): Algorithm Descriptions,"* PL-TR-94-2114, Phillips Laboratory, Hanscom AFB, MA, 1994. (UNCLASSIFIED)

Holman, J. P., *Experimental Methods for Engineers,* McGraw-Hill, NY, 1978, p. 344. (UNCLASSIFIED)

Jones, A. S., and T. Vonder Haar, "Passive Microwave Remote Sensing of Cloud Liquid Water Over Land Regions," *J. Geophys. Res.*, Vol. 95, 1990, pp. 16673-16683. (UNCLASSIFIED)

Liu, G., J. A. Curry, and R. Sheu, "Classification of Clouds Over the Western Equatorial Pacific Ocean Using Combined Infrared and Microwave Satellite Data", *J. Geophys. Res.*, Vol. 100, 1995, pp. 13811-13826. (UNCLASSIFIED)

McCann, D. W., "A Neural Network Short-Term Forecast of Significant Thunderstorms," *Forecast. Tech.,* Vol. 7, September 1992, pp. 525-534. (UNCLASSIFIED)

Peak, J. E., and P. M. Tag, "An Expert System Approach for Prediction of Maritime Visibility Obscuration," *Mon. Wea. Rev.*, Vol. 117, 1988, pp. 2641-2653. (UNCLASSIFIED)

Salby, M. L., et al., "Analysis of Global Cloud Imagery from Multiple Satellites," *Bull. Amer. Meteor. Soc.*, Vol. 72, No. 4, April 1991, pp. 467-480. (UNCLASSIFIED)

Sarkisian, C. P. et al., *Support of Environmental Requirements for Cloud Analysis and Archive (SERCAA): Algorithm Descriptions,* PL-TR-94-2114, Phillips Laboratory, Hanscom AFB, MA, 1994. (UNCLASSIFIED)

Welch, R. M. et al., "Polar Cloud and Surface Classification Using AVHRR Imagery: An Intercomparison of Methods," *J. Appl. Meteor.*, Vol. 31, May 1992, pp. 405-420. (UNCLASSIFIED)

Weng, F., and N. C. Grody, "Retrieval of Cloud Liquid Water Using the Special Sensor Microwave Imager (SSM/I)," *J. Geophys. Res.*, Vol. 99, 1994, pp. 25535-25551. (UNCLASSIFIED)

APPENDIX A
DATA

Data for three study regions were provided as the primary database for the WCPM. All three regions (EASA—East Asia, CNSA—Central and South America, EMDA—Eastern Mediterranean Sea) were tropical (Figure A-1). The total data set is listed in Table A-1 and includes the SERCAA, NOGAPS, RTNEPH and terrain data.

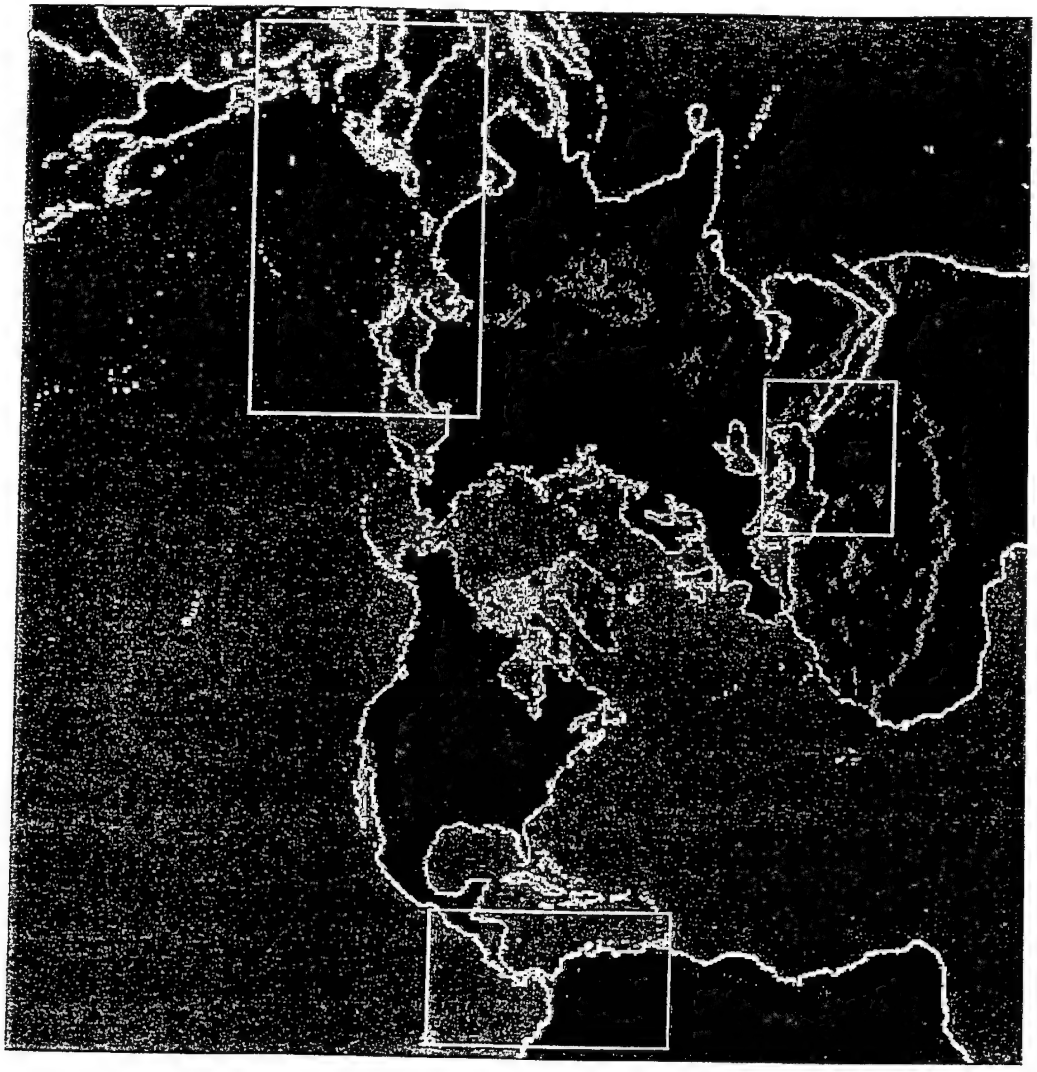

Figure A-1. Regions for which SERCAA data was supplied.

Table A-1. WCPM datbase.

Type	Description	Size (MB)
Numerical weather prediction	NOGAPS Feb-Apr 1993 and 1994 May-Jul 1993 and 1994	1,656
Terrain	TACNEPH	2
	SERCAA	
	Elevation	63
	Geography	17
Nephanalysis	RTNEPH Feb-Apr 1993 and 1994 May-Jul 1993 and 1994	6,660
	SERCAA	
	EASA 22-30 Mar 1993	1,180*
	EASA 22-31 Jul 1993	1,323
	CNSA 22-31 Mar 1994	495
	EMDA 12-21 Mar 1994	313

SERCAA data processing was still being developed during the first year of this contract. Much of the EASA and CNSA data received at PSR was unsuitable for our purposes due to the presence of processing artifacts. Hence, neural network training focused on the EMDA data. In addition, Level 4 SERCAA processing (the integrated results from all available satellites) was unusable due to poor satellite merging and equalization. WCPM processing utilized only the GOES-6 data in the SERCAA Level 3 data set.

A.1 TERRAIN DATA.

Figure A-2 shows the input SERCAA land type data for area EMDA. Five land types were utilized in this study.

A.2 SERCAA DATA.

SERCAA algorithms incorporate high-resolution sensor data from multiple military and civilian satellites, polar and geostationary, into a real-time cloud analysis model and apply multispectral cloud analysis techniques that improve the detection of clouds. The SERCAA algorithms consist of a number of processes involved in integrating cloud analyses from multiple satellite

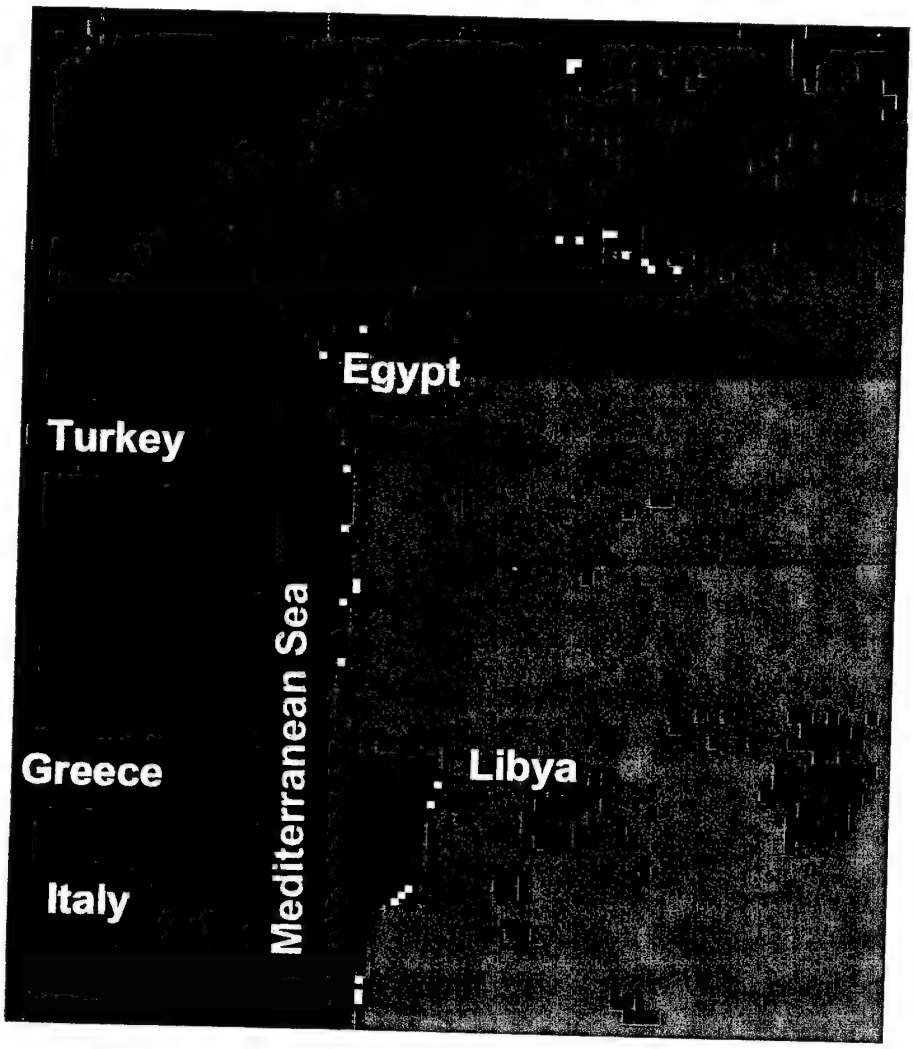

Key:	
Ocean	black
Land	green
Desert	red
Coast	blue
Desert coast	white

Figure A-2. Location and land type map for EMDA.

platforms into a single cloud analysis product. The steps required to process the raw sensor data, collected from each of the platforms, into each of the individual cloud analysis products include total cloud algorithms for DMSP, AVHRR, GOES, METEOSAT and geostationary platforms, cloud layer and type algorithms, and an analysis integration algorithm (see Sarkisian et al., 1994).

SERCAA products are available with three levels of processing. Level 1 represents raw, individual satellite data. Level 2 represents corrected satellite data. Level 3 represents individual satellite nephanalyses. Level 4 merges the individual satellite Level 3 analyses. Final SERCAA products are reported on a 16^{th} mesh and include total cloud cover fraction, number of cloud layers (4 maximum), cloud layer coverage fraction, cloud type, cloud height, and a measure of confidence.

The primary data used for analysis is shown in Figure A-3. Although hourly images (with a few gaps) are available, the Level 3 total cloud fraction is shown at three hour increments.

A.3 NOGAPS DATA.

NOGAPS "data" is provided by FNMOC. NOGAPS is the output of a large NWP code that also assimilates satellite weather observations to produce a current prediction of the numerical parameters previously shown in Table 3-2 and a 12 hour forecast of those parameters. A complete description of the NOGAPS algorithms is beyond the scope of this report. The reader is referred to reports specifically related to NOGAPS for model details. NOGAPS does not produce a nephanalysis.

NOGAPS provides a global analysis and a 12-hour forecast twice daily at 00 and 12 Z on a 2.5×2.5 degree latitude/longitude grid. The resolution at 60° N is 139 km, decreasing to 278 km at the equator. In contrast, SERCAA data is available hourly (nominally) and the resolution of 16th-mesh SERCAA data at 60° N is 23.8 km, increasing toward the equator. The current NOGAPS operational model is higher resolution (0.75×0.75 degree) but unfortunately no archived data is available for the 1993 and 1994 times corresponding to the SERCAA data sets.

Figures A-4 and A-5 show NOGAPS data corresponding to the SERCAA EMDA data.

Total Cloud Fraction

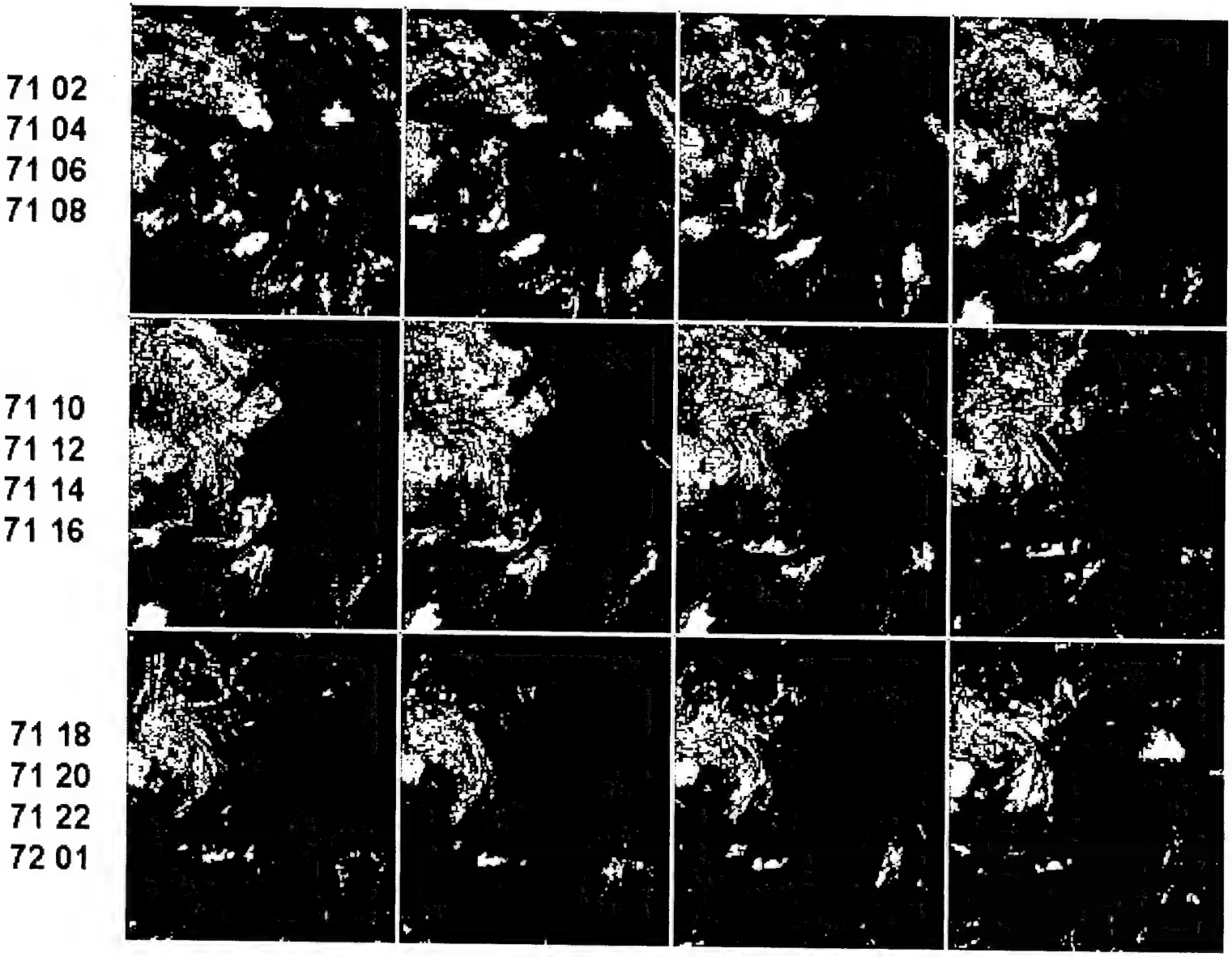

Figure A-3. SERCA level 3 total cloud fraction on days 71 through 81 for EMDA.

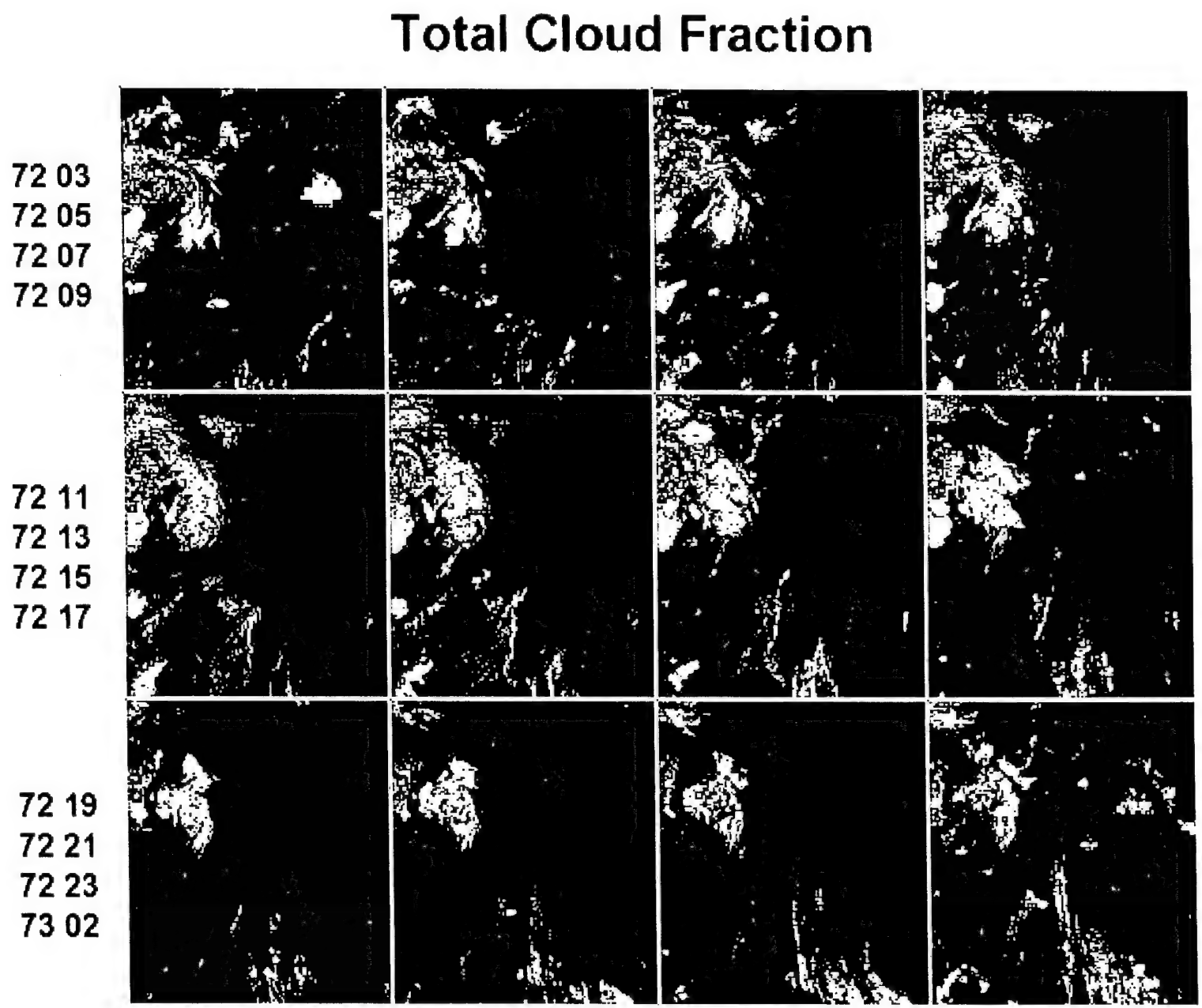

Figure A-3. SERCA level 3 total cloud fraction on days 71 through 81 for EMDA (Continued).

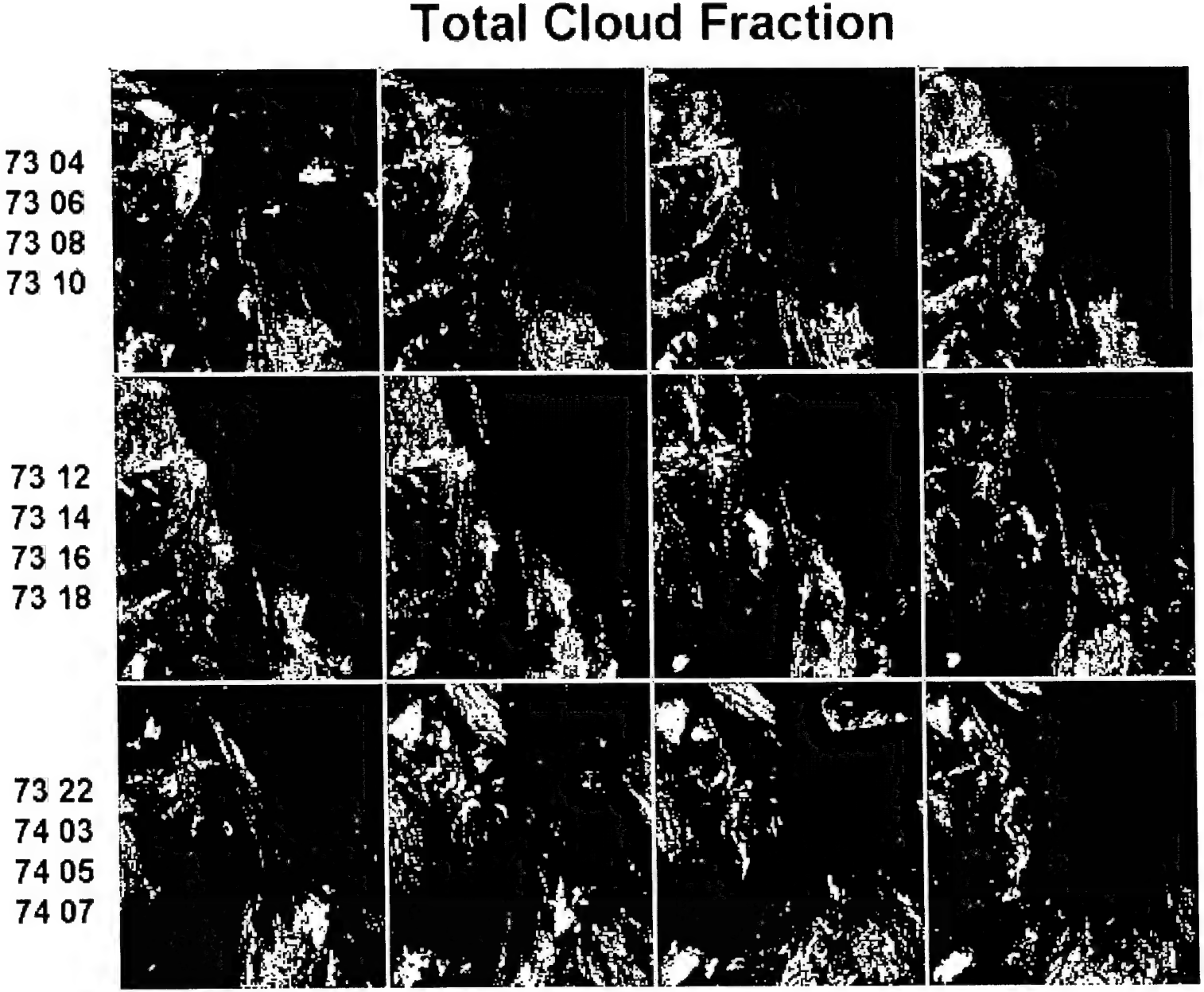

Figure A-3. SERCA level 3 total cloud fraction on days 71 through 81 for EMDA (Continued).

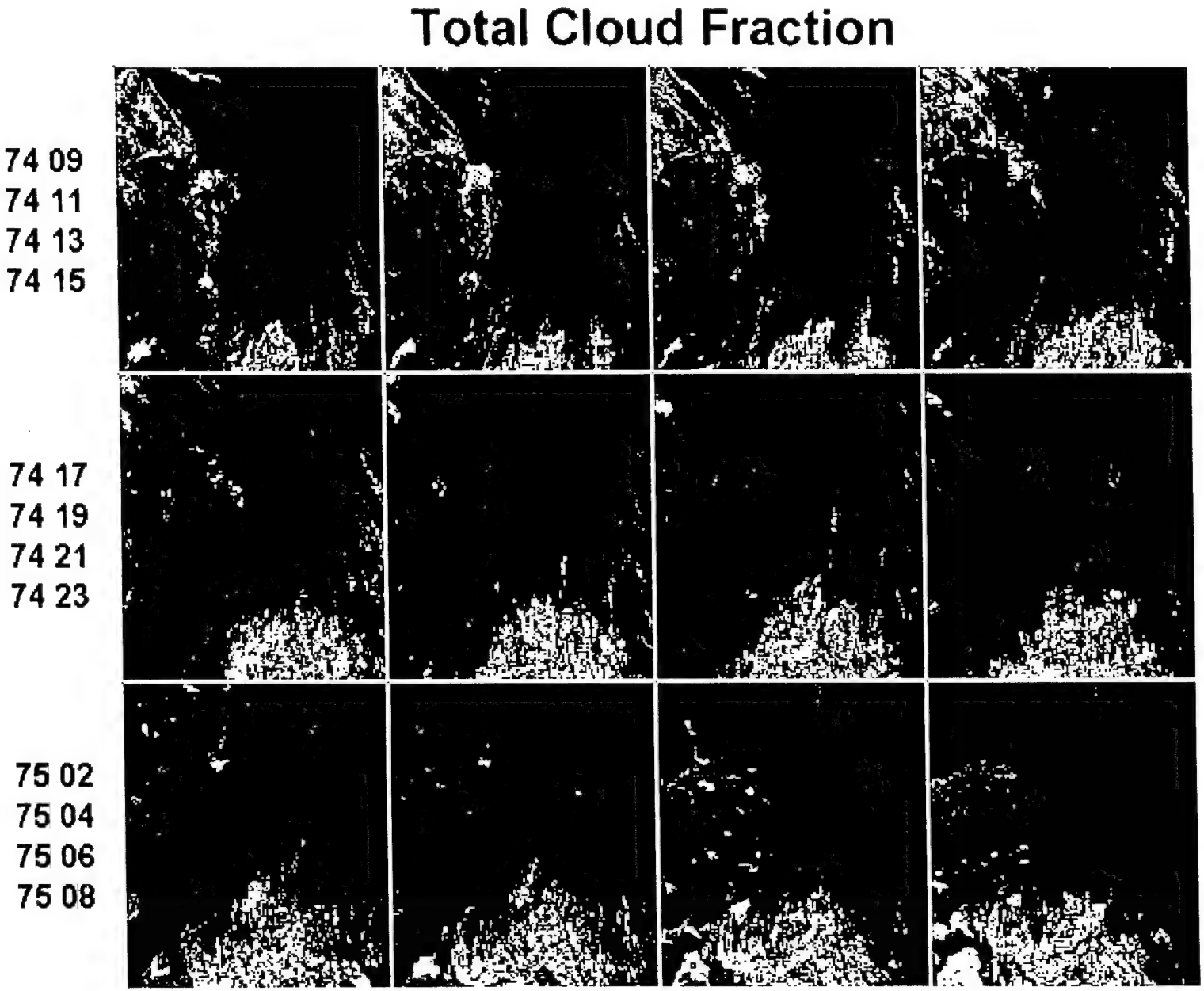

Figure A-3. SERCA level 3 total cloud fraction on days 71 through 81 for EMDA (Continued).

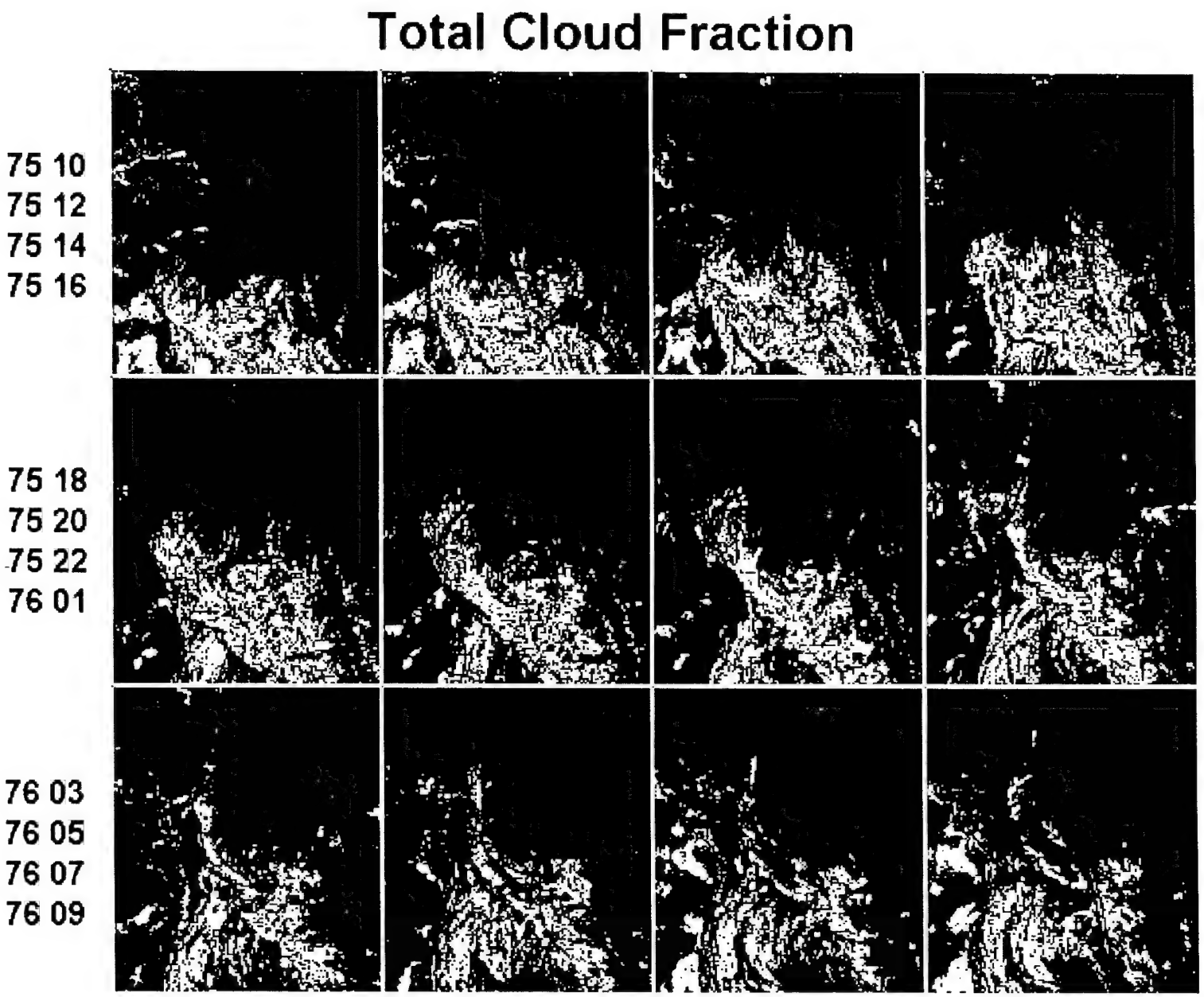

Figure A-3. SERCA level 3 total cloud fraction on days 71 through 81 for EMDA (Continued).

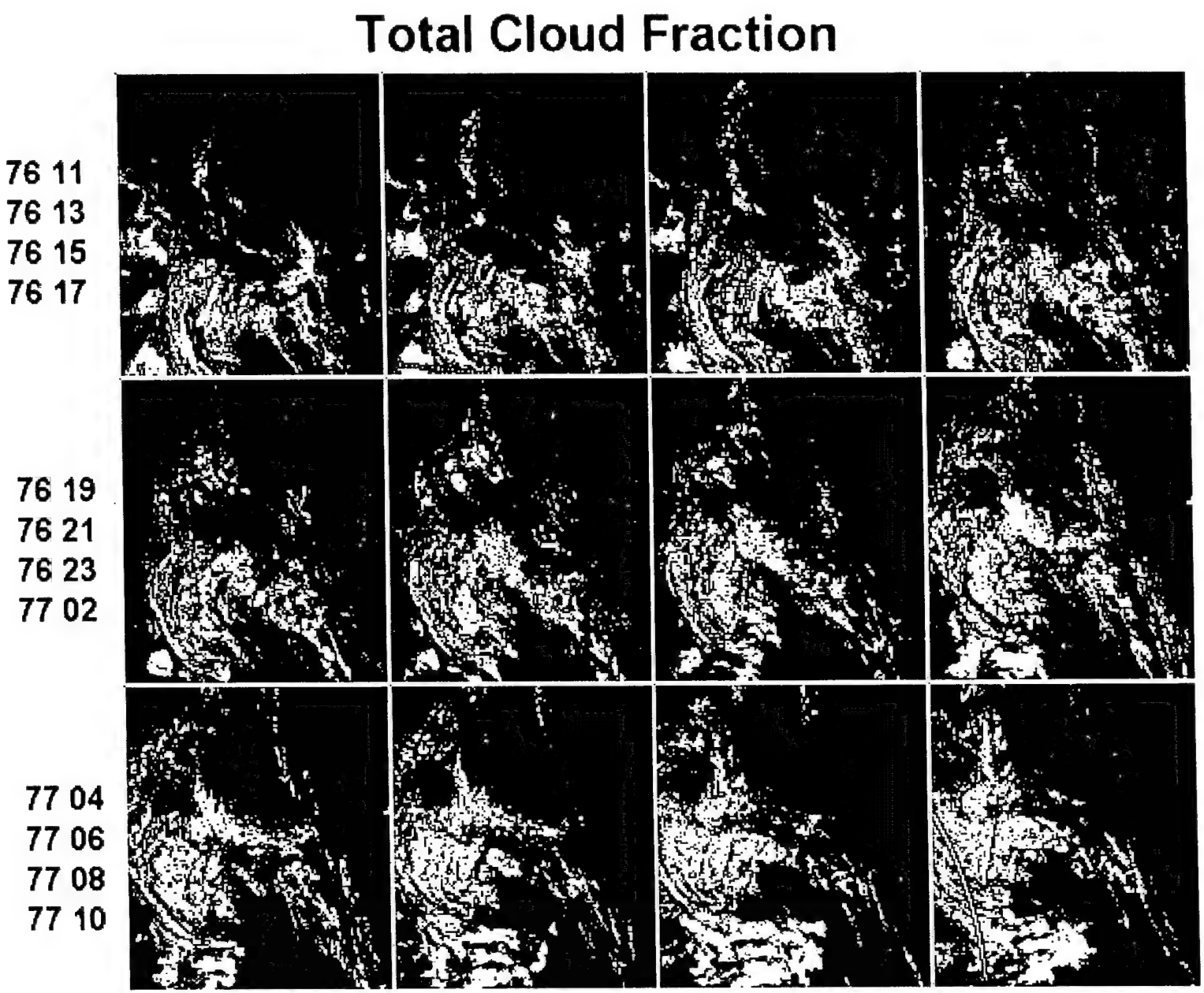

Figure A-3. SERCA level 3 total cloud fraction on days 71 through 81 for EMDA (Continued).

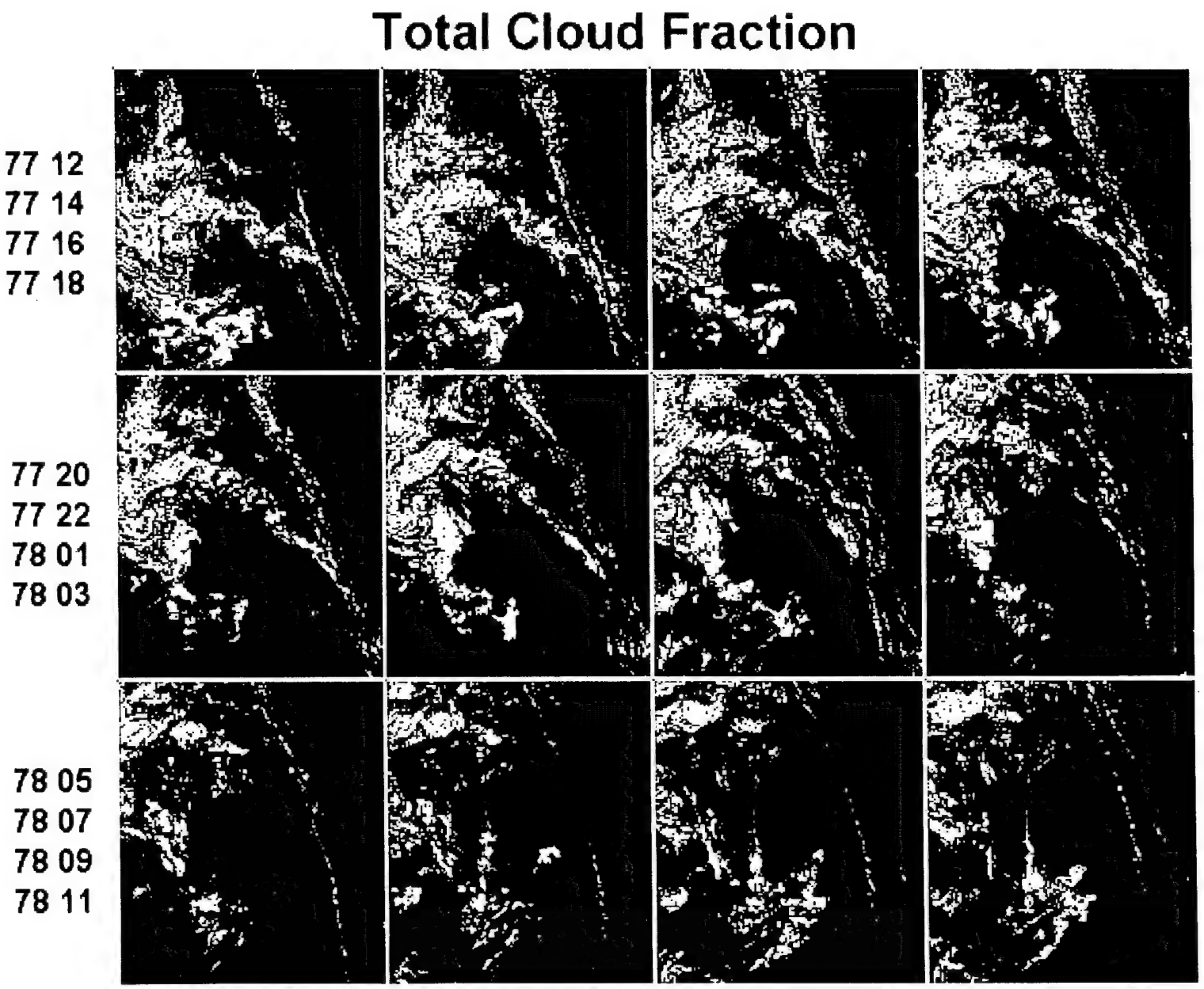

Figure A-3. SERCA level 3 total cloud fraction on days 71 through 81 for EMDA (Continued).

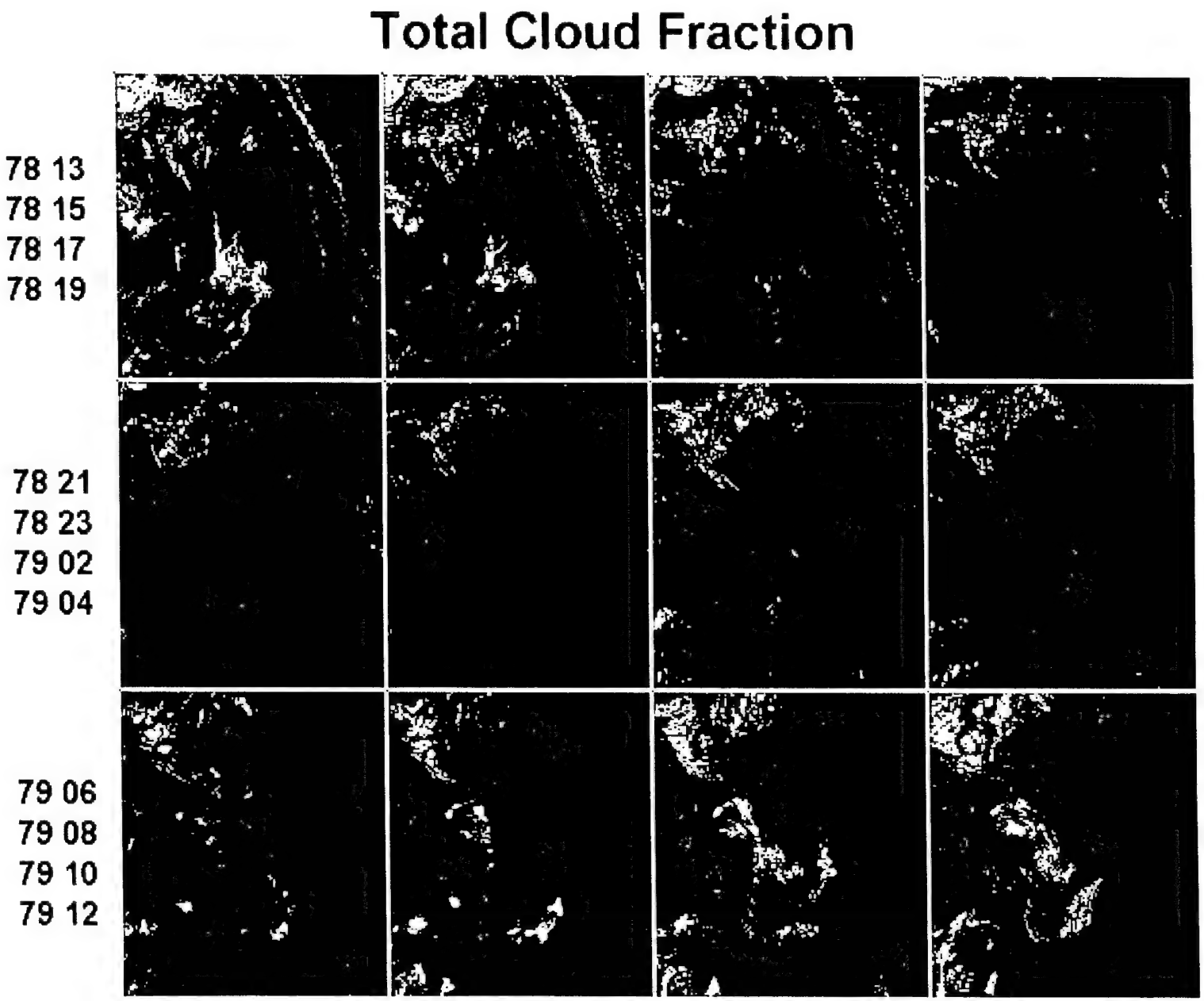

Figure A-3. SERCA level 3 total cloud fraction on days 71 through 81 for EMDA (Continued).

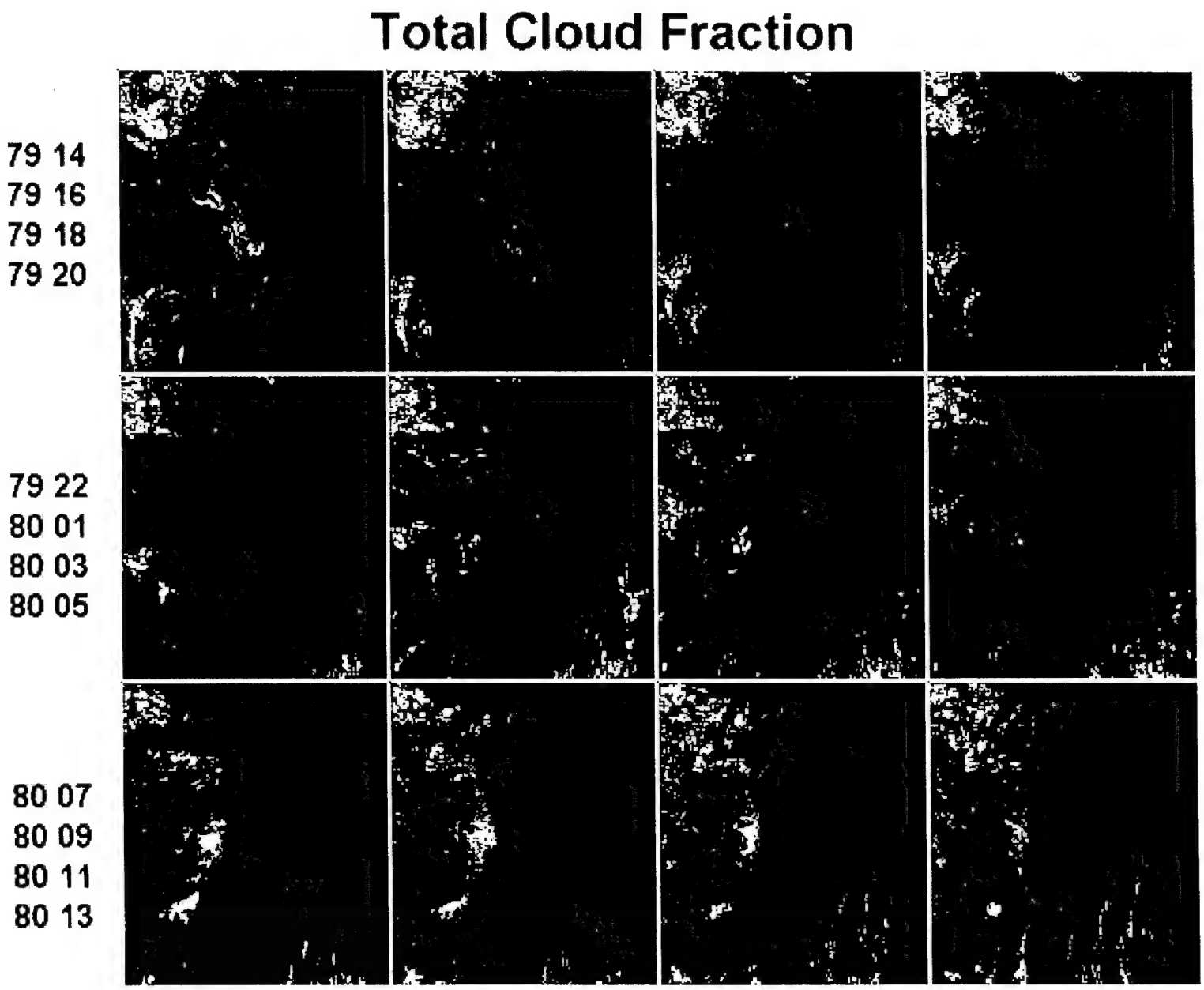

Figure A-3. SERCA level 3 total cloud fraction on days 71 through 81 for EMDA (Continued).

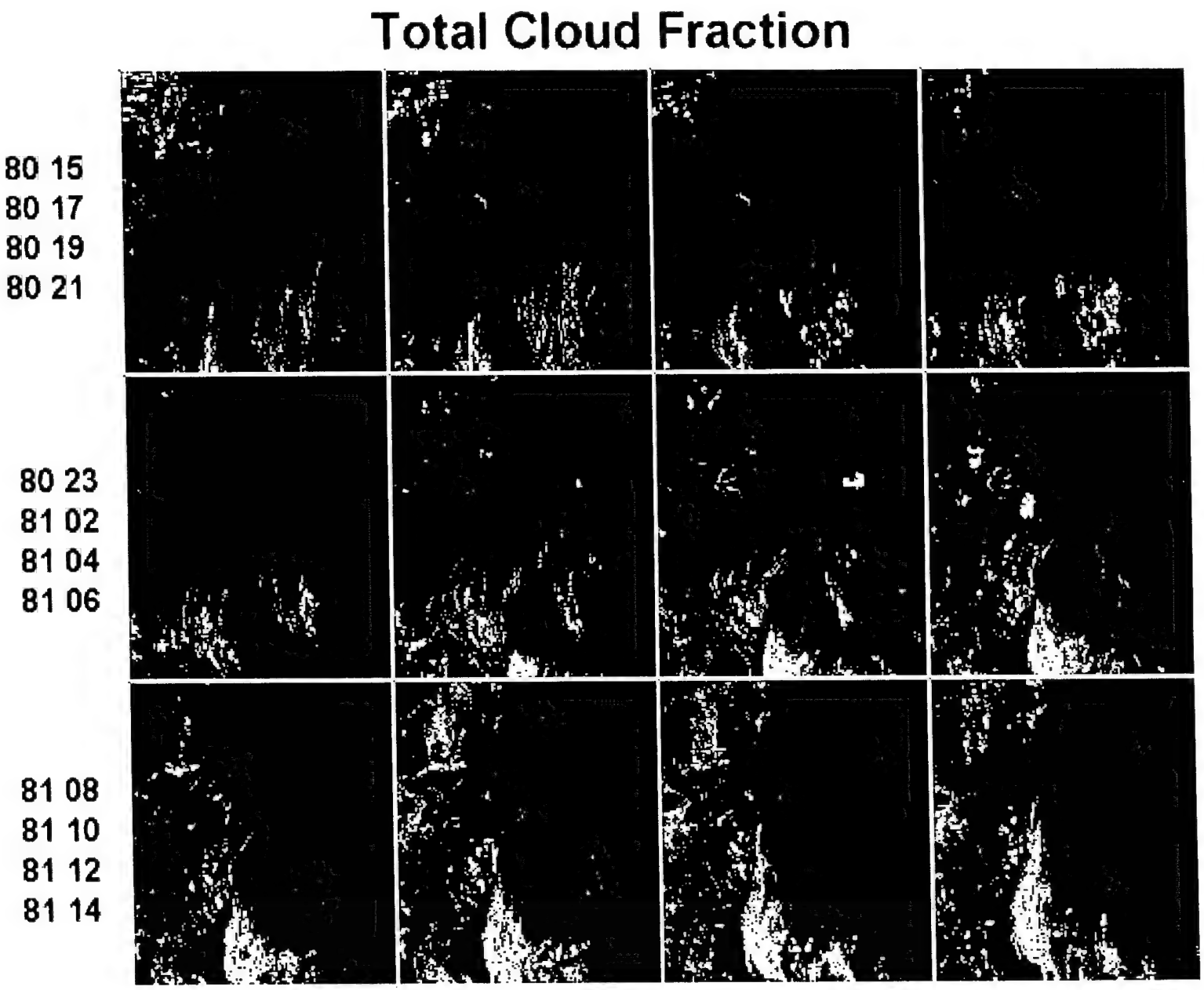

Figure A-3. SERCA level 3 total cloud fraction on days 71 through 81 for EMDA (Continued).

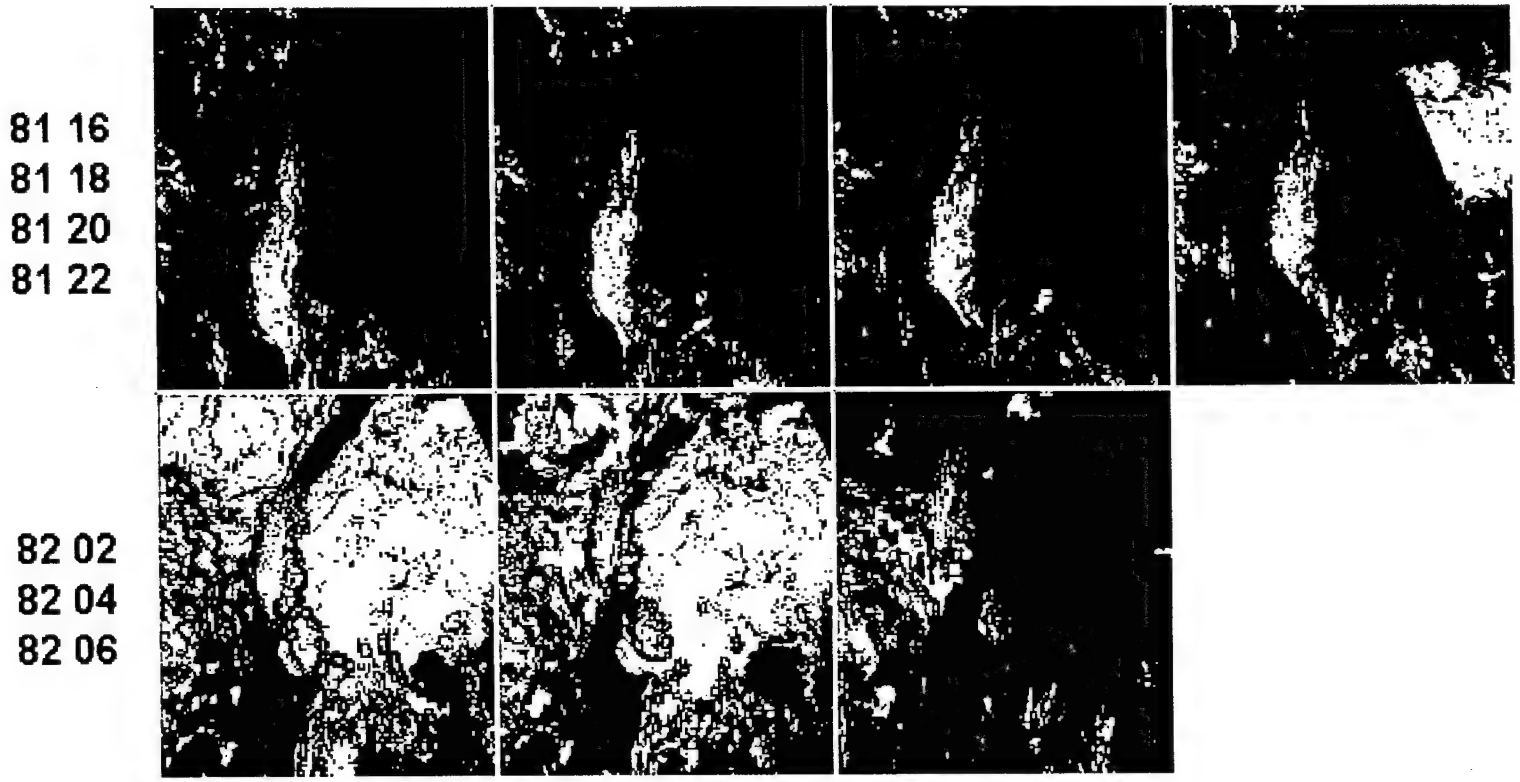

Figure A-3. SERCA level 3 total cloud fraction on days 71 through 81 for EMDA (Continued).

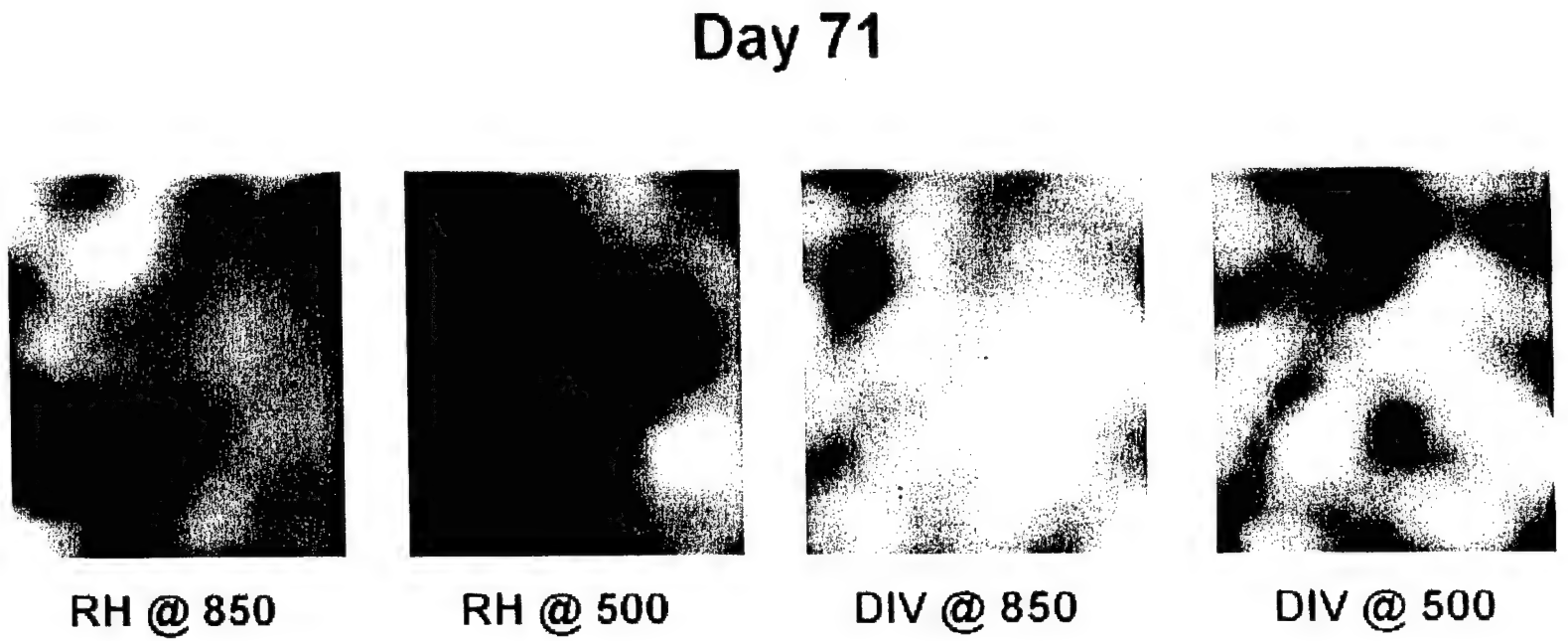

Figure A-4. NOGAPS relative humidity and velocity divergence data at two altitudes on days 71 through 82 for EMDA.

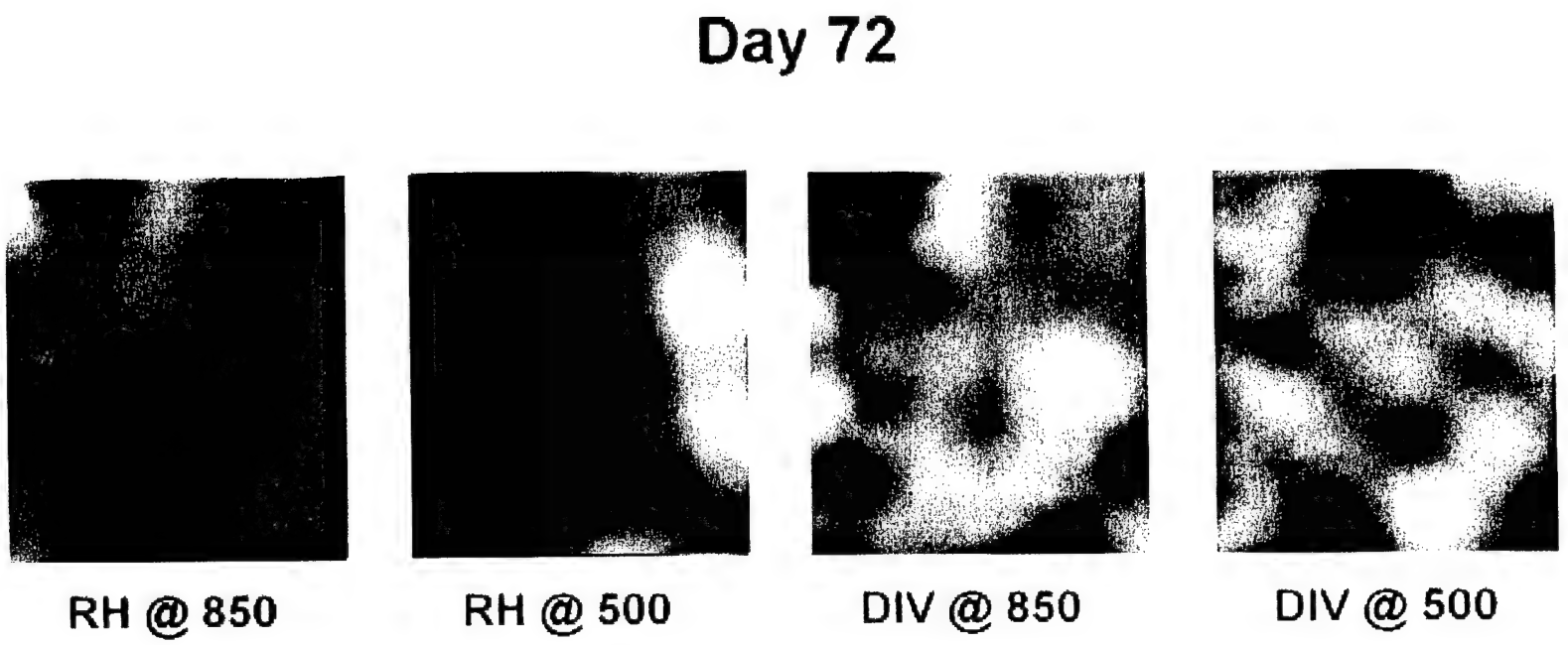

Figure A-4. NOGAPS relative humidity and velocity divergence data at two altitudes on days 71 through 82 for EMDA (Continued).

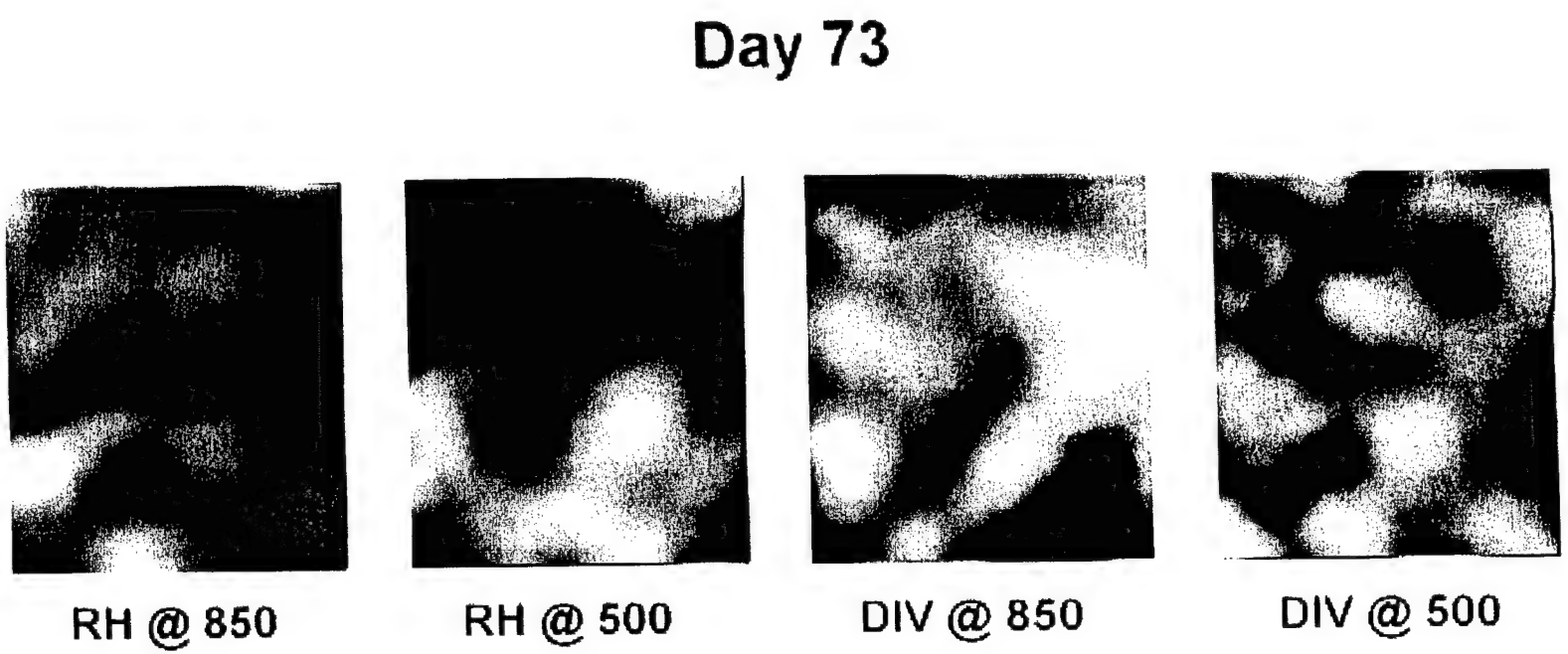

Figure A-4. NOGAPS relative humidity and velocity divergence data at two altitudes on days 71 through 82 for EMDA (Continued).

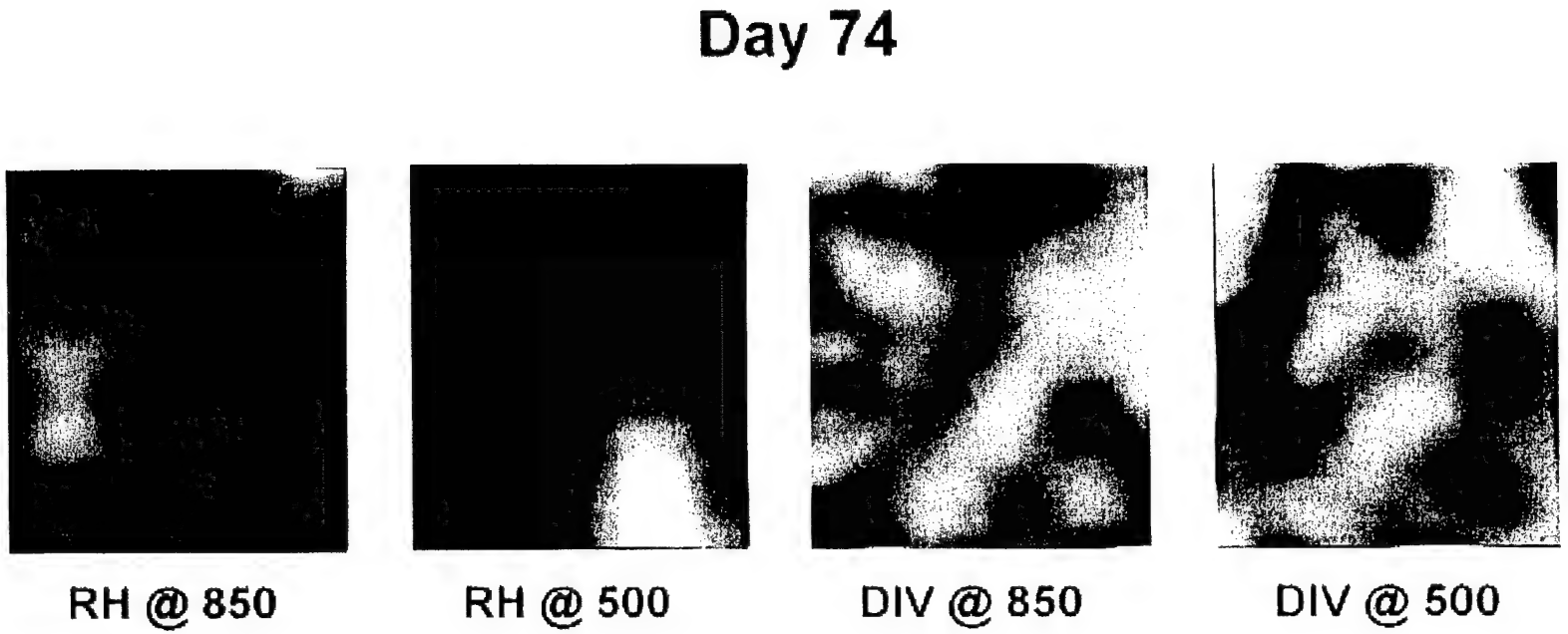

Figure A-4. NOGAPS relative humidity and velocity divergence data at two altitudes on days 71 through 82 for EMDA (Continued).

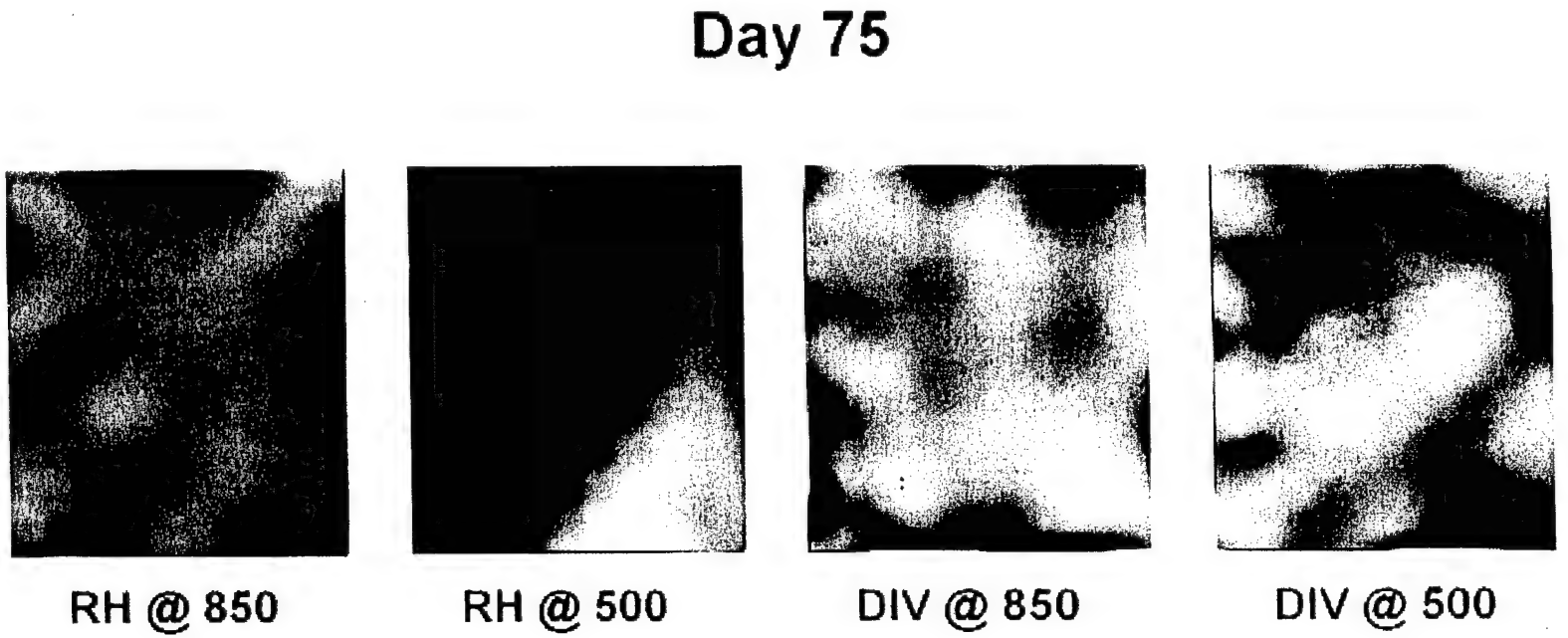

Figure A-4. NOGAPS relative humidity and velocity divergence data at two altitudes on days 71 through 82 for EMDA (Continued).

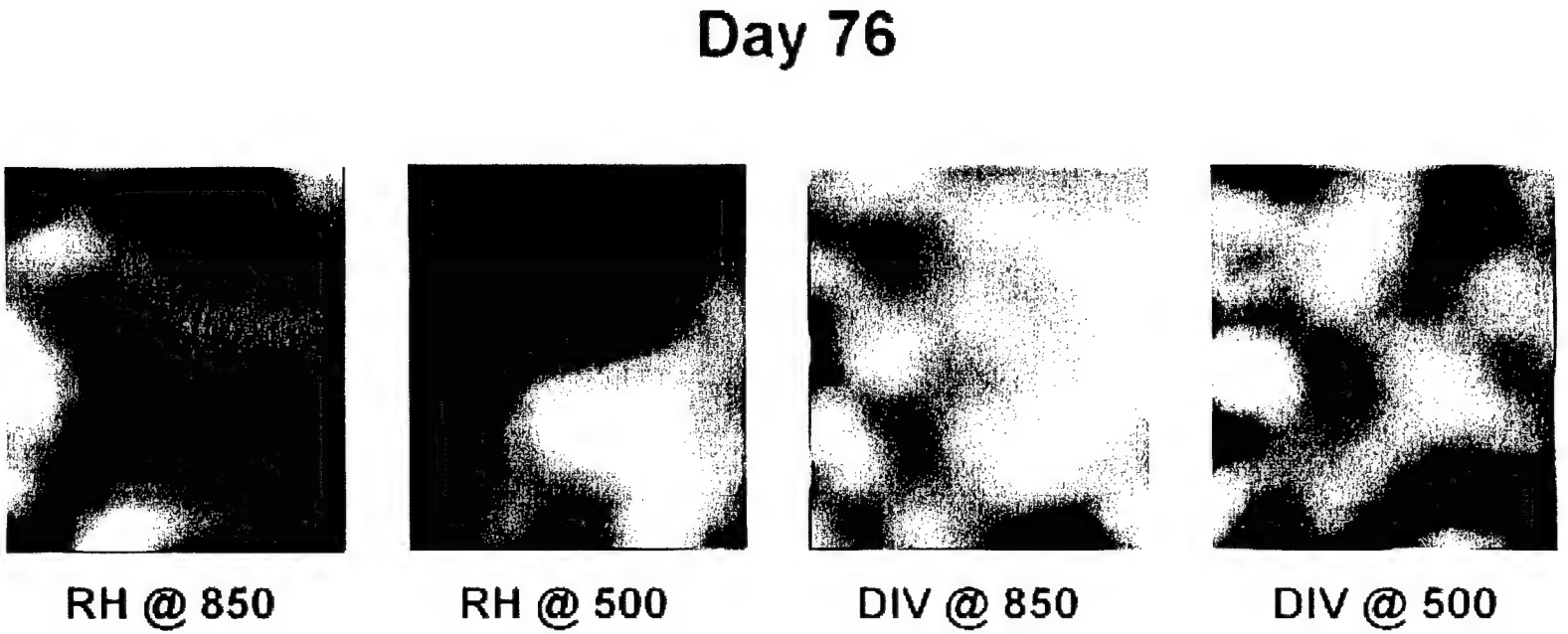

Figure A-4. NOGAPS relative humidity and velocity divergence data at two altitudes on days 71 through 82 for EMDA (Continued).

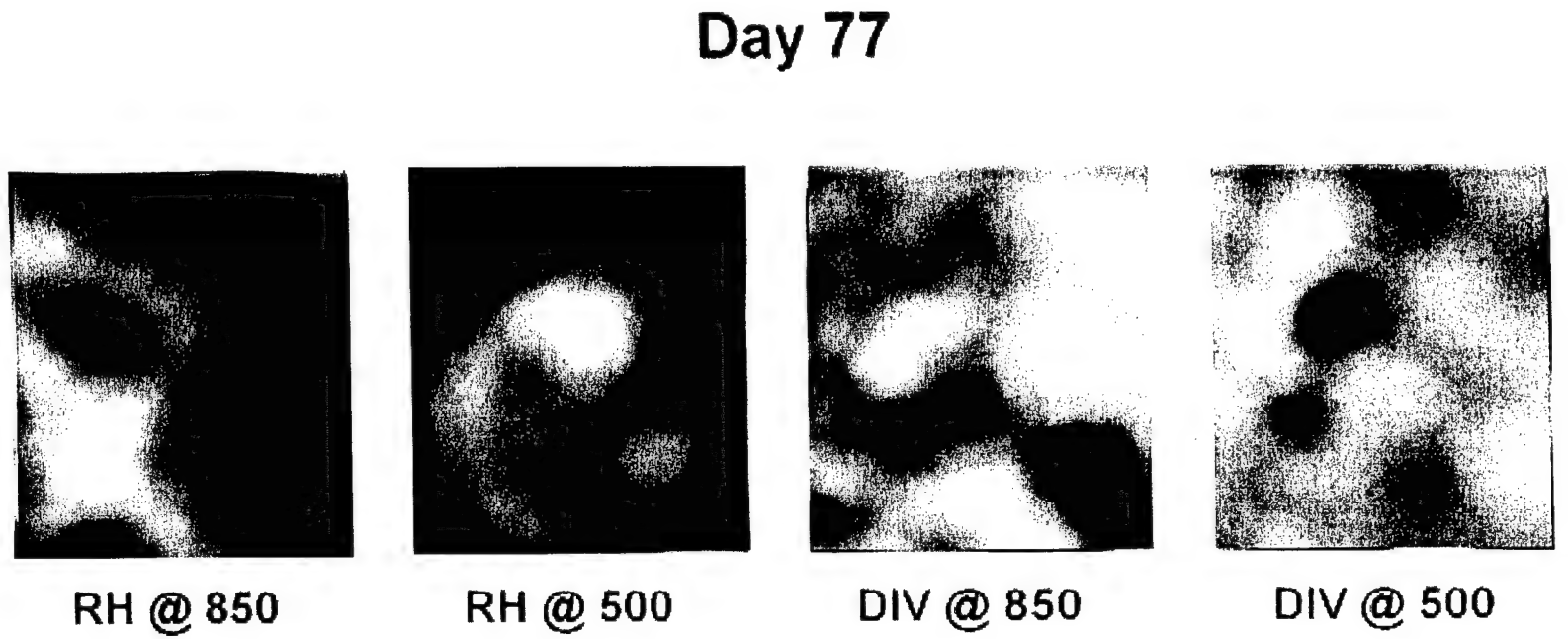

Figure A-4. NOGAPS relative humidity and velocity divergence data at two altitudes on days 71 through 82 for EMDA (Continued).

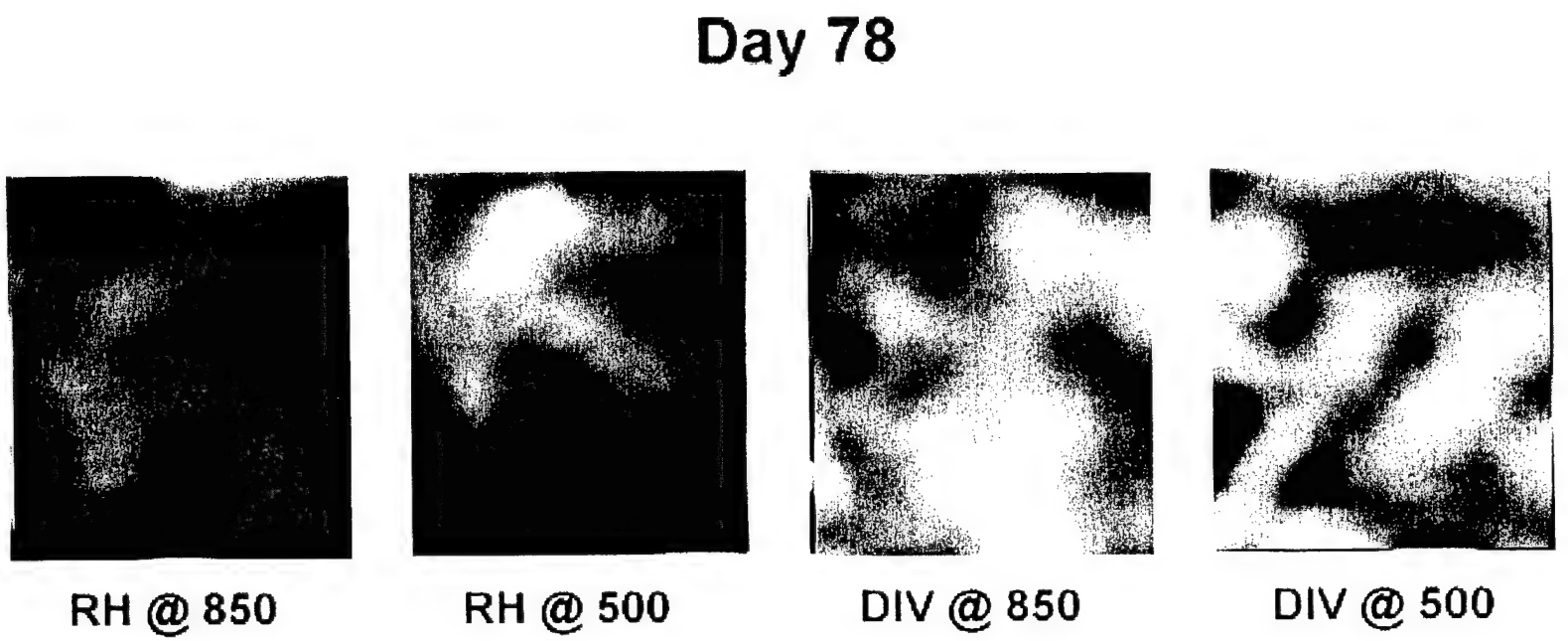

Figure A-4. NOGAPS relative humidity and velocity divergence data at two altitudes on days 71 through 82 for EMDA (Continued).

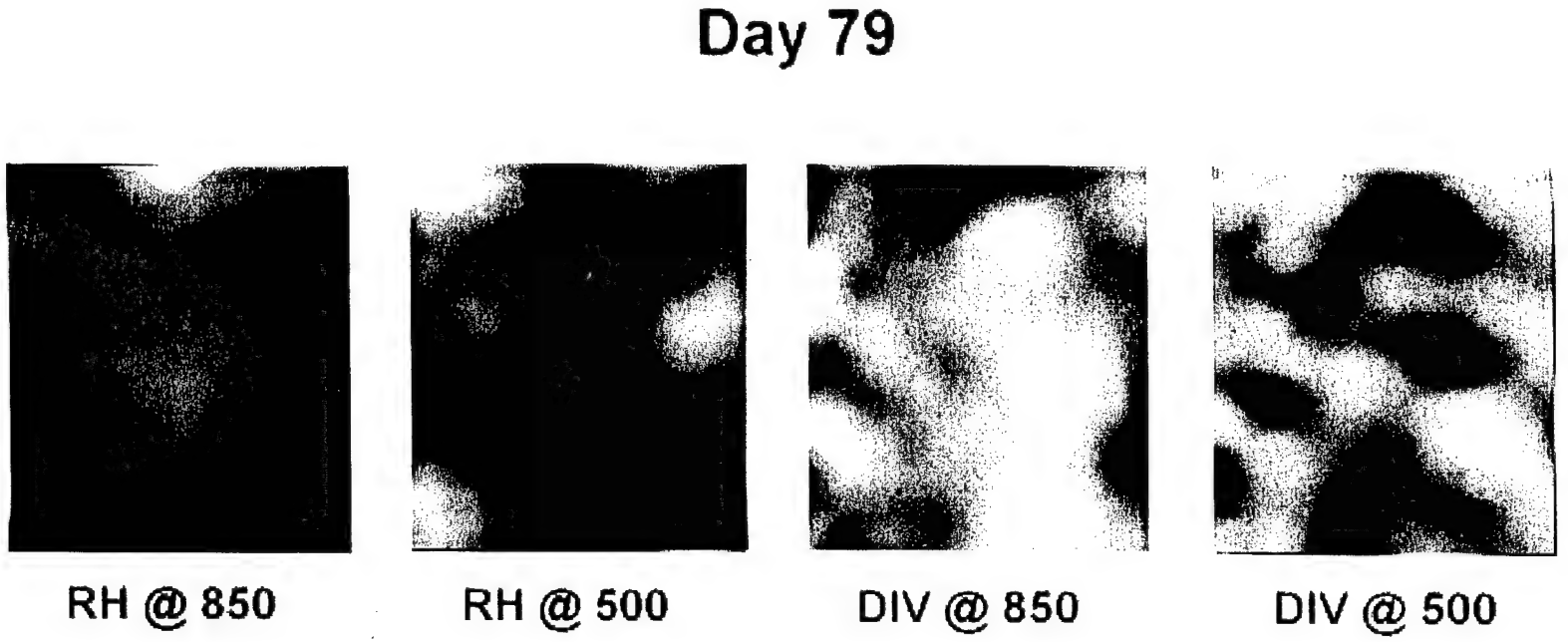

Figure A-4. NOGAPS relative humidity and velocity divergence data at two altitudes on days 71 through 82 for EMDA (Continued).

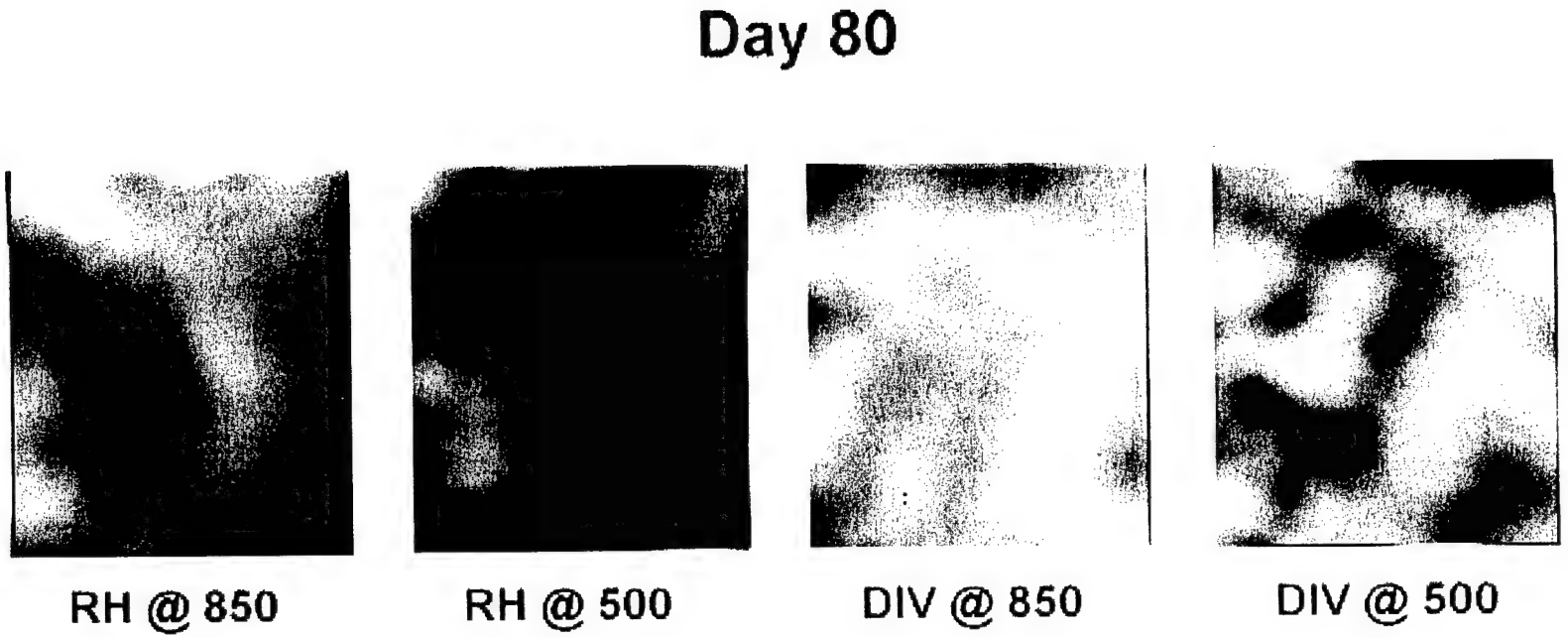

Figure A-4. NOGAPS relative humidity and velocity divergence data at two altitudes on days 71 through 82 for EMDA (Continued).

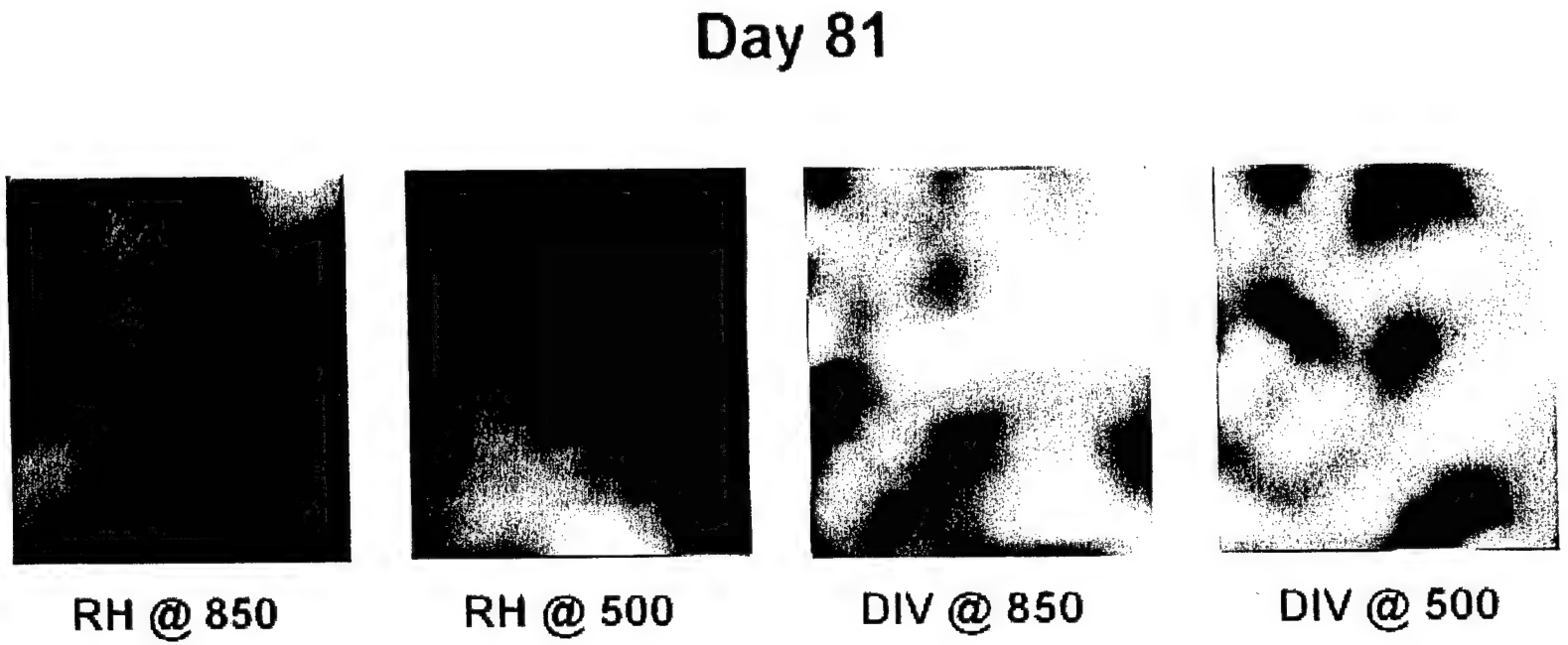

Figure A-4. NOGAPS relative humidity and velocity divergence data at two altitudes on days 71 through 82 for EMDA (Continued).

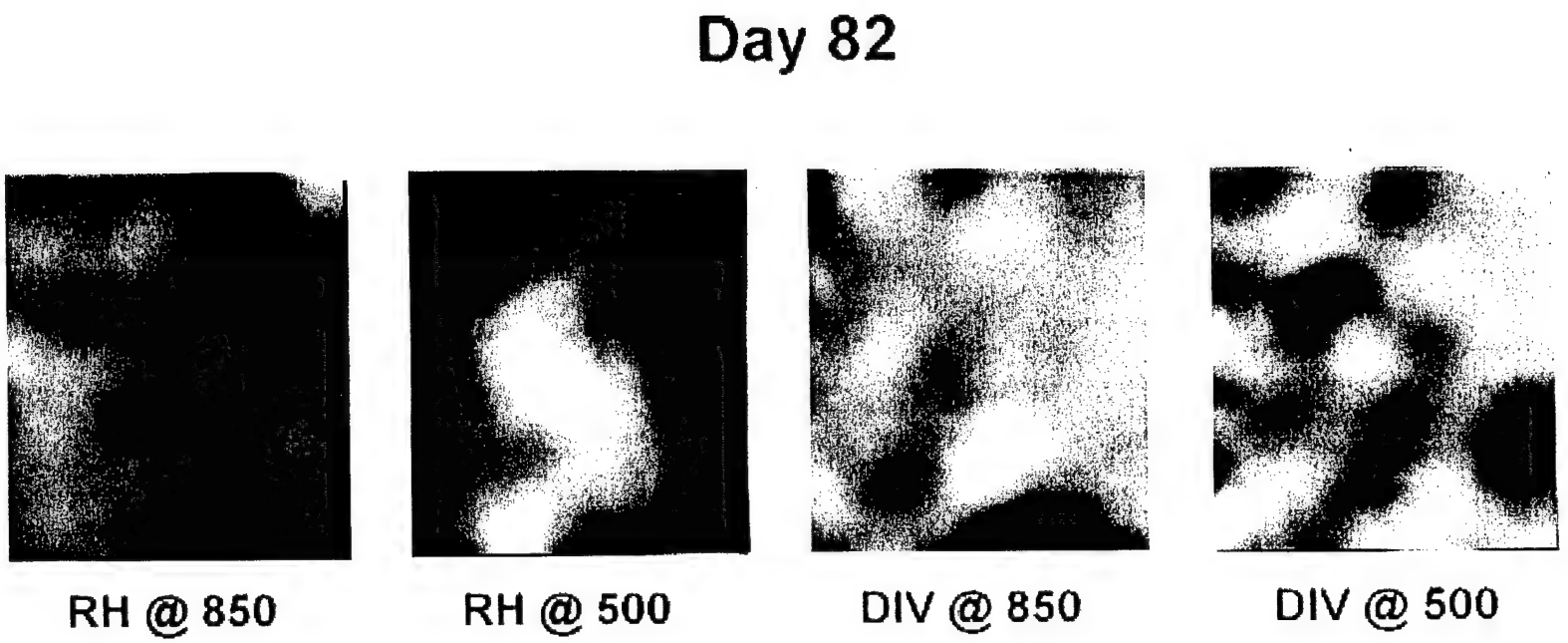

Figure A-4. NOGAPS relative humidity and velocity divergence data at two altitudes on days 71 through 82 for EMDA (Continued).

Total Cloud Fraction - CNSA

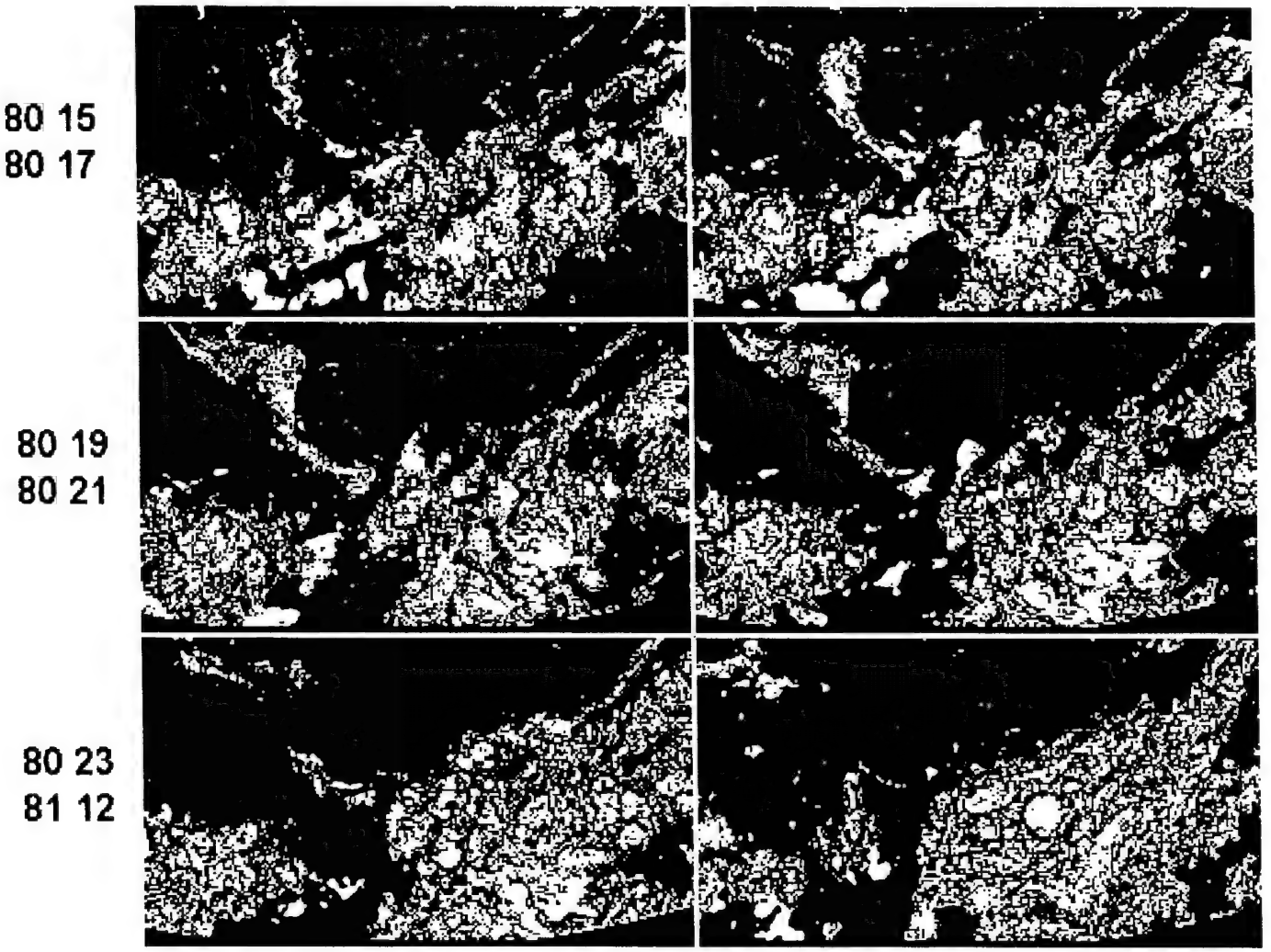

Figure A-5. SERCA level 3 total cloud fraction on days 80 through 91 for CSNA.

Total Cloud Fraction - CNSA

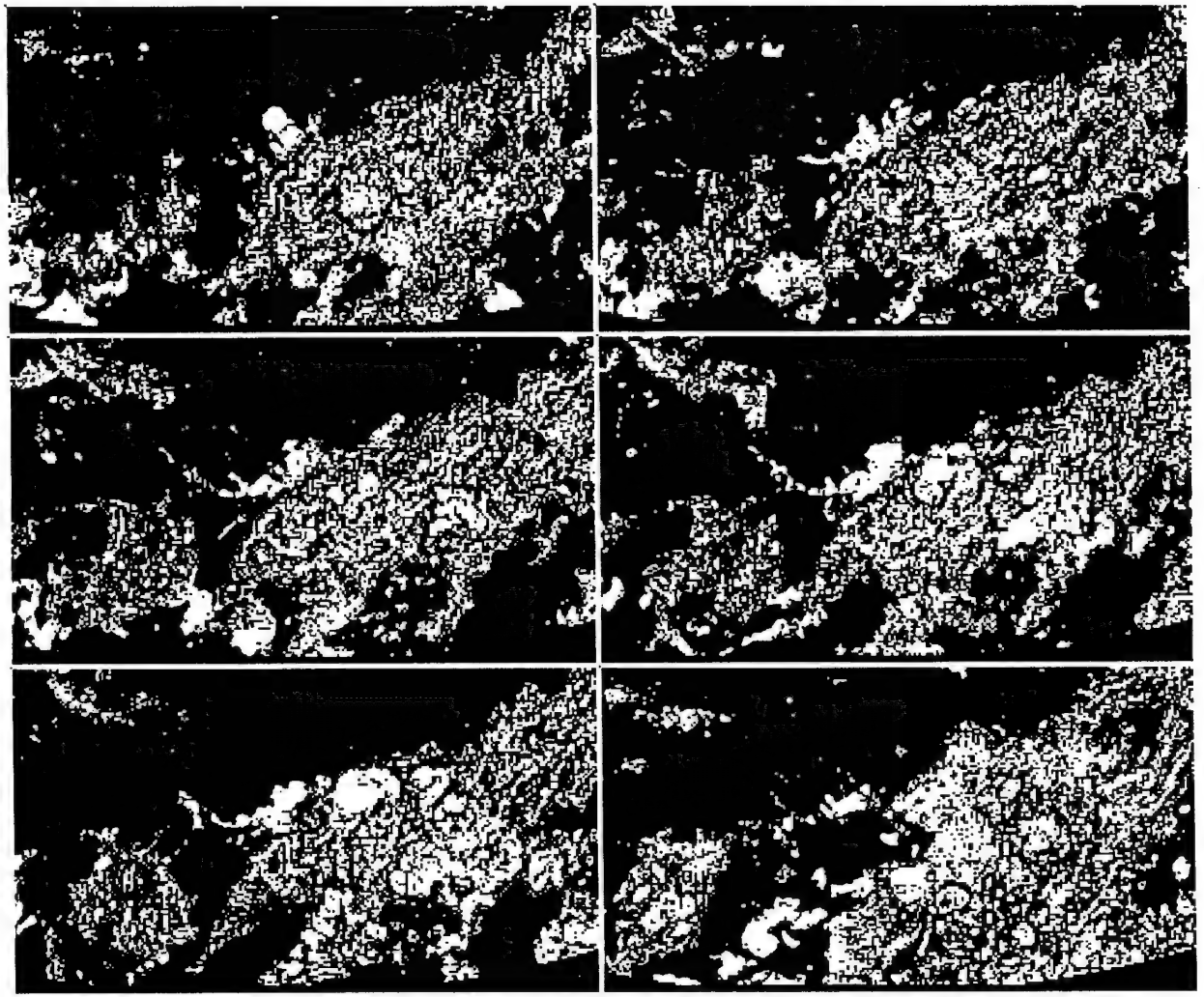

Figure A-5. SERCA level 3 total cloud fraction on days 80 through 91 for CSNA (Continued).

Total Cloud Fraction - CNSA

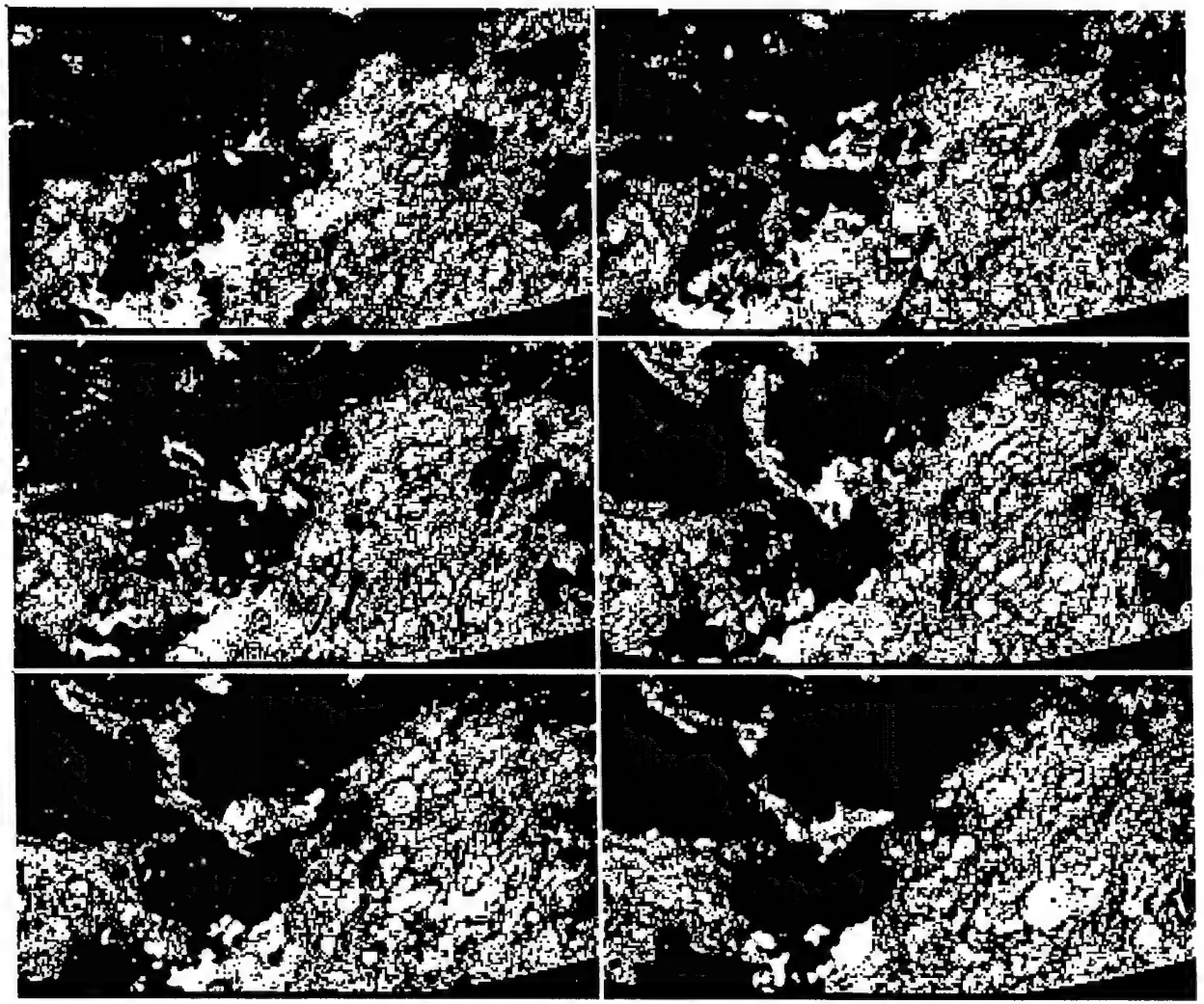

Figure A-5. SERCA level 3 total cloud fraction on days 80 through 91 for CSNA (Continued).

Total Cloud Fraction - CNSA

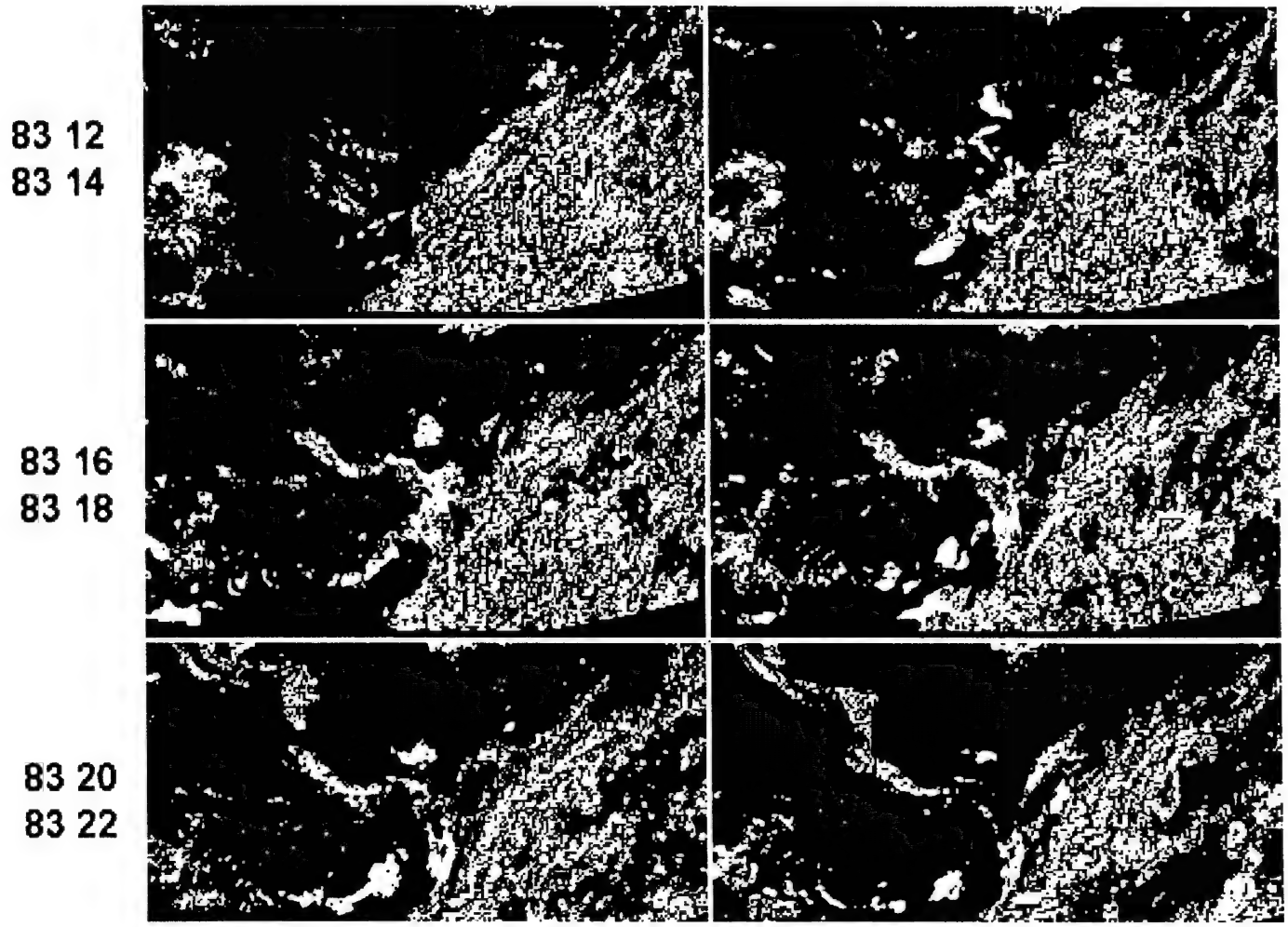

Figure A-5. SERCA level 3 total cloud fraction on days 80 through 91 for CSNA (Continued).

Total Cloud Fraction - CNSA

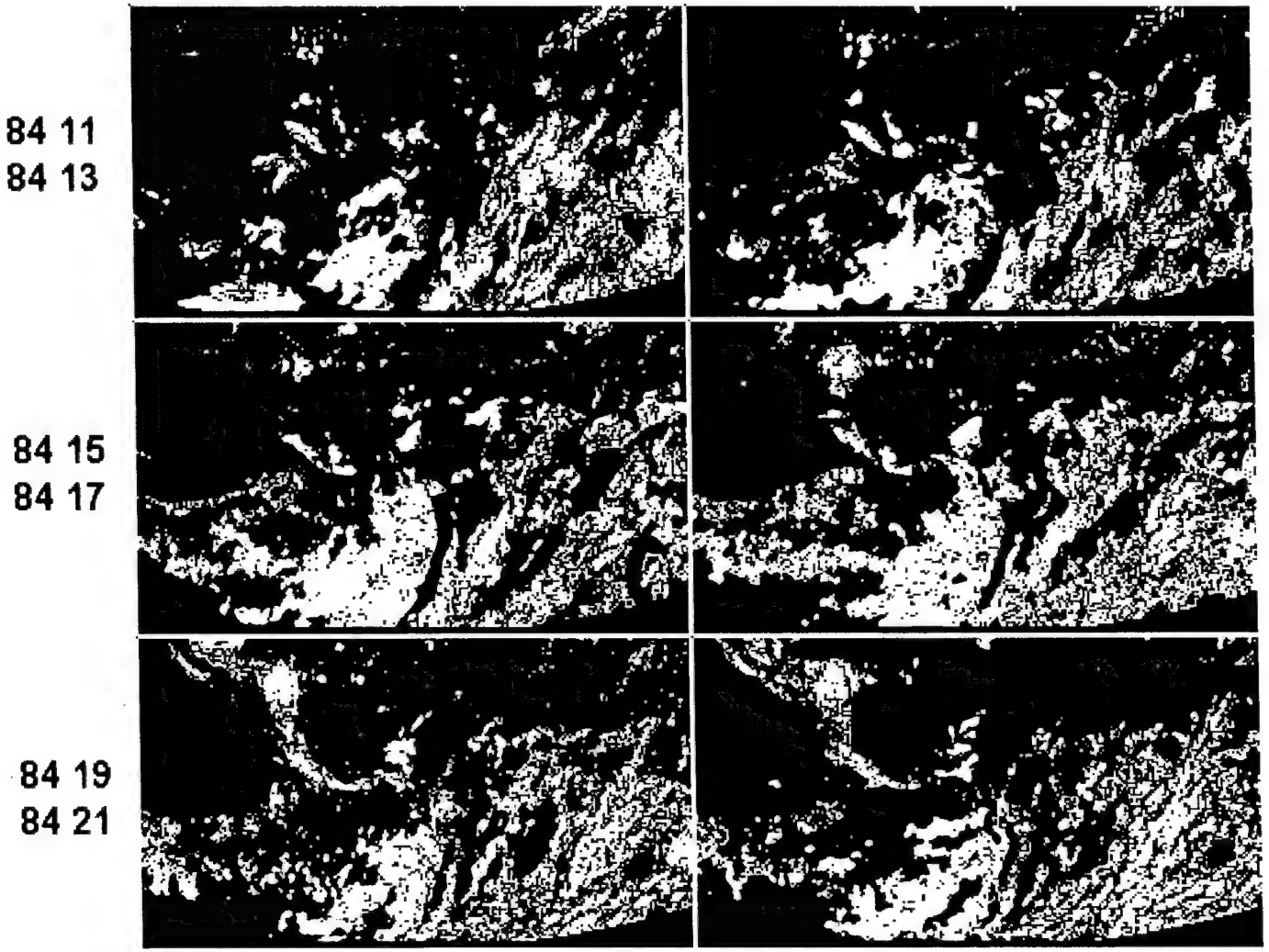

Figure A-5. SERCA level 3 total cloud fraction on days 80 through 91 for CSNA (Continued).

Total Cloud Fraction - CNSA

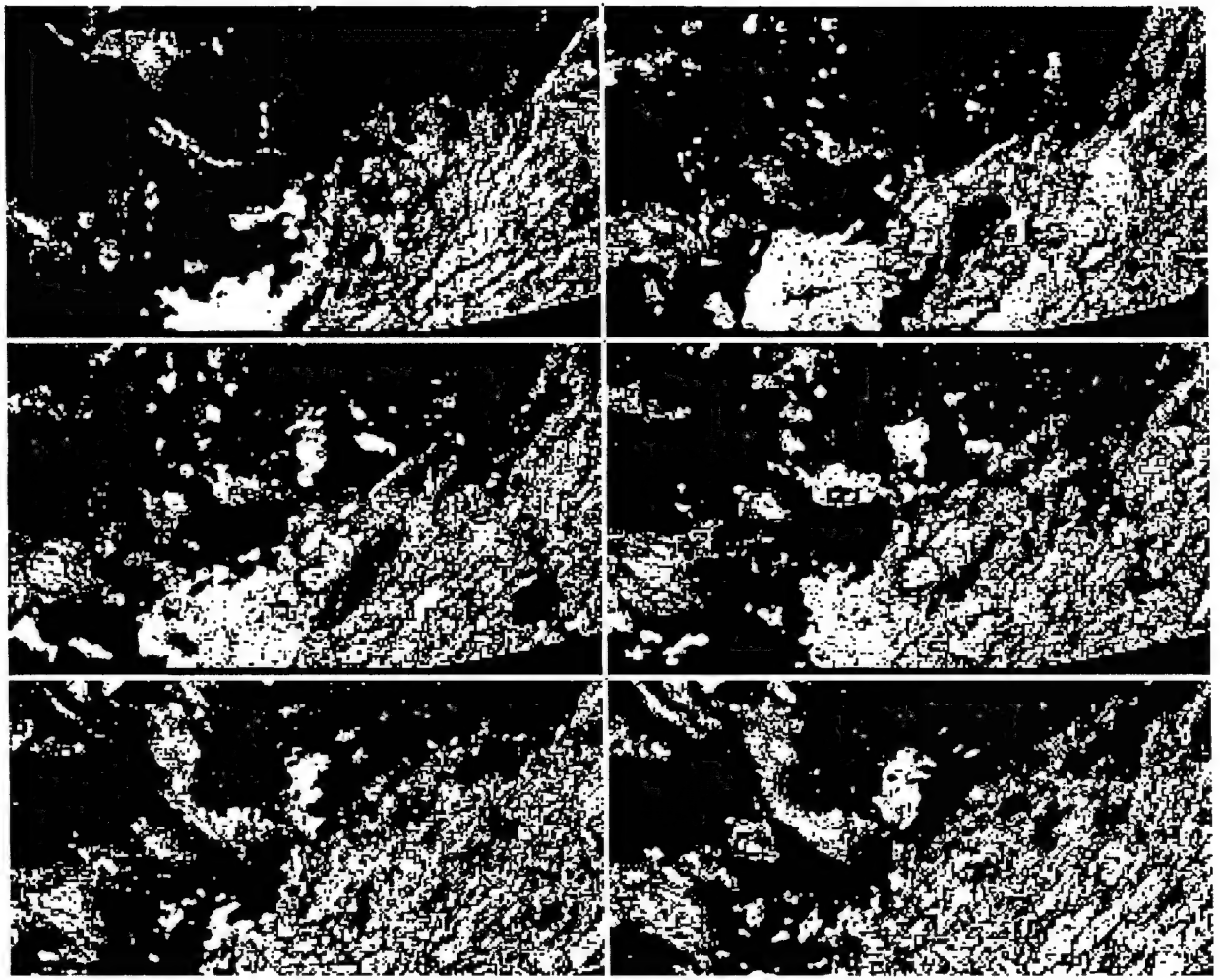

Figure A-5. SERCA level 3 total cloud fraction on days 80 through 91 for CSNA (Continued).

Total Cloud Fraction - CNSA

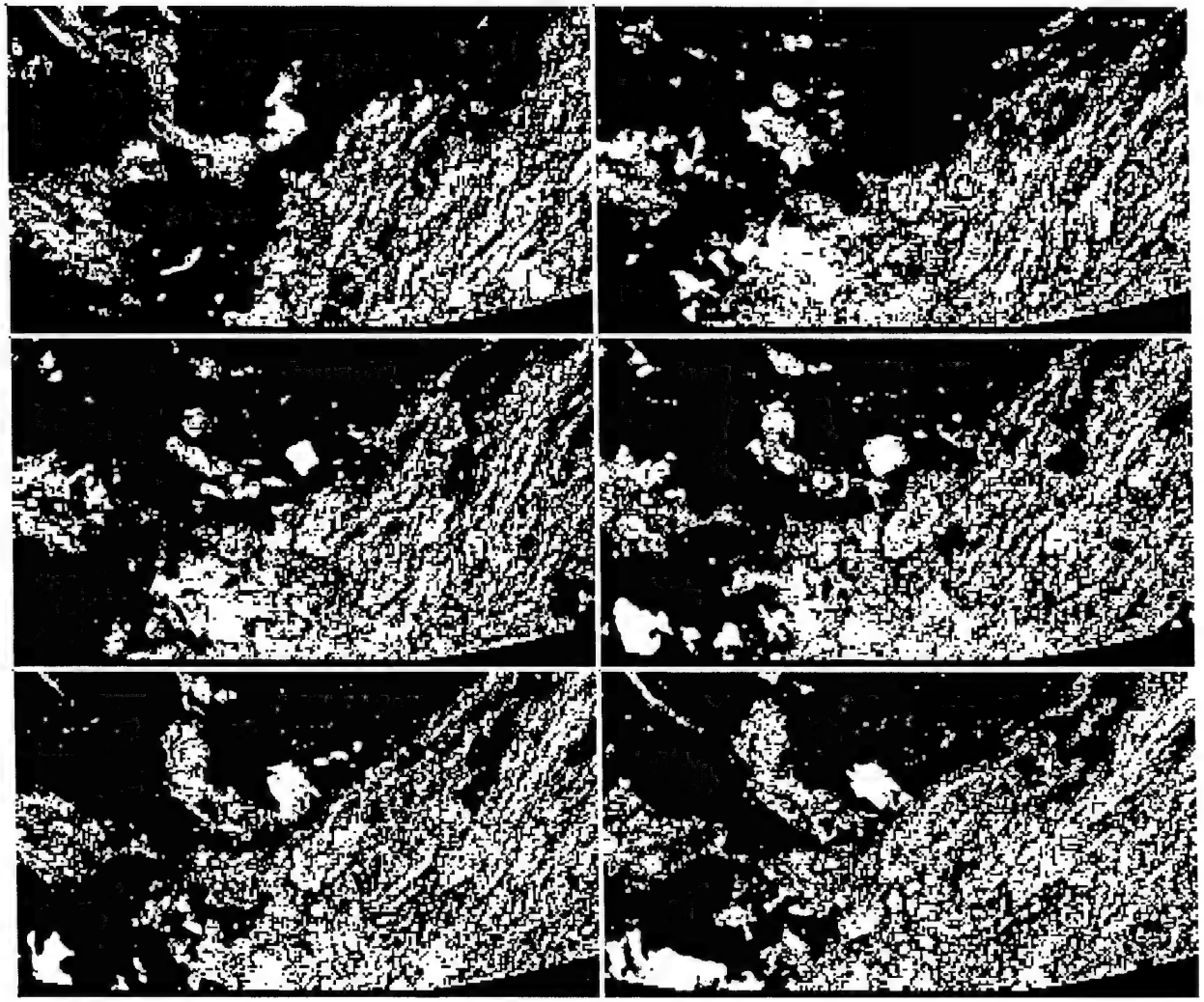

Figure A-5. SERCA level 3 total cloud fraction on days 80 through 91 for CSNA (Continued).

Total Cloud Fraction - CNSA

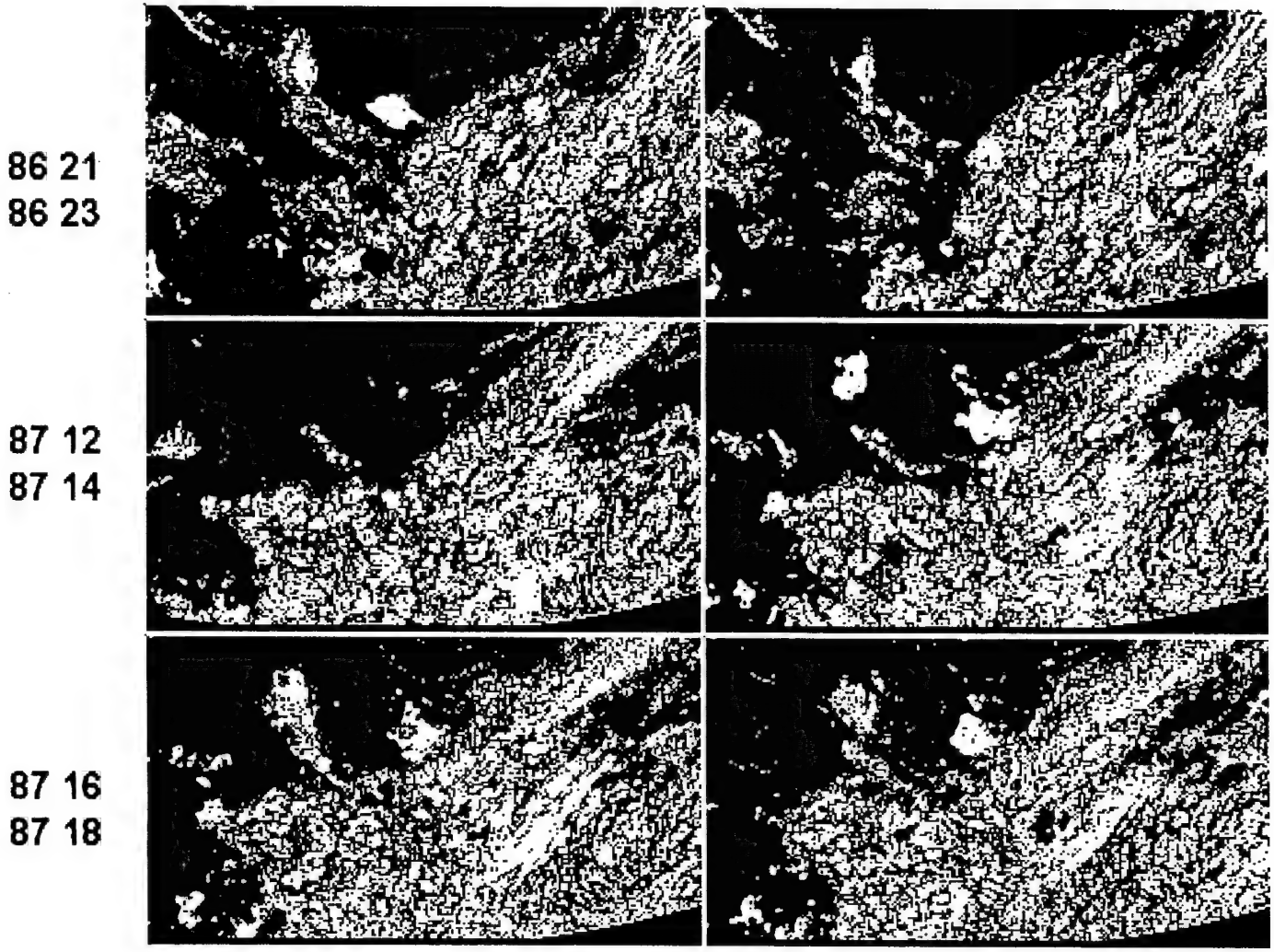

Figure A-5. SERCA level 3 total cloud fraction on days 80 through 91 for CSNA (Continued).

Total Cloud Fraction - CNSA

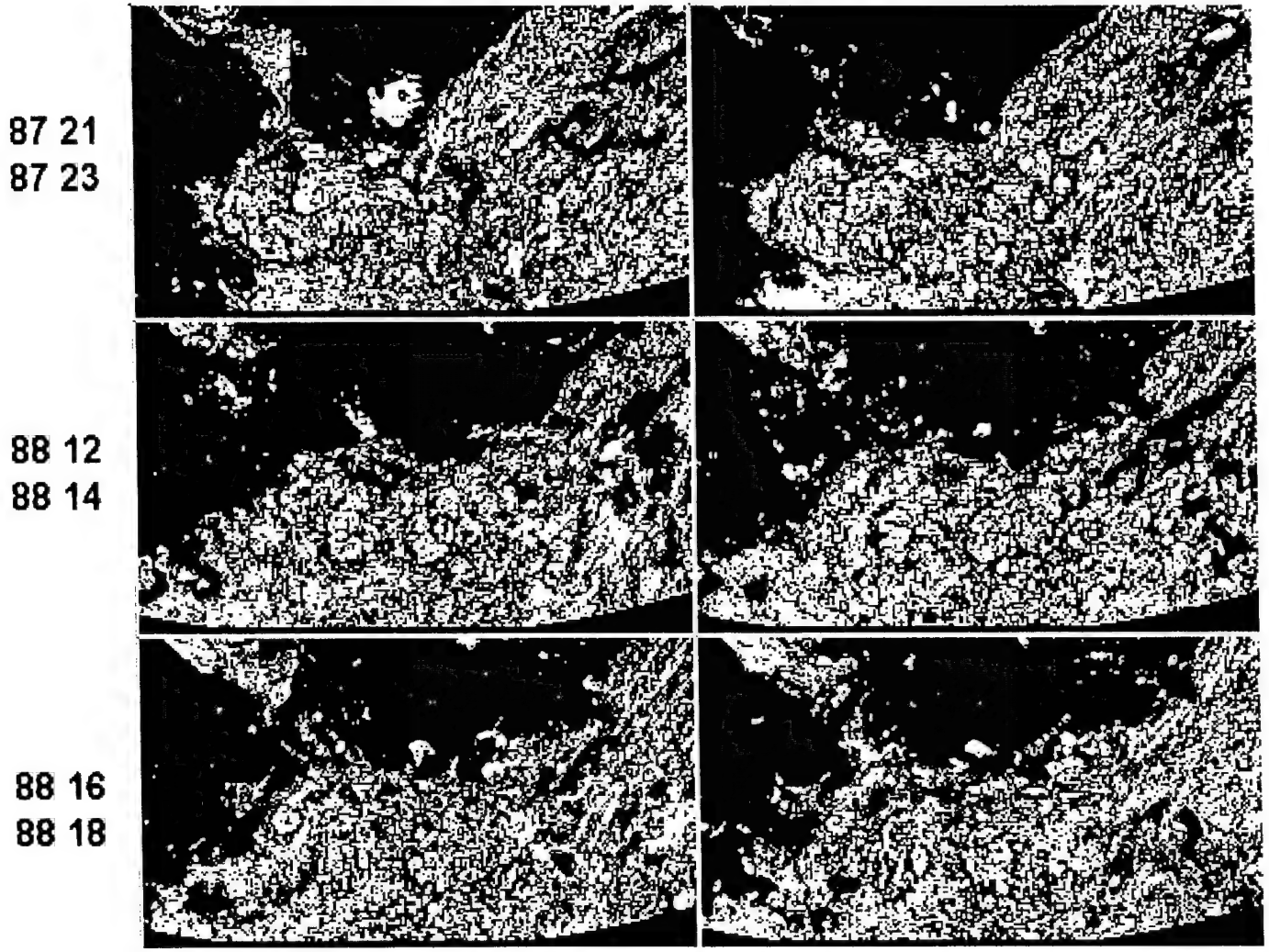

Figure A-5. SERCA level 3 total cloud fraction on days 80 through 91 for CSNA (Continued).

Total Cloud Fraction - CNSA

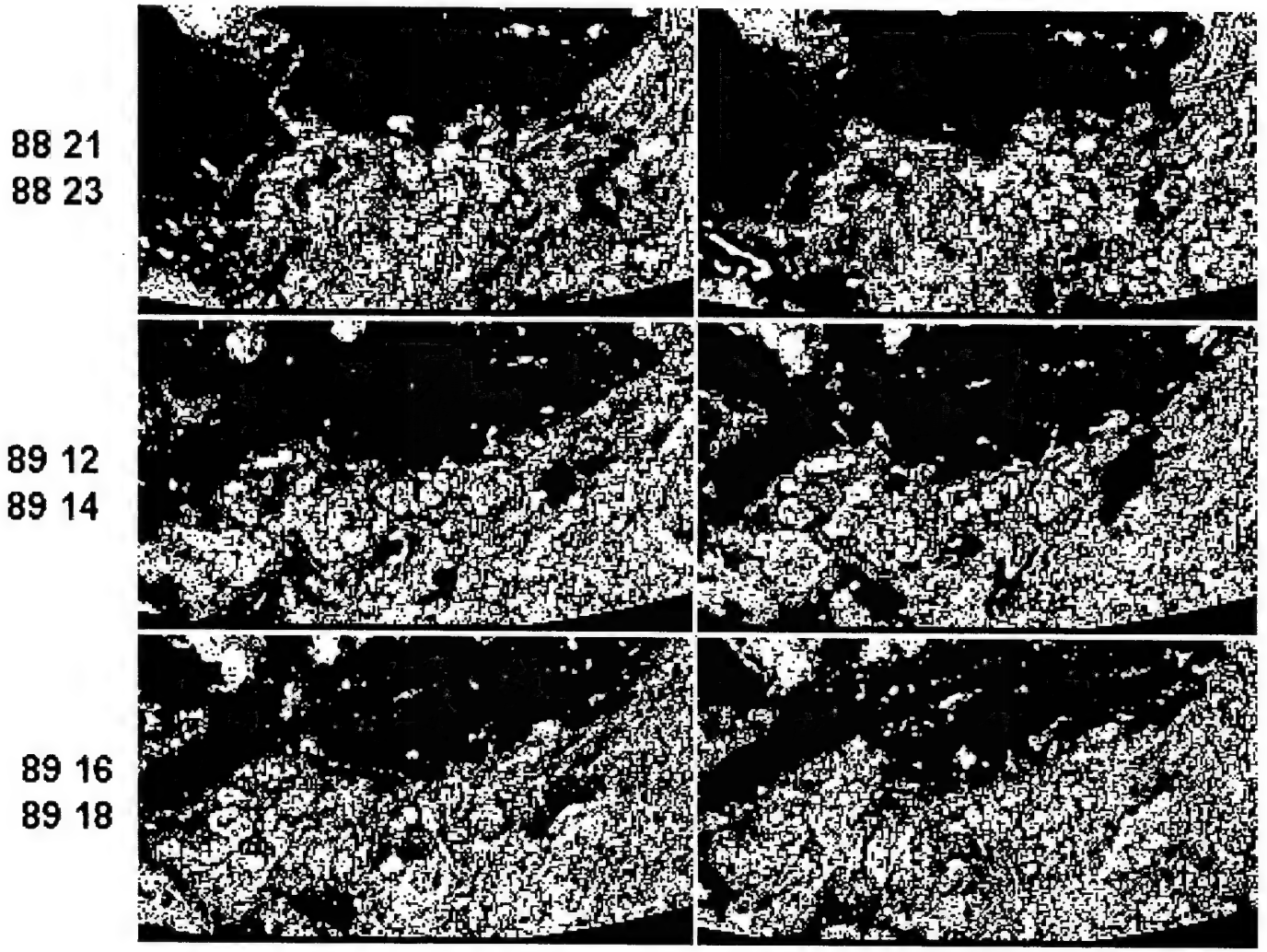

Figure A-5. SERCA level 3 total cloud fraction on days 80 through 91 for CSNA (Continued).

Total Cloud Fraction - CNSA

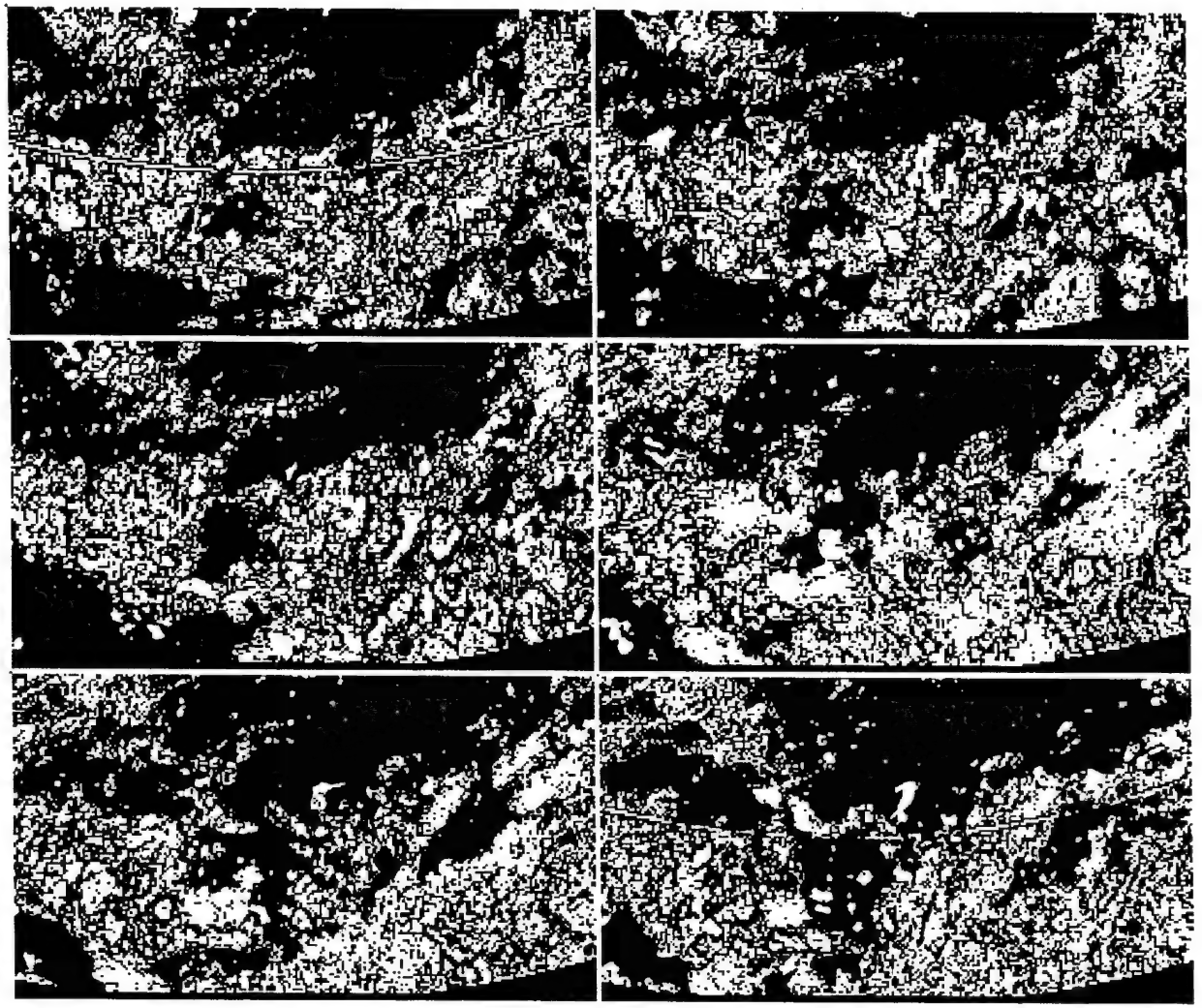

Figure A-5. SERCA level 3 total cloud fraction on days 80 through 91 for CSNA (Continued).

Total Cloud Fraction - CNSA

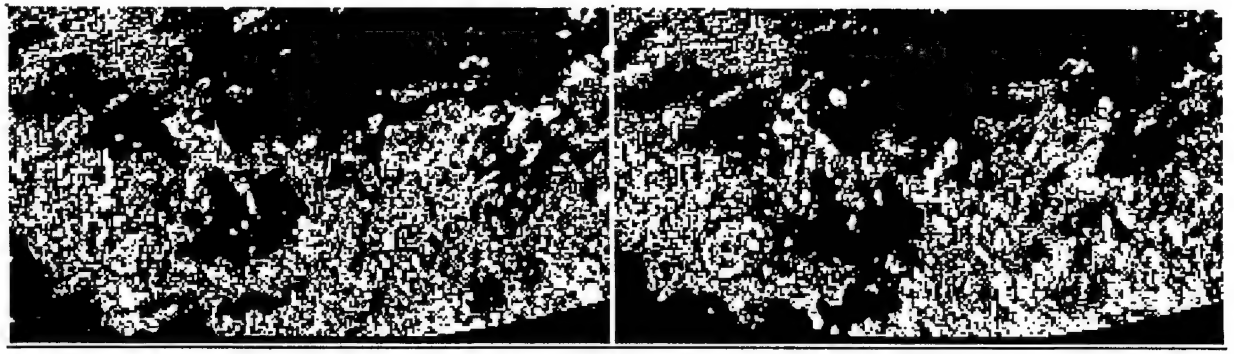

Figure A-5. SERCA level 3 total cloud fraction on days 80 through 91 for CSNA (Continued)

APPENDIX B

SKILL SCORE DEFINITION

The skill scores used in this study are completely defined and described in Gandin and Murphy (1992). For completeness, a short definition of each is provided below.

Brier Score:

The Brier score is the standard measure of the mean square error between the forecast and the truth. There is not selective weighting or penalty. The score is normalized to range from 0 to 1 with a score of 0 being perfect.

Equitable Skill Score (ESS):

The ESS is defined to emphasize an ability to accurately forecast the unusual in an image. ESS also penalizes for poor forecasts. To accomplish this ESS weights points approximately inversely proportional to their fractional occurrence. Therefore, the correct forecast of an isolated feature is very heavily weighted while the correct forecast of the most commonly occurring values is lightly weighted. Conversely, incorrect forecasts are negatively weighted according to their fractional occurrence. Negative ESS is therefore possible. ESS can range from -1 to +1 with +1 being perfect.

Evaluating the ESS is very difficult because the concept of a "good" score is image dependent. Low, but positive, ESS (0.1 to 0.2) is expected for the cloud fields shown in Figures A-2 to A-5. The cloud fields are very broken. Isolated pixels of clouds are observed and are randomly populated. The opportunity for forecast penalties is very large due to these isolated pixels.

20/20:

The 20/20 score simply measures the ability of the forecast to predict within ±20% of the correct value. There is no weighting according to the chance of occurrence for that value. Scores range between 0 and 1 with a score of 1 being perfect.

The EMDA data is dominated by areas of no clouds (about 70% of the pixels have no clouds). The 20/20 score should be high if the model accurately forecasts "no clouds". In regions of uniform clouds (no clouds or all clouds) the scores are expected to exceed 0.8. In areas of scattered clouds lower scores of 0.5 to 0.6 are expected.

Correlation (CORR):

This is the standard zero-lag image correlation coefficient given by

$$CORR = \frac{1}{N}\sum_{i,j}^{N} x_{ij} y_{ij} \qquad \text{(B.1)}$$

where x_{ij} and y_{ij} are pixels in the forecast and truth images each containing N pixels. This score emphasizes the correct forecasting of larger features in the images. Since cloudless pixels have a value near zero, the cloudy pixels contribute most to the correlation.

DISTRIBUTION LIST

DSWA-TR-97-13

DEPARTMENT OF DEFENSE

DEFENSE INTELLIGENCE AGENCY
ATTN: TWJ
ATTN: TWP - 6, G WEBER

DEFENSE SPECIAL WEAPONS AGENCY
2 CY ATTN: TRC
ATTN: WEL
2 CY ATTN: WEL, LTC JIM HODGE
ATTN: WEL, L WITTWER
ATTN: WEL, MAJ T SMITH

DEFENSE TECHNICAL INFORMATION CENTER
2 CY ATTN: DTIC/OCP

FC DEFENSE SPECIAL WEAPONS AGENCY
ATTN: FCT - S, G BALADI
ATTN: FCTO

JOINT CHIEF OF STAFF
ATTN: J8 WAR FIGHTING DIV

DEPARTMENT OF THE ARMY

ARMY RESEARCH LABORATORIES
ATTN: AMSRL - SL - CE

DEPARTMENT OF THE ARMY
ATTN: DAMO - NCZ

US ARMY RESEARCH LAB
ATTN: AMSRL - WT - TA, G BULMASH
ATTN: SLCBR - SS - T, TECH LIB

DEPARTMENT OF THE NAVY

NAVAL RESEARCH LABORATORY
ATTN: CODE 5227, RESEARCH REPORT

NAVAL SURFACE WARFARE CENTER
ATTN: CODE K42, L VALGE

DEPUTY CHIEF OF NAVAL OPERATIONS
ATTN: BRANCH HEAD, N514

DEPARTMENT OF THE AIR FORCE

AF WEATHER TECHNICAL LIBRARY
ATTN: KAY MARSHALL

AIR FORCE LABORATORY
ATTN: PL/WS, MR SHARP

AIR FORCE SPACE COMMAND
ATTN: LTCOL CROSS

AIR FORCE WEATHER AGENCY/DNXM
ATTN: MAJ RANDY LEFEVRE

AIR UNIVERSITY LIBRARY
ATTN: AUL - LSE

HQ USAF/XOWX
ATTN: XOWX

DEPARTMENT OF ENERGY

LAWRENCE LIVERMORE NATIONAL LAB
ATTN: ALLEN KUHL
ATTN: L - 81, R PERRETT

LOS ALAMOS NATIONAL LABORATORY
ATTN: A S MASON
ATTN: J NORMAN
ATTN: ESS - 5, R W WHITAKER
ATTN: WX - 1/B SHAFER

DEPARTMENT OF DEFENSE CONTRACTORS

APPLIED RESEARCH ASSOCIATES, INC.
ATTN: C NEEDHAM

HORIZONS TECHNOLOGY, INC.
ATTN: B KREISS

ITT INDUSTRIES
ATTN: DASIAC
ATTN: DASIAC/DARE

LOGICON RDA
ATTN: RAY POPE
ATTN: TOM MAZOLLA

MISSION RESEARCH CORP
ATTN: BRUCE BAUER

PACIFIC-SIERRA RESEARCH CORP.
2 CY ATTN: DAVID CRANDALL
ATTN: H BRODE

2 CY ATTN: KENNETH HETKES
2 CY ATTN: KENNETH POEHLS
2 CY ATTN: KEVIN O'ROUKE

SCIENCE APPLICATIONS INTL CORP
ATTN: J MANSHIP

SCIENCE APPLICATIONS INTL CORP
ATTN: D BACON
ATTN: J COCKAYNE
ATTN: J MCGAGHAN

SCIENCE APPLICATIONS INTL CORP
ATTN: A LAGANELLI
ATTN: A MARTELLUCCI
ATTN: J SONTOWSKI

THE AEROSPACE CORP
ATTN: DR MIKE PLONSKI

TITAN CORPORATION (THE)
ATTN: R ENGLAND

THE TITAN CORPORATION
ATTN: M ROSENBLATT

TRW S. I. G.
ATTN: NORMAN LIPNER

VISIDYNE, INC.
ATTN: J DEVORE